IN-SITU STERIC STABILIZATION OF ULTRAFINE TITANIA PARTICLES SYNTHESIZED BY A SOL-GEL PROCESS

by

Vidhu JaiKishen Nagpal

Dissertation submitted to the Faculty of the
Virginia Polytechnic Institute and State University
in partial fulfillment of the requirements for the degree of
Doctor of Philosophy
in
Materials Engineering Science

Approved:

Richey M. Davis, Chairman

Seshu B. Desu

Garth L. Wilkes

J.S. Riffle

Tom C. Ward

August 30, 1993
Blacksburg, Virginia

IN-SITU STERIC STABILIZATION OF ULTRA-FINE TITANIA PARTICLES SYNTHESIZED BY A SOL-GEL PROCESS

Vidhu J. Nagpal
Richey M. Davis, Chairman
Materials Engineering Science Program

Abstract

This dissertation concerns the synthesis of ultra-fine titania particles starting with titanium ethoxide as a precursor. The particle size and morphology was controlled using polymeric stabilizers which imparted in-situ steric stability during the particle growth. An attempt was made to elucidate the factors which govern the particle size and morphology by studying the solvent-polymer-particle surface interactions. For this purpose, the effects of polymer concentration, molecular weight, structure, and the solvent system were studied.

Titanium dioxide particles were synthesized via the hydrolysis of tetraethylorthotitanate in ethanol in the presence of hydroxypropylcellulose, HPC, as an in-situ steric stabilizer. The effects of HPC concentration, molecular weight, and water concentration on TiO_2 particle size and morphology were determined along with the effect of HPC on the particle growth rate. The particle size decreased by ten-fold upon the addition of HPC at high water concentrations due to the combined effects of increased HPC adsorption and increased nucleation rates. Water was shown to segregate at the TiO_2 surface and to promote HPC adsorption through enhanced hydrogen bonding.

Mean particle diameters as small as 70 nm were obtained. The particles grown with HPC had surface morphologies that suggest the particles aggregated by flocculating initially into a secondary energy minimum followed by condensation reactions that welded the aggregates together. Particle growth rate studies show that HPC can undergo an alcoholysis reaction with tetraethylorthotitanate when mixed in the absence of water. Electrophoresis measurements show the absence of any significant electrostatic stabilization effects under conditions giving the smallest particle sizes.

In another related study, titanium dioxide particles were synthesized via the hydrolysis of tetraethylorthotitanate, TEOT, in mixtures of ethanol and tetrahydrofuran, THF, in the presence of hydroxypropylcellulose, HPC, as an in-situ steric stabilizer. The effects of THF concentration on the particle size and growth rate were studied at fixed concentrations of water, TEOT, and HPC. Particles grown in the absence of HPC were highly aggregated while the size of the primary particles comprising the aggregates decreased with THF concentration. The particle growth rate increased significantly with THF concentration due to the decrease in the hydrogen bonding capability of the solvent system which increased the activity of the water. In the presence of HPC, both the growth rate and the particle size decreased dramatically with increasing THF concentration. The decrease in the solubility of HPC with THF concentration presumably enhanced HPC adsorption at the particle surface which led to increased colloid stabilization. Particles as small as 50 nm in diameter were obtained when the particles were grown in 1:1 THF:ethanol volume mixtures.

In an attempt to study the effect of polymer structure and structure on particle size

and morphology, a low molecular weight (Mw = 2000) polymer with poly(propylene oxide) back-bone was end functionalized to make it a suitable in-situ steric stabilizer. Effects of polymer concentration, functionality at chain-ends, and molecular weight on the particle size were studied. The polymer functionalized at both ends imparted in-situ steric stability at $C_p > 8$ g/l. Particles having mean size of 0.2 microns were obtained at $C_p = 16$ g/l. This work demonstrated that end-functionalized low molecular weight polymers offer a novel way to synthesize in-situ steric stabilizers.

An application of the synthesized ultra-fine titania particles was studied. For this purpose, novel thin films of ultra-fine titanium dioxide particles dispersed in a matrix of hydroxypropylcellulose polymer were made on quartz and silicon substrates. The TiO_2/HPC composite films were transparent in the visible region and completely blocked ultra-violet radiation at 300 nm. These films were crack-free and uniform in composition and thickness. Transparent films of amorphous TiO_2 were made by burning out the HPC at 500°C. These films were highly uniform and had no macroscopic cracks. X-ray diffraction revealed a transition to the anatase form upon sintering at 600°C. A film sintered at 700°C had a porosity of 38%. The crystalline films remained transparent until they densified at 800°C.

Acknowledgements

First and foremost, I would like to thank my advisor, Professor Rick Davis, whose guidance and insightful suggestions made this work meaningful and success. He always encouraged new ideas and free thinking which made this work an exciting and rewarding experience for me. I thank him for being so inspiring, tolerant, patient, and understanding and I consider myself fortunate to have him as my advisor.

I would also like to express my sincere thanks to Professor Judy Riffle, Professor Seshu Desu, and Professor Garth Wilkes, for their invaluable contributions and helping me stay focussed in my work. I consider myself very fortunate for having an opportunity to attend the courses in the area of polymer science taught by the two of the best teachers, Professor Garth Wilkes and Professor Tom Ward. These brilliantly taught courses laid a strong theoretical foundation in me for which I am forever indebted to them.

I would also like to thank my lab-mates for being so co-operative and tolerant of my mood swings. My sincere thanks to Steve McCartney for helping me with his expertise in electron microscopy and for being a good friend. Steve, you have always accommodated me at a short notice and I appreciate that.

My special thanks to Kumud Ajmani for being a great friend over the years. People like him make this world a better place to live.

Natasha, I cannot thank you enough for coming into my life and filling it with happiness. You have been extremely patient and understanding and taken care of smallest of my needs. Your love and affection has helped me see through the roughest of times and I feel so lucky to have you as my partner for the rest of my life. For this I am thankful to Drs. Anand and Sita Bhatia for trusting me with their daughter and marrying us off at such a short notice.

I would like to thank my father, Jai Kishen Nagpal, who encouraged me for graduate studies in the United States. He is a very hard working man and I have always been inspired by his enthusiasm and dedication to work. Papa, you have been my role model and this thesis is for you. The love, affection and dedication of my mother, Susheel, and my sister, Ritu, has been instrumental in the completion of this thesis.

Table of Contents

List of Figures

List of Tables

Preface

The paper versions of Chapters 2 and 3 were submitted to *Colloids and Surfaces*, and the *Journal of Non-Crystalline Solids* respectively. Both the papers were co-authored with Professor Judy Riffle in the Department of Chemistry.

The paper version of Chapter 5 was submitted to *Langmuir* and was co-authored with Professor Riffle and Dr. Q. Liu in the Department of Chemistry.

The paper version of Chapter 6 was submitted to the *Journal of Materials Research* and was co-authored with Professor Seshu Desu in the Department of Materials Science and Engineering.

This thesis is dedicated to my Parents, Susheel and Jai Kishen Nagpal, without whose everlasting love and support this work wouldn't have been possible.

Chapter 1

Introduction

The synthesis and processing of ultra-fine ceramic powders is critically important for the manufacture of functional and structural ceramics. Submicron powders find applications in the ceramic industry when high performance materials are required [1]. Ceramic powders are used as catalysts, pigments, abrasives, and fillers. They are employed in fabricating electronic, optical, and magnetic storage media devices. The mechanical, electrical, and optical properties of these materials and their uses depend significantly on the size, morphology and the porosity of the starting ceramic particles.

In optical applications, it is often important to control the transmission of light through a ceramic by minimizing light scattering from within the ceramic. This can be done by reducing the size of the ceramic particles comprising the body or of pores within the ceramic body to much less than the wavelength of visible light [2]. Optical coatings alter the reflectance, transmission, or absorption of the substrate. The reflectance and absorption are controlled by the refractive index of the coating which is affected by porosity. Anti-reflective coatings coatings have been prepared this way [3]. IROX^{R} (TiO_2/Pd) coated glass structures have been used extensively where the IROX controls the transmission of sun-light by controlling the reflectance, transmission and absorption of incident light [4].

In structural ceramics, relatively monodispersed spherical particles are precursors for making dense ceramic bodies for load-bearing applications by slip casting or injection molding. Smaller particles lead to close packing and approach the theoretical density of the green body, thus reducing the size and number of flaws which have a deleterious effect on mechanical properties, particularly strength and impact resistance. Sintering time and temperature of the green body also can be significantly reduced as the particle size reduces [5]. These examples clearly indicate the imperative need to control the size, porosity, and morphology of particles to make high performance ceramic materials.

This chapter is organized as follows. After a brief review of some aspects of the chemistry of particle synthesis from alkoxides, the role of colloid stabilization in particle formation is reviewed with a focus on polymer-induced steric stabilization. In-situ steric stabilization is a key part of this work. This involves precipitating and growing particles in the presence of a soluble polymer solution from which polymer chains adsorb onto the growing particles, ultimately preventing further particle aggregation and resulting in relatively small particles. The factors affecting in-situ steric stabilization are discussed next. The final part of the chapter details the goals of this research and the overall organization of the thesis.

Particle Synthesis

Processes for making ceramic particles can be broadly classified into two

categories: solution (sol-gel) techniques and techniques involving reactions or phase changes in a gas phase. The latter include the formation of particles from aerosols, evaporative decomposition of solutions, and vapor-phase reactions such as flame, plasma, or laser-induced reactions. These techniques have been reviewed by Matijevic and Gherardi [6], Brinker and Scherer [7], and Livage et al. [8]. Sol-gel techniques include particle synthesis from aqueous metal salts and alkoxide precursors. One important advantage of the sol-gel process over other processes is it's ability to transform completely from the molecular precursor to the solid material. This permits better control of the entire process and allows the synthesis of tailor-made powders, particularly when mixed oxides are desired [8].

Metal alkoxides are particularly versatile precursors for the sol-gel synthesis of oxides. The molecular structure of metal alkoxides consist of a M-O-C linkage where M is metal, O is oxygen, and C is carbon element. The electropositivity of the metal atom coupled with the electronegativity of oxygen polarizes the M-O bond and makes it susceptible towards an attack by nucleophilic reagents like water. While many metal oxide systems have been made in the form of relatively large, irregular aggregated particles, (size typically much larger than 1 micron [7]), most of the studies of fine particle formation done with alkoxides with the purpose of making relatively monodisperse, well-defined spherical particles have concerned the hydrolysis and condensation of silicon alkoxide systems $Si(OR)_4$ because silicon alkoxides have relatively low reactivity and hence offer a better control over the synthesis. The reaction scheme

of hydrolysis and condensation of metal alkoxides is shown in reaction scheme 1 in Figure 1.1 [7].

Acid or base catalysts are typically employed to accelerate the reaction kinetics. Particle formation is favored under basic conditions whereas gel formation is favored under acidic conditions. The Stober process [9] is used routinely now to make monodispersed silica particles in the range 0.1 to over 1 micron by hydrolysis and condensation of silicontetraethoxide (TEOS) at water concentration ranging from R (=[H_2O/[TEOS]) = 20 to 50 and ammonia concentration ranging between 1 to 7 M.

By contrast with silicon alkoxides, less work has been done in using sol-gel processes to make relatively monodisperse, well-defined spherical particles from transition metal alkoxides systems $M(OR)_4$. Their more rapid reaction kinetics make fundamental studies of hydrolysis and condensation of $M(OR)_4$ more difficult than $Si(OR)_4$. For example, the hydrolysis rate constant for $Si(OEt)_4$ is reported [10] as k_h = 5 x 10^{-9} M^{-1} s^{-1} presumably at room temperature at pH 7 whereas k_h = 10^{-3} M^{-1} s^{-1} for $Ti(OR)_4$ approximately [11] at the same pH. Also, the condensation rate was faster for TiO_2 precipitated from $Ti(OEt)_4$, i.e., the condensation constant $k_c(Si(OEt)_4)$ = 10^{-4} M^{-1} s^{-1} [12] whereas $k_c(Ti(OEt)_4)$ = 30 M^{-1} s^{-1} [13]. Transition metal alkoxides are much more reactive than silicon alkoxides because (i) transition metals are more electropositive than Si and thus less stable towards nucleophilic reactions, and (ii) transition metals exhibit multiple stable coordination states and hence coordination expansion occurs spontaneously when attacked by water. Hence, acid or base catalysts are not necessarily

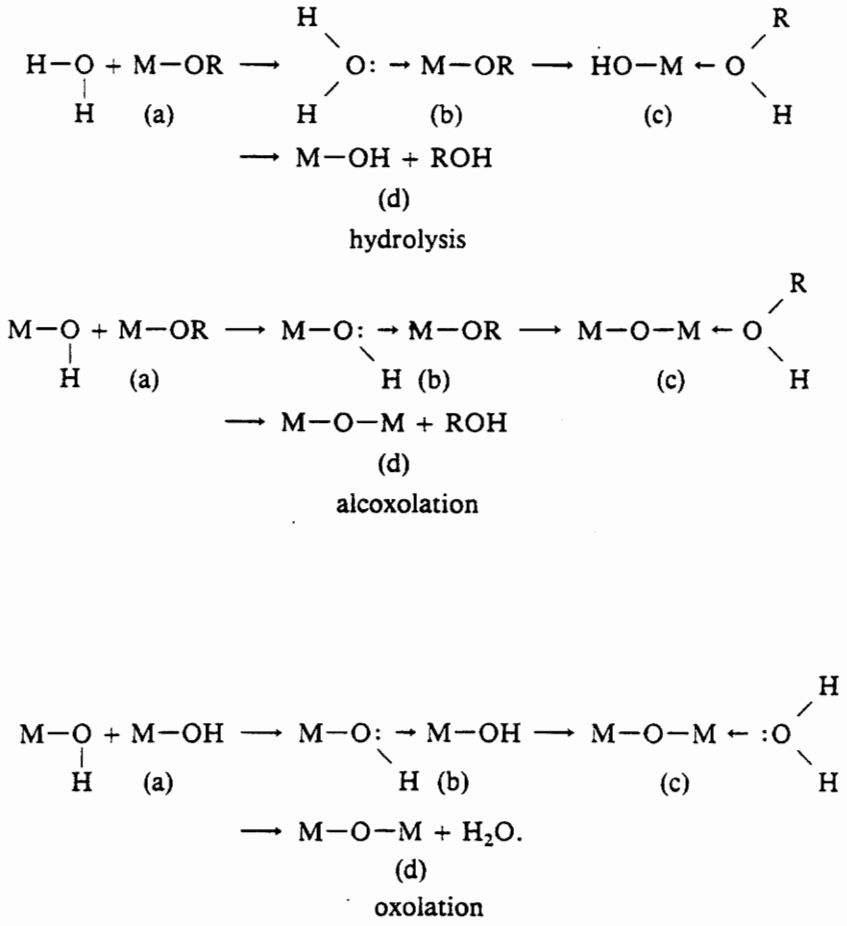

Figure 1.1. Reaction scheme 1 of nucleophilic attack of water resulting in the hydrolysis and condensation of $M(OR)_4$.

required for practical studies of the hydrolysis and condensation of $M(OR)_4$ systems - the reactions are often carried out under neutral conditions unlike $Si(OR)_4$ systems.

This work concerns the synthesis of ultrafine, relatively monodisperse TiO_2 particles via the hydrolysis and condensation of tetraethylorthotitanate $Ti(OC_2H_5)_4$, referred to henceforth as TEOT, at neutral conditions in the presence of a soluble polymer solution from which polymer chains adsorb onto the growing particles. The adsorbed chains provided steric stabilization that limited particle aggregation to very small sizes in some cases. TEOT was chosen firstly because prior work using electrostatic [14] and steric stabilization techniques [15] demonstrated that it was possible to make well-defined particles less than 1 micron in diameter with careful control of reaction conditions. The prior work on steric stabilization left many issues unresolved such as the role that polymer structure and polymer/solvent/particle interactions played in stabilizing the growing TiO_2 particles. These issues form the bases of much of the present work and will be discussed later in more detail. The approach taken in this work with TEOT is sufficiently general that it is believed the findings of this research will provide guidance towards the synthesis of ultrafine particles of other transition metal oxides. e.g., zirconia and tantalum oxides. In terms of applications, titania particles are extensively used in the paint, coatings, and paper industries as pigments and opacifiers.

In the presence of water, TEOT undergoes step-wise hydrolysis and condensation reactions according to the reaction scheme 1. As shown in this scheme, the condensation reaction could be via either oxolation or alcoxolation. Livage et al. [8] developed the

partial charge model which predicts that condensation by alcoxolation is preferred over oxolation in the cases of both silicate and titanate systems. However, Assink and Kay [16] showed that oxolation is favored over alcoxolation in silicates. No such study has been done on titanate systems and it is entirely possible that both alcoxolation and oxolation occur simultaneously given the rapid condensation kinetics.

Particle Formation

A general model commonly used to explain particle formation by the sol-gel process was developed by LaMer and Dinegar [17] as shown in Figure 1.2. In the case of hydrolysis and condensation of TEOT, LaMer's theory holds that the concentration of hydrolyzed species initially increases rapidly until the critical concentration C_N is reached where nucleation occurs very rapidly. This is followed by formation of very small (2-4 nm) size nuclei which reduces the soluble species concentration below the supersaturation point C_o where further nucleation does not occur. Further particle growth then occurs by the diffusion of the soluble species to and adsorption onto the existing nuclei until the concentration decreases to the equilibrium solubility, C_s. According to this model, it is possible to make monodispersed particles only if a single burst of nucleation is achieved. Prolonged nucleation would lead to highly polydisperse particles. However, this model cannot account for the characteristics of silica particles grown from TEOS. For instance, the model holds that particle growth occurs by the diffusion of molecular species which should result in high density, non-porous, and crystalline

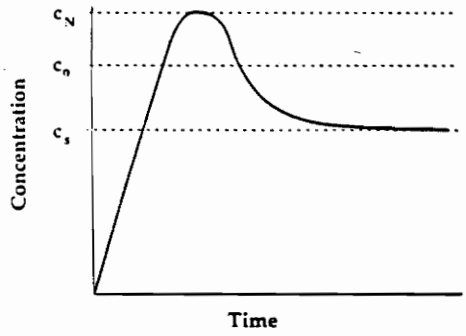

Figure 1.2. Schematic illustration of concentration of precipitating species before and after nucleation. After LaMer and Dinegar [17].

spheres. However, silica particles produced by the Stober processs are porous, amorphous and have relatively low densities [18].

Based on their work on silica synthesized by the Stober process, Zukoski et al. [18] concluded that the classical model by LaMer and Dinegar applied only up to the formation of nuclei and thereafter the particle growth occurred by aggregation of primary particles which resulted in the formation of porous and amorphous powders. Perhaps the most convincing evidence against the LaMer theory of particle growth came from the fact that Zukoski et al. obtained monodisperse silica particles (relative standard deviation $\leq$ 1.1) even though nucleation continued throughout most of the particle formation period. In their later work, Bogush and Zukoski [19] developed a model of particle growth where they assumed that particle growth occurred solely by aggregation with primary particles which were constantly being formed due to the hydrolysis and condensation of the silicon alkoxide. This model linked the morphology of the resulting particles to parameters which governed colloid stability of the growing solid phase. Their model could successfully predict the final particle size over a wide range of reagent concentrations. The success of their model strongly suggests the fact that colloid stability and not the duration of the nucleation period is the key to controlling the size and morphology of the resulting particles.

Colloid Stabilization

Colloid stabilization can be explained by the Deryaguin-Landau-Verwey-Overbeek

(DLVO) theory which predicts the total potential V_T between the approaching particles as a function of distance of surface to surface separation h. A general expression for V_T is given as:

$$V_T = V_A + V_E + V_S \qquad [1]$$

where V_T is the total potential energy, V_A is the Van der Waal's attractive potential, V_E is the electrostatic repulsion potential, and V_S is the steric repulsion potential. Aggregation occurs due to the Van der Waal's attractive potential between the particles. Colloid stabilization can either be electrostatic or steric in nature. Electrostatic repulsion results due to the presence of fixed charges or adsorbed ions at the particle surface. The mobile counterions in solution form an electrical double layer which screens charge repulsion and limits their range. Electrostatic stabilization is sensitive to any changes in pH or electrolyte concentration since the double layer is compressed at high ion concentrations. Steric stabilization results from the adsorption of polymer chains on a particle surface. Repulsive forces between two interpenetrating polymer layers on particles approaching each other. Details of each of these effects are discussed below.

Van der Waal's Attractive Potential V_A

The attractive potential between two spherical particles of material 1 in a liquid medium of material 2 was derived by Hamaker [20] as:

$$V_A = -\frac{A}{12}\left[\frac{1}{x^2+2x} + \frac{1}{x^2+2x+1} + 2\ln\frac{x^2+2x}{x^2+2x+1}\right] \qquad [2]$$

where A is the composite Hamaker constant and is given by :

$$A = (\sqrt{A_{11}} - \sqrt{A_{22}})^2 \qquad [3]$$

where A_{11} is the Hamaker constant of the particle, e.g.TiO_2, and A_{22} is the Hamaker constant of the solvent medium. The interparticle separation is expressed as x = h/2r where r is the particle radius and h is the surface-to-surface separation. The negative sign denotes attraction between particles.

Electrostatic Repulsion Potential $\mathbf{V_E}$

Electrostatic repulsion results from the presence of charged groups on the particle surface. The charges may be fixed, e.g. SiO^-, or adsorbed as low molecular weight ions,

or adsorbed as charged polymer chains, e.g. polyelectrolytes. These surface charges require mobile charges of opposite sign in the solvent phase for electroneutrality. These mobile charges form an electrical double layer which screens the charges and determines the range of electrostatic forces. The range is characterized by the Debye length, κ^{-1} which is defined by:

$$\kappa^{-1} = [\epsilon kT/4\pi I]^{1/2} \qquad [4]$$

where ϵ is the solvent dielectric constant, k is Boltzmann's constant, T is temperature, and I is the ionic strength. In the case for small $r\kappa$, i.e. where the double layer is small compared to the particle size, the energy term V_E is given by:

$$V_E = \frac{\varepsilon r \zeta^2}{(2r+h)} \ln[1+\exp(-Kh)] \qquad [5]$$

where ζ is the zeta potential - the potential at the shear slip plane [21]. This potential can be measured by electrophoresis.

From equations [4] and [5], it is seen that the Debye length κ^{-1} and the energy term V_E depend on the ionic strength. In addition, the term V_E depends on the pH since

the pH determines the sign and magnitude of the fixed charge density. For TiO_2, the pH at which the net surface charge is zero, i.e. the iso-electric point IEP, in water is ~ 6.2. For pH < IEP, the surface has a net positive charge due to the protonation of the surface Ti-OH groups. Hence, electrostatic stabilization is sensitive to changes in pH and electrolyte concentration.

Steric Stabilization

For steric stability to occur, several criteria must be met: (i) the polymer should adsorb so strongly that it does not desorb due to collisions between particles, (ii) the polymer should effectively cover the surface to avoid bridging flocculation (a form of particle aggregation caused due to the adsorption of polymer on the surface of more than particles), (iii) the thickness of the adsorbed layer (steric layer) should be sufficiently thick to overcome the range of attractive Van der Waal's forces, and (iv) the non-adsorbing part of the polymer chain (tails) should be well solvated by the liquid, i.e. $\chi < 0.5$ [22].

Structure of Adsorbed Polymer Layers

Steric repulsion between two particles occurs due to the adsorbed polymer at the surface. The spatial extension of an adsorbed polymer chain depends upon the mode of attachment. If the chains are terminally attached at one end they are referred to as tails. Attachment through two or more points results in loops. Flat adsorption of the chain at

the surface results in the formation of trains. Only the loops and tails contribute to the steric repulsive forces. Tails, trains, and loops are illustrated in Figure 1.3.

Physical adsorption of a polymer chain can be characterized in terms of the polymer-surface interaction parameter χ_s, a dimensionless segmental free energy of adsorption, and the polymer-solvent interaction (Flory-Huggins) parameter χ [23]. When a polymer adsorbs, it loses some entropy due to constraints placed on the segment positions at a surface. In order for adsorption to occur, the enthalpy change must be sufficiently negative (due to hydrogen bond formation, dipole interactions, or electrostatic attraction) to overcome this entropy loss. Physical adsorption is enthalpy-driven. Thus, the segmental adsorption energy χ_s must exceed a certain critical adsorption energy χ_{sc} for adsorption to occur. This critical energy, which can be estimated and measured experimentally, typically has a magnitude on the order of 0.1-1 kT. Values of χ_s for polymers that adsorb by hydrogen bonding can range from 3-5 kT [24]. It has been shown theoretically and experimentally that the amount of adsorbed polymer on a given surface and the fraction of the adsorbed segments in the train conformation increases with χ_s for a fixed value of χ. It has also been shown that, for a fixed value of χ_s, the amount of adsorbed polymer increases as the solvent quality becomes poorer, i.e. for increasing values of χ.

If a homopolymer adsorbs at a surface, i.e. if $\chi_s > \chi_{sc}$, the chain may adsorb in trains, tails, and loops because each adsorbing group along the homopolymer backbone has the tendency to adsorb at the surface. Also, since only a portion of the polymer

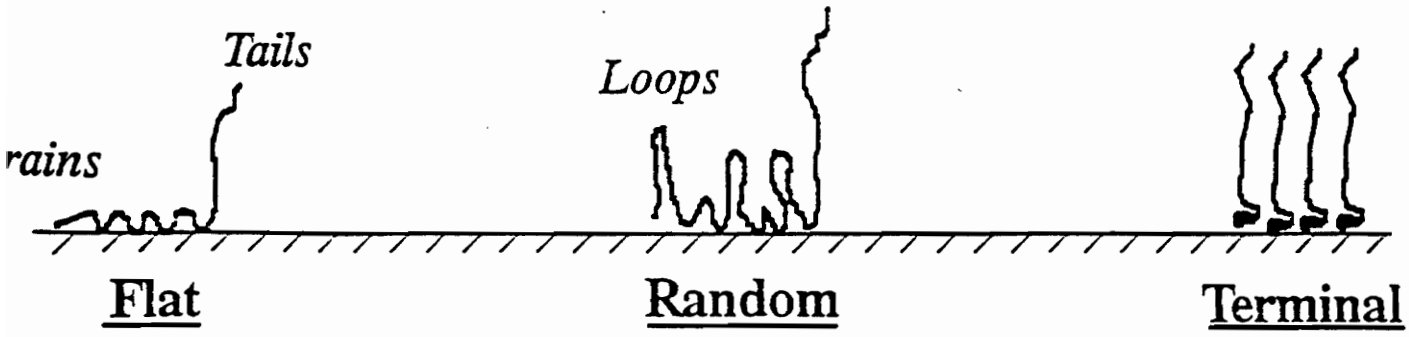

Figure 1.3. Modes of polymer adsorption: Flat adsorption occurs in the form of trains and is characteristic of block copolymer adsorption. Random adsorption occurs in the form of tails, trains, and loops and is characteristic of homopolymer adsorption. Terminal adsorption results if the polymer adsorbs through the chain end and is characteristic of end-functionalized polymer adsorption.

segments are in the tail and loop forms, a relatively high molecular weight of the polymer is required to achieve sufficient steric layer thickness. Nonionic homopolymers are not as efficient stabilizers as are terminally-attached chains or block copolymers.

Tail adsorption is observed in the case of end-functionalized homopolymers which may attach either by physical adsorption or by covalent bonds. Terminal adsorption can result in a very high concentration of adsorbed polymer. This leads to steric repulsion between the tails and ultimately to the extension of tails. This extension is enhanced even further if the polymer segments do not adsorb on the surface, i.e. if $\chi_s < \chi_{sc}$. A relatively thick steric layer is obtained in this mode of adsorption.

Trains and tails are characteristic of block copolymers where the anchor block adsorbs strongly at the surface and the tail block remains in solution. A diblock copolymer optimized for steric stabilization typically has $n_{tail}/n_{anchor} \sim$ 4-10, where n is the degree of polymerization [25, 26]. With these block length ratios, the tail blocks can experience significant chain extension of tails, the adsorbed layer thickness $\delta \propto n_{tail}$ and hence high steric layer thicknesses can be achieved with relatively low molecular weight chains.

Steric Repulsion Potential Energy $\mathbf{V_s}$

In deriving the equation for steric potential it is important to know the segment density distribution in the adsorbed layer. Napper and co-workers [27, 28] gave an expression for two simple segment density distributions: (a) uniform segment distribution

where the segment density in the layer is assumed constant away from the surface, and (b) exponential distribution where the segment density is assumed to decay exponentially away from the surface. These two distributions represent useful bounds - for many cases the segment-density profiles lie between these two. In the case of terminally anchored polymer chains, the uniform segment-density profile is approached whereas, in the case of homopolymers adsorption, the exponential distibution has been suggested as more appropriate.

Fischer [29] derived the expression for steric potential in terms of excess free energy of mixing $_{\Delta}G^{M}$ when the steric layer attached to two spheres overlap in a volume element dV. The excess free energy of mixing is related to the excess osmotic pressure π_E due to chain overlap and can be written as follows:

$$\Delta G^{M}=x\int_{V}\pi_{E}dV \qquad [6]$$

where π_E can be expressed by the virial expansion as:

$$\pi_{E}=RTA_{2}C_{2}^{2}+\ldots \qquad [7]$$

where A_2 is the second virial coefficient. The lens-shaped volume dV representing the overlap of two interpenetrating polymer layers can be expressed as:

$$dV=\frac{2}{3}\pi(\delta-\frac{h}{2})^2(3r+2\delta+\frac{h}{2}) \qquad [8]$$

Combining equations [6], [7] and [8] and assuming a uniform segment density in the adsorbed layer, the steric energy V_S term derived by Fischer can be written as:

$$\frac{V_s}{kT}=\frac{4}{3}\pi A_2 C_i^2(\delta-\frac{h}{2})^2(3r+2\delta+\frac{h}{2}) \qquad [9]$$

where N_{Av} is Avagadro's number, C_i is the polymer concentration in the adsorbed layer in g/cm^3, δ is the steric layer thickness in nm, r is the radius of particle in nm, and h is the surface to surface distance of separation between the particles. Equation [9] is valid only for $h < 2\delta$.

Thermodynamic Treatment of Steric Stability

Steric stabilization can be both enthalpic and entropic in origin [21, 22]. This can be explained using classical thermodynamics. Consider two particles coated with polymer approaching each other due to Brownian motion. The change in their free energy ΔG_F on close approach can be given as:

$$\Delta G_F = \Delta H_F - T\Delta S_F \qquad [10]$$

where ΔG_F is the change in free energy of flocculation (the opposite of stabilization), ΔH_F and ΔS_F are the changes in enthalpy and entropy respectively upon close approach and T is the temperature. For stabilization to occur, ΔG_F should be positive over the appropriate distance of close approach. The various possible combinations of signs and magnitudes of ΔH_F and ΔS_F give rise to steric stabilization.

Steric stabilization is then classified as: enthalpic, entropic, or combined enthalpic-entropic in origin. In enthalpic stabilization, both ΔH_F and ΔS_F are positive so that the enthalpy change on close approach of the particles promotes stabilization, whereas the corresponding entropy change promotes flocculation. Their relative contributions to ΔG_F are such that the enthalpic contribution dominates. Enthalpic stabilization is characterized by flocculation on heating since on raising the temperature $T\Delta S_F$ increases and overcomes ΔH_F in magnitude so that ΔG_F becomes negative. Hence, colloidal suspensions which flocculate on heating are enthalpically stabilized.

By contrast, entropic stabilization occurs when both ΔH_F and ΔS_F are negative so that enthalpy of close approach promotes flocculation but the entropy term opposes it. In this case, their relative contributions to ΔG_F are such that the entropic term dominates. This is characterized by flocculation on cooling.

In the case of combined enthalpic-entropic stabilization, ΔH_F is positive and ΔS_F is negative and both contribute towards steric stabilization. Here, the suspension cannot be flocculated by temperature changes. However, sufficiently large temperature changes may change the signs of either ΔH_F or ΔS_F so that the mode of stabilization becomes either enthalpic or entropic and then temperature changes can cause flocculation.

Criteria for Colloid Stabilization

Figure 1.4 is the plot of V_T versus the distance of separation h between the particles [21b]. Positive values of the potential energy V_T represent net repulsion between particles. Colloid stability is characterized by the stability ratio W which measures the effectiveness of the potential barrier in preventing particles from flocculating [21a]. W is defined as the ratio (number of collisions between particles/number of collisions that result in flocculation) and is related to V_T by:

$$W=2r\int_0^{\infty}\frac{\exp(V_T/kT)dh}{(h+2r)^2} \qquad [11]$$

In the absence of an energy barrier, i.e., $V_T = 0$, W = 1 and rapid agglomeration is obtained. For the primary maximum $V_{max} = 15$ kT, W is of the order of 10^5 and for $V_{max} = 25$kT, W is about 10^9 which gives a suspension that is stable on the order of several months.

Another important feature of this potential energy diagram in Figure 1.4 is the presence of an attractive secondary minimum well which leads to flocculation when the particles begin to approach each other. If the depth of the well is between 1-2 kT then the flocculation is reversible and the particles can be easily redispersed by mechanical agitation or stirring. The primary minimum well is typically deeper than the secondary minimum and hence particle aggregation in primary minimum is nearly irreversible.

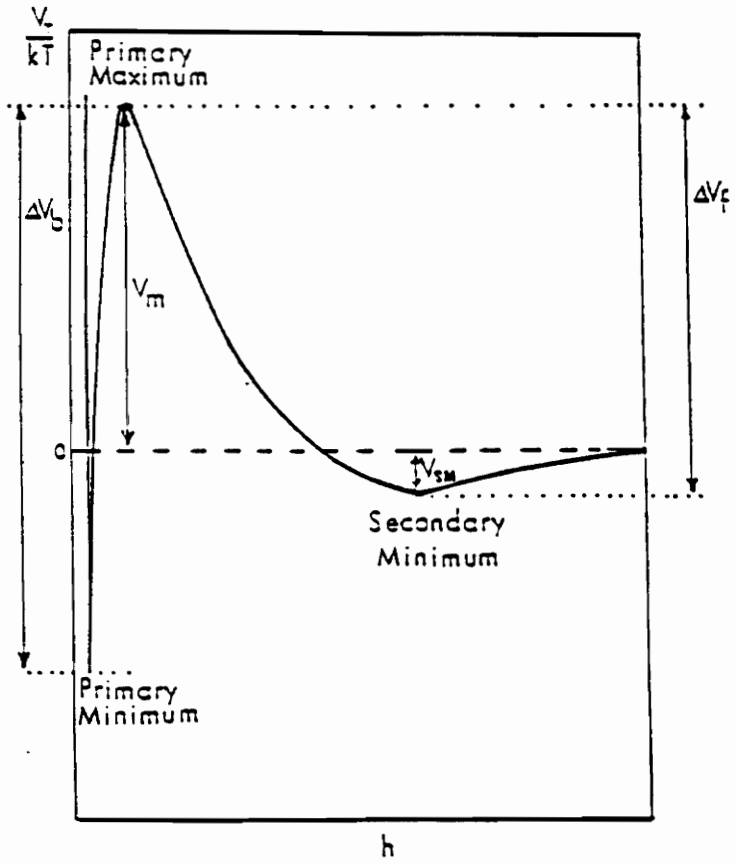

Figure 1.4. Schematic illustration of total potential energy V_T versus distance of seperation h between a pair of approaching particles with radius r. From reference [21b].

Conditions Relevant to This Work

When electrostatic effects can be assumed to be negligible as is the case in this work, the total potential can be written as:

$$V_T = V_A + V_S \qquad [12]$$

For a given particle size r, V_A is constant for a given system and is negative. The total potential V_T can then be increased and made positive by increasing the steric potential V_S such that $V_{max} > 15$ kT. Hence, it becomes critical to identify factors which affect V_S.

In-Situ Steric Stabilization

In the case of in-situ steric stabilization, particle growth by aggregation and condensation of soluble Ti-containing species occurs in the presence of a polymer which adsorbs onto the growing particle and forms a steric layer. The amount of polymer adsorbed and steric layer thickness should be enough to generate a sufficiently large value of V_S to inhibit further particle growth. The diffusion of polymer to the particle surface competes with the diffusion of condensing species as well as with particle diffusion and aggregation. It is reasonable that smaller final TiO_2 particles result the earlier that a sufficiently thick steric layer of HPC can be established. Thus, the relative kinetics of particle growth and polymer adsorption determine the ultimate size of the

particles.

The parameters which govern steric potential between particles of given size r are seen from equation [9] to be the second virial coefficient A_2, the polymer concentration in the adsorbed layer C_i, and the steric layer thickness δ. Solution paramters which affect these parameters are summarized as follows:

(a) Polymer solubility: V_s increases linearly with A_2. Also, an increase in A_2 leads to an increase in δ due to chain swelling. Finally, an increase in A_2 (decreasing χ) leads to an decrease in the amount of adsorbed polymer [23]. Therefore the effect of solvent on the polymer solution thermodynamics plays a crucial role in determining steric stability.

(b) Polymer molecular weight: An increase in molecular weight increases δ and the amount of polymer adsorbed at equilibrium [23]. However, increasing molecular weight may slow polymer adsorption relative to particle growth so that stabilization becomes poorer.

(c) Polymer-particle surface interactions: The segmental adsorption energy $\chi_s kT$ determines, along with the χ parameter, the polymer conformation at the surface, i.e. trains, tails, and loops as shown in Figure 1.3. All three conformations are typical of homopolymer adsorption. Since only a fraction of these segments are in the tail and loop forms, a relatively high molecular weight of the homopolymer is required to get a sufficiently thick steric layer to produce steric stabilization.

A di-block copolymer optimized for steric stabilization typically consists of a relatively short adsorbing anchor block and a longer non-adsorbing block tail block that

should be well solvated. If the anchor block is short compared to the tail block, then close packing of the polymer occurs at the surface which leads repulsion between tail blocks. Hence the chains tend to extend in solution, leading to relatively high values of the steric layer thickness δ for relatively low molecular weights.

If the polymer chain has adsorbing groups on one or both chain ends and adsorption occurs only at those ends, then the chain is terminally adsorbed. Terminal adsorption also leads to chain extension. Thus, for both block copolymers and terminally attached polymers, it is possible to achieve steric stability with relatively lower molecular weights than for physically adsorbed homopolymers. In addition, low molecular weight polymers (Mw $<$ 10 kg/mole) generally have higher solubilities than their higher molecular weight homologues. Hence low molecular weight steric stabilizers can be used in a variety of solvents and therefore have wider applications. In addition, low molecular weight polymers do not affect the suspension viscosity significantly which leads to easier processing.

Thesis Research Goals

Titanium dioxide particles were synthesized via a sol-gel process using in-situ steric stabilization to limit particle size. The hydrolysis and condensation of titanium tetraethoxide (TEOT) in ethanol was studied as a model system. The findings of this research are expected to provide guidance to study other transition metal-alkoxide systems. Interactions between polymer, solvent, TEOT, and TiO_2 were studied to

determine the roles they played in controlling particle size and morphology. Finally, applications for the synthesized ultra-fine particles were explored. Hence, the principal goals of this doctoral research can be stated as:

1. Explore novel synthetic routes to the formation of ultra-fine TiO_2 particles using soluble polymers as in-situ steric stabilizers.

2. Investigate the applications of the ultra-fine TiO_2 particles made by in-situ stabilization.

These goals are described in more detail below.

Goal 1 In order to fulfill the first objective, the following studies were undertaken:

Effect of Solvent Composition on Particle Formation

(a) Elucidate polymer/solvent/particle interactions where the solvent composition is varied by the addition of water, a reactant.

(b) Elucidate polymer/solvent/particle interactions where the solvent composition is varied by the addition of an inert diluent tetrahydrofuran THF which nonetheless affects the hydrogen bonding behavior of the reacting species. The polymer used in (a) and (b) was hydroxypropylcellulose, HPC.

Effect of Polymer Structure on Particle Formation

(c) Study the effect of polymer structure on the final particle size and morphology of TiO_2 particles. In (a) and (b) the polymer used was homopolymer HPC which adsorbs in the form of loops, trains and tails. End-functionalized polymer attaches terminally at the particle surface which leads to a high polymer concentration in the adsorbed layer C_i and presumably to chain extension. These two conditions can, in principle, lead to steric stabilization with a low molecular weight polymer. In-situ steric stability was studied when the polymer was terminally attached. For this purpose, poly(propylene oxide) was end-functionalized to make it suitable for steric stabilization.

Goal 2 In order to fulfill the second objective, the functional properties of ultra-fine TiO_2 particles were investigated. For this purpose, thin titania/HPC composite films were fabricated by spin coating and then characterized. By controlling the reaction conditions, it was possible to synthesize TiO_2 particles less than 50 nm in diameter suitable for making thin films. A relatively inexpensive and simple process was developed to make thin ceramic films. The films were characterized for thickness, refractive index, uniformity, crystallinity, transparency, and ultra-violet barrier properties. These films can find applications in areas of coatings, nano-composites, catalysts, membranes, polymer-ceramic composites, and in the fabrication of narrow band-pass optical filters.

Thesis Organization

Chapters 2 to 6 are written in a manuscript format. Each chapter has its own introduction and literature review, experimental procedure, results and discussions, conclusions, and references.

Chapter 2 concerns the synthesis and characterization of TiO_2 particles synthesized in the presence of homopolymer hydroxypropylcellulose (HPC). Effects of HPC concentration, molecular weight, and water concentration on particle size and morphology are discussed. The water concentration in the reaction medium had a profound effect on the particle size. By carefully controlling the polymer and water concentrations, TiO_2 particles having mean sizes of 0.07 microns were synthesized.

In the work discussed in Chapter 2 the liquid phase composition was changed with the addition of water which was one of the reactants. The purpose of the work in **Chapter 3** was to study particle formation when the liquid phase composition was affected by the addition of the inert diluent tetrahydrofuran THF but did affect the hydrolysis and condensation reactions by changing the hydrogen bonding behaviour of the reacting species. The effects of THF concentration on the particle size and growth rate were studied at fixed concentrations of TEOT, water, and HPC.

Work mentioned in Chapters 2 and 3 involved the use of the homopolymer HPC as an in-situ steric stabilizer. As discussed in the earlier section, homopolymers adsorb randomly and hence a relatively high molecular weight polymer is required to achieve steric stability. The purpose of work described in **Chapter 4** was to end-functionalize

poly(propylene oxide) based on a low molecular weight polymer, Jeffamine D2000, so that it could adsorb terminally and impart in-situ steric stability to the growing TiO_2 particles. In this chapter, the end-capping reaction chemistry is discussed along with its performance as an in-situ steric stabilizer.

If one end of a di-block copolymer can adsorb strongly at the particle surface then it can serve as an effective steric stabilizer. The diblock of poly(2-ethyl-2-oxazoline)-b-poly(dimethylsiloxane) was originally studied as an in-situ steric stabilizer for the synthesis of TiO_2 particles via the hydrolysis and condensation of titanium isopropoxide in isopropanol. However, it was found that this copolymer formed micelles in water-isopropanol mixtures and hence was not suitable for steric stabilization. Thus, **Chapter 5** focuses on a study of micelle formation as a function of water-isopropanol mixtures was studied by dynamic light scattering for two diblock copolymers with block molecular weights ranging from 8-20 kg/mole for PEOX and 2-5 kg/mole for PDMS.

Chapter 6 discusses the fabrication and characterization of thin titania/HPC films. Thin films on quartz and silicon wafers were formed by spin casting. These films were characterized for their optical properties and uniformity. Heating temperature affected the film transparency, refractive index, and crystallinity. Some suggested future work is discussed in **Chapter 7**.

References

1. J. Livage, MRS Bulletin, 15(1) (1990) 18.

2. E. Matijevic, MRS Bulletin, XIV(12) (1989) 18.

3. B.E. Yoldas, Applied Optics, 23 (1984) 1418-1424.

4. H. Dislich and E. Hussman, Thin Solid Films, 77 (1981) 129.

5. E. Barringer, N. Jubb, B. Fegley, R.L. Pober, and H.K. Bowen in Ultrastructure Processing of Glasses, Ceramics, and Composites, eds., L.L. Hench, and D.R. Ulrich, Wiley, New York, 1984, p. 315.

6. E. Matijevic and P. Gherardi, Transformation of Organometallics into Common and Exotic Materials: Design and Activation, NATO ASI series E, no. 141, ed. R.M. Laine (Martinus Nijhoff, Dordrecht, 1988), p.279.

7. Sol-Gel Science: The Physics and Chemistry of Sol-Gel Processing, Academic Press, CA, 1990.

8. J. Livage, M. Henry, and C.Sanchez, Prog. Solid St. Chem. 18, (1988) p.259.

9. W. Stober, A. Fink, and E. Bohn, J. Colloid and Interface Sci., 26 (1968) 62.

10. G. Orcel and L. Hench, J. Non-Cryst. Solids, 79 (1986) 177.

11. G. Winter, Oil and Colour Chemist's Association, 34 (1953) 30.

12. M.F. Bechtold, R.D. Vest, and L. Plambeck, J. Am. Chem. Soc., 90 (1968) 4590.

13. B.J. Ingebrethsen and E. Matijevic, J. Colloid Interface Sci., 100 (1984) 1.

14. J-L Look, and C.F. Zukoski, Faraday Discuss. Chem. Soc., 90 (1990) 345.

15. J.H. Jean and T.A. Ring, Colloids and Surfaces, 29 (1988) 273.

16. B.D. Kay and R.A. Assink, J. Non-Crystalline Solids, 104 (1988) 112.

17. V.K. LaMer and R.H. Dinegar, J. Am. Chem. Soc., 72(11) (1950) 4847-4854.

18. G.H. Bogush and C.F. Zukoski in Ultrastructure Processing of Advanced Ceramics, eds. J.D. Mackenzie and D.R. Ulrich (Wiley, New York, 1988, p.477-486. 19. J. Colloid Interface Sci., 142, (1991) p.1 and ibid p.19.

20. C.H. Hamaker, Physica, 4 (1937) 1058.

21. (a) Foundations of colloid Science, Volume 1, edited by R.J. Hunter, Oxford Science Publications, 1987. (b) R. Buscall, et al., in 'Polymer Colloids' eds. R. Buscall et al., Elsevier Applied Science Publishers, London, Chapter 5 (1985).

22. Polymeric Stabilization of Colloidal Dispersions, D.H. Napper, Academic Press, 1983.

23. M.A. Cohen Stuart, G.J. Fleer, and J.M.H.M. Scheutjens, Journal of Colloid Interface Science, 97 (9184) 515.

24. C. Chen, and R.M. Davis , "Measurements of the Segmented Adsorption Energy of PEOX on Silica in Water and Ethanol, submitted to Macromolecules.

25. C.M. Marques and J.R. Joanny, Macromolecules, 21 (1988) 1454.

26. D. Guzonas, D. Boils, and M. Hair, Macromolecules, 24 (1991) 3383.

27. D.H. Napper, in Colloid dispersions, J.W. Goodwin (ed.), The Royal Society of Chemistry, London (1982) p. 99-128.

28. J.B. Smitham, and D.H. Napper, Colloid and Polymer Sci., 257 (1979) 748.

29. E.W. Fischer, Kolloid-Z, 160 (1958) 120.

Chapter 2

In-Situ Steric Stabilization of Titanium Dioxide Particles Synthesized by a Sol-Gel Process

Introduction

The synthesis and processing of fine ceramic particles less than 100 nm in diameter has received considerable attention in recent years due to their novel optical, electronic, and densification properties [1-3]. Applications of particles in this size range include (i) ceramics with densities approaching the theoretical maximum, resulting in superior mechanical properties, (ii) ceramic composites with heterogeneities controlled at the $\approx$10-50 nm length scale, and (iii) grain boundary engineered capacitors. Techniques for making ultra-fine metal oxide particles include vapor phase pyrolysis [4], liquid phase hydrolysis of metal salts [5], and the hydrolysis and condensation of metal alkoxides [6,7]. In liquid phase processes, the final particle size distribution and morphology is a function of the interparticle forces that govern colloid stabilization. In particular, liquid phase reactions of metal alkoxides have been used to produce fine particles of a variety of metal oxides [8-12]. Previous studies have focussed on how particle growth and the final size distribution is affected by interparticle forces generated by electrostatic, hydrodynamic, and

polymer-induced steric stabilization effects. TiO_2 was chosen for the present study because some aspects of the formation and properties of titanium dioxide particles from alkoxide reactions have already been studied by various groups [13-25] and because it is a metal oxide used extensively in coatings and ceramics [26,27]. This paper focuses on the formation of discrete titanium dioxide particles from the hydrolysis and condensation of tetraethylorthotitanate, TEOT, in the presence of a polymeric steric stabilizer, hydroxypropylcellulose, HPC, that is soluble in the reaction medium.

The outline of this paper is as follows. After a brief review of particle growth mechanisms in reacting alkoxide solutions, the experimental procedures will be described. The results are then presented with a focus on the effect of solvent composition on polymer-particle interactions and the role these interactions play in determining particle size and morphology.

Particle Formation Mechanisms

The TiO_2 particles are made from the step-wise hydrolysis and condensation reactions of titanium alkoxide precursors which are written in abbreviated form as [4]:

$$Ti(OC_2H_5)_4 + 4H_2O \rightarrow Ti(OH)_4 + 4C_2H_5OH \text{ ..... Hydrolysis}$$

$$Ti(OH)_4 \rightarrow TiO_2 \cdot xH_2O + (2 - x)H_2O \text{ ..... Condensation}$$

In the first reaction, titanium ethoxide hydrolyzes in a step-wise manner and, in the subsequent step-wise condensation reaction, forms discrete particles of TiO_2. The ratio of water molarity to alkoxide molarity is defined as $R = [H_2O]/[TEOT]$ and is a crucial parameter that controls the hydrolysis reaction kinetics and the resulting metal oxide morphology. For $R > 2.5$, discrete particles are obtained whereas polymeric gels and fibers are obtained for $R < 2.5$ [13]. All of the present work was done in the range $5.3 \leq R \leq 60$.

Bowen and Barringer first demonstrated that it was possible to form submicron TiO_2 particles with relatively narrow size distributions via sol-gel chemistry [13,14]. The aggregate size was of the order of 3-4 microns when the hydrolysis and condensation reactions were carried out in the absence of any added acid or base catalysts. The large agglomerates could be broken by ultrasonication and stabilized electrostatically in water at $pH = 9.5$. This procedure yielded spherical TiO_2 particles having an average diameter of 0.5 micron.

Work by Harris and Byers revealed that the step-wise hydrolysis reactions up to the hydrolysis of the third ethoxide group was much faster than the condensation rate, leading to relatively rapid conversion of TEOT to the partially hydrolyzed species $(TiOC_2H_5)(OH)_3$ which then condensed to form TiO_2 particles [23]. Later work by Zukoski and co-workers [15-17] showed that under a variety of conditions of water, acid, and electrolyte concentrations, elevated supersaturation levels of soluble titanium species persisted for extended periods of time during the particle growth and

that the rate limiting step was the condensation reaction. This resulted in prolonged nucleation with nuclei sizes estimated to be $\approx$ 2-6 nm. Particle growth occurred by the aggregation of nuclei formed initially as well as by aggregation at later stages of larger, older particles with nuclei formed later in the growth process. This work showed clearly that the growth process was governed by colloidal stability effects which could be explained in terms of the pair interaction energy given by the DLVO theory. Ionic strength, pH, and the scaled water concentration "R" were manipulated to control the height of the primary maximum and the location and magnitude of secondary minima. A short-range repulsive hydration force was included with electrostatic and Van der Waals forces in calculating the interaction energy to account for the effect of solvent conditions and shear rate on aggregate size and morphology. Secondary minima in the interaction energy curves correlated well with the formation of aggregates consisting of smaller particles 5-20 nm in size that initially flocculated into the minima and were then welded together by the condensation of reactive monomer or oligomeric species [17]. The presence of reactive oligomeric species is supported by fast-freeze cryogenic transmission electron microscopy studies by MecCartney et al. [25] which showed the formation of very small oligomeric polymer species which subsequently collapsed and condensed to form TiO_2 particles. Average final particle sizes ranged between 0.15-0.7 microns depending upon the growth conditions with a relative standard deviation of about 12%. In the absence of any electrolyte, aggregates of the size of about 1.5 micron were obtained.

Ring and coworkers showed that significant particle size reduction could be achieved when the hydrolysis and condensation reactions occur in a solution of hydroxpropyl cellulose (HPC) polymer [18-20]. HPC acts as a steric stabilizer by adsorbing onto TiO_2 particles as they nucleate and aggregate, thus limiting the final size of the TiO_2 aggregates. The structure of HPC shown below in Figure 2.1(a) consists of a cellulose backbone with an average of three hydroxypropyl groups substituted per anhydroglucose unit. The hydroxypropyl groups make HPC soluble in water and ethanol due principally to hydrogen bonding. The adsorption of a steric stabilizer such as HPC increases the magnitude of the primary maximum V_{max} of the pair interaction energy curve.

The TiO_2 particle size decreased with increasing polymer concentration up to $C_p = 1.7$ g l^{-1} beyond which no appreciable decrease in particle size was observed [19,20]. This was attributed to near or complete particle surface coverage by HPC. Adsorption isotherms established that HPC was indeed adsorbing onto the TiO_2. However, the effect of water concentration, or "R", on adsorption was not studied. Average particle sizes as small as 0.3 micron with a relative standard deviation of about 10 % were obtained as determined by TEM for typical growth conditions of [TEOT] = 0.075 M, $[H_2O] = 0.5$ M and $C_p = 1.7$ g l^{-1}. The presence of polymer did not affect the extent of conversion of TEOT and it was concluded that HPC acted only as a stabilizer and did not participate in the reactions. In all of these experiments, the water concentrations were in the range $5 \leq R \leq 12$.

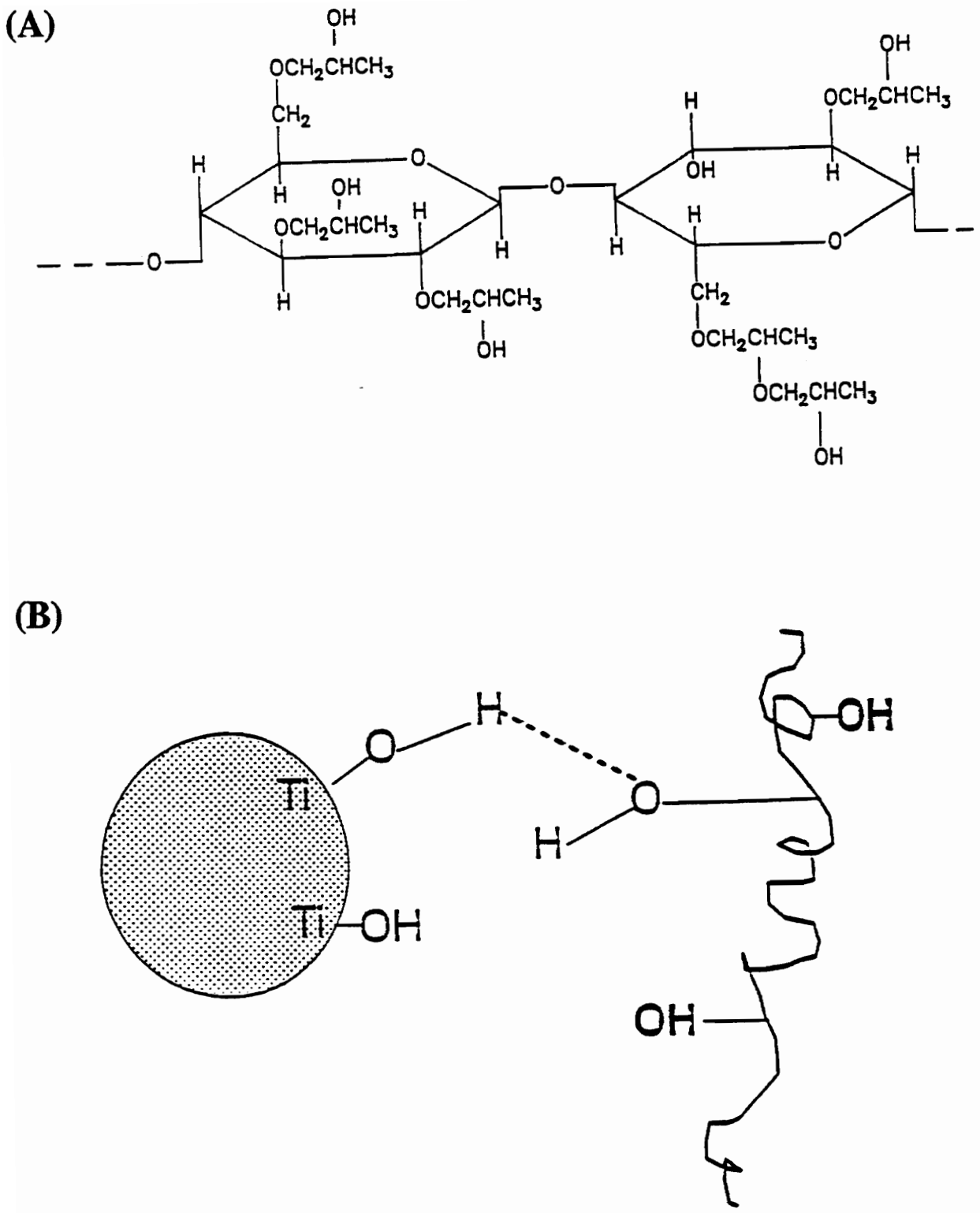

Figure 2.1. (A) Two monomer units of Hydroxypropylcellulose, HPC (B) Hydrogen bonding mechanism between the hydroxyl groups on the polymer and the TiO_2 surface.

The HPC molecular weight in the range 60-300 kg $mole^{-1}$ did not have any significant effect on the particle size. It was concluded that particle growth occurred by the classical nucleation mechanism proposed by La Mer, i.e. nucleation occurred early in the particle growth step and ceased once supersaturation was relieved. Particle growth then occurred by the deposition of oligomeric TiO_2 species onto the nuclei. However, the diffusion coefficients derived by fitting particle growth rate data to this model were 2-3 orders of magnitude larger than that expected for the oligomeric species.

These studies of in-situ steric and electrostatic stabilization of TiO_2 demonstrate the crucial role that colloid interactions play in governing particle size distribution and growth rate. For steric stabilization, it is important to understand the underlying effects of solvent composition, polymer structure, molecular weight, and concentration on the polymer-particle interactions. A general goal of this research is to learn what chemical and architectural features are necessary for a polymer to effectively adsorb onto and stabilize metal oxide particles derived from alkoxides. A specific focus of this work is the role that solvent composition, specifically water concentration, plays in controlling polymer adsorption since this and its subsequent effects on electrophoretic mobility have not been reported previously. In addition, this study reports sizes of particles grown over a much broader range of water concentration and HPC molecular weight than previously reported.

Experimental Procedure

Materials

Titanium ethoxide (95 weight % TEOT, 5% ethanol) was obtained from the Alfa Chemical Company and was used as received. Anhydrous ethanol, 200 proof, was obtained from the Aaper Alcohol and Chemical Company. Samples of hydroxypropylcellulose, HPC, were kindly donated by the Aqualon Company, a subsidiary of Hercules, Inc. The nominal molecular weights used in this study were 60 kg $mole^{-1}$ (lot # 6684) and 1150 kg $mole^{-1}$ (lot # 4899) with the designated grades E and H, respectively. The molecular weight of the HPC E polymer was analyzed with a gel permeation chromatograph equipped with a VISKOTEK™ intrinsic viscosity detector which measured the absolute molecular weight distribution [28]. The stationary phase was MicroStyragel HT (crosslinked polystyrene from Waters, Inc.) and the mobile phase was N-methylpyrrolidinone (HPLC grade) containing 0.5 weight % LiBr. The analysis was done at 60°C, giving the following: M_n = 40 kg $mole^{-1}$, M_w = 68.5 $kgmole^{-1}$, $[\eta]$ = 82 cm^3/g. The HPC H sample apparently formed gel particles in the mobile phase and thus could not be analyzed accurately.

Elemental analysis revealed that both HPC samples contained 28 ppm of silica powder having a particle diameter range of 10-30 nm which was added as an anti-caking agent [29]. The amount of silica in both polymer samples was determined by Inductively Coupled Plasma Spectrometry (ICP) (Jarrell-Ash Atomscan 2400) on

aqueous HPC solutions with polymer concentration $C_p = 1.7$ g l^{-1} that had been filtered through 0.2 micron filters. The instrument was first calibrated for silicon with a Spex Plasma Standard PLS19-2X and the silicon was detected at a wavelength of 251.6 nm. The detection limit of this instrument ranges from 0.01 to 3000 ppm for silicon. The possibility of silica particles acting as heterogenous nucleating agents during TiO_2 particle growth is examined and dismissed as discussed below in the section on growth rate.

The HPC samples were dried in a vacuum oven at room temperature for about 4 hours and then at 100°C for about 20 hours prior to their use in the TiO_2 particle growth experiments. Homogeneous, gel-free stock solutions of HPC in anhydrous ethanol were prepared with typical concentrations of 2 g HPC E/100 ml ethanol and 0.5 g HPC H/100 ml ethanol by stirring at room temperature for twenty four hours. Deionized water with a resistivity of 16-18 x 10^6 ohm-cm was used in all of the experiments. Fisher-certified 50% hydrogen peroxide and concentrated sulfuric acid ($\sim$ 36 N) were obtained from Fisher Scientific and were used as received as part of a spectrophotometric assay for HPC. All glassware was cleaned first with a detergent and then soaked in a saturated solution of alcoholic KOH for 24 hours followed by soaking in 2M HCl solution for another 24 hours. This was followed by washing thoroughly with tap water and finally washed 4 times with deionized water. The glassware was then dried in air in a laminar flow hood for at least two days before being used for experiments.

Mixing Procedures

For particle synthesis, equal volumes of solutions of TEOT in ethanol, denoted as solution A, and a solution of HPC in ethanol and water, denoted as solution B, were mixed rapidly and shaken for 5 seconds and were then allowed to sit quiescently for 24 hours before the particles were analyzed. Solution A consisted typically of a 5 ml mixture of titanium ethoxide and anhydrous ethanol mixed in a nitrogen glove bag to prevent early hydrolysis of the ethoxide by atmospheric moisture. Solution B consisted typically of a mixture of an HPC stock solution and water. Both solutions were filtered with a 0.2 micron Gelman filter. The 5-second mixing procedure was followed for all of the results reported in this paper after it was found that slow stirring of the reacting solutions with HPC for 24 hours resulted in relatively aggregated TiO_2 particles. This is consistent with the shear-induced aggregation reported earlier by Look and Zukoski [16]. The water concentrations in these experiments were R(=$[H_20]$/[TEOT]) = 5.3, 13, 30, and 60. All particle growth experiments were performed at a fixed initial titanium ethoxide concentration of 0.075 M. Prior to making stock solutions and samples, all glassware was purged 4 or 5 times with dry nitrogen in a glove bag.

Dynamic Light Scattering

The effect of solvent composition on the hydrodynamic diameter of HPC was measured to determine the qualitative effect of solvent composition on the solubility of

HPC. The hydrodynamic diameter, D_h, was measured with a Brookhaven model 2030AT variable angle dynamic light scattering machine equipped with a digital correlator with 136 channels and a Lexel 95-2 argon ion laser operated at a wavelength of 514.5 nm. Measurements were made at a scattering angle of 90 and a temperature of 25.0 $\pm$ .1°C. The hydrodynamic diameters were calculated using the second cumulants method described elsewhere [30]. The measurements were conducted in ethanolic solutions of HPC H, $M_w \approx 1150$ kg mole^{-1}, at a fixed HPC concentration of $C_p = 1.7$ g l^{-1} and for water mole fraction X_w in the range $0.1 \leq X_w \leq 0.12$, which corresponded to $5.3 \leq R \leq 60$. The hydrodynamic diameter of HPC H was also measured in pure water. The TiO_2 particle growth rate was measured by dynamic light scattering at [TEOT] = 0.04 M and R = 6.2 as a function of HPC concentrations. Further details are given below in the Results section.

Extent of Conversion of TEOT

The extent of conversion of the TEOT after 24 hours was determined by measuring the amount of soluble titanium species in solution by a spectrophotometric method using hydrogen peroxide [31]. Titanium ions form a yellow complex with hydrogen peroxide $[TiO.H_2O_2]^{2+}$ which can be detected by spectrophotometry at a wavelength of 410 nm.

TiO_2 Particle Characterization

Particle Size Measurements

TiO_2 particle sizes were determined by transmission electron microscopy (TEM) with a Philip 420T Scanning Transmission Electron Microscope which was interfaced with a Tracor Northern Model 5500 image analyzer. Particle sizes from the TEM micrographs were determined with an image size analyzer by counting at least 100 particles to obtain a mean number particle diameter as well as a standard deviation for the particle size distribution. Particle surface morphology was studied with a scanning electron microscope.

Degree of Crystallinity

TiO_2 particles were grown with and without the polymer HPC at R = 5.3 and 60. The reaction mixture was centrifuged and the precipitate was dried at 100°C to obtain a dry powder. The dry powder was then analyzed for crystallinity by X-ray diffraction using a Nicolet I2/V 2000 Transmission Wide Angle X-Ray diffractometer using CuK_α radiation. Samples were scanned through 2θ values of 3° to 60° at 0.05° increments at a dwell time of 10 seconds.

HPC-TiO_2-Solvent Interactions

The effect of solvent composition on the interaction of HPC with TiO_2 was characterized by measuring the adsorption isotherms of the two HPC samples on TiO_2

particles and by measuring the electrophoretic mobility of the particles as a function of solvent composition, molecular weight, and polymer concentration. The interaction of water with TiO_2 was characterized by studying water segregation on and in TiO_2 particles by Karl-Fischer titrations and by electrophoresis. The solvent composition was controlled by varying the mole fraction of water X_w in ethanol/water mixtures corresponding to $0.01 \leq X_w \leq 0.12$ or $5.3 \leq R \leq 60$.

To perform these experiments, a large batch of TiO_2 was synthesized in the absence of HPC at $R = 5.3$. Over 24 hours, TiO_2 precipitated and settled at the bottom of the container. The supernatant was then decanted and a large excess of fresh anhydrous ethanol was added to the precipitate, shaken vigorously for few minutes, and allowed to sit for twenty four hours after which the supernatant was decanted and fresh ethanol added. The ethanol washing step was repeated 3 times after which a concentrated slurry of 18 wt % TiO_2 was obtained and used for adsorption experiments. This procedure of using TiO_2 as a wet precipitate was preferred over using dry TiO_2 powder since wet TiO_2 precipitate was more easily redispersed into a solvent and since drying would alter the TiO_2's microstructure by changing the pore sizes and may alter the surface chemistry. Before carrying out any experiments, the TiO_2 slurry was sonicated for five minutes to break any agglomerates that may have formed.

HPC Adsorption Isotherms

The effect of water concentration on the polymer adsorption was studied at two extreme concentrations, C_p = 0.24 g l^{-1} and C_p = 1.7 g l^{-1}, corresponding to partial and complete coverage of TiO_2 particles as determined from the particle growth experiments. A measured mass of polymer solution was mixed with the ethanolic suspensions of TiO_2 particles grown in the absence of HPC along with water so that the water concentrations R = 5.3-60. The TiO_2 concentration was typically 10 wt%. The mixtures were agitated at room temperature for 24 hours on a wrist-action shaker. The samples were then centrifuged at 16,000 g-force for 20 minutes and the clear supernatant was filtered through a 0.45 micron Acrodisc™ filter. The supernatants were diluted further with the ethanol/water mixtures corresponding to their respective values of R. The concentration of HPC in solution was measured with a standard colorimetry assay for cellulose involving phenol and H_2SO_4 [19] which forms a colored complex that was measured with an Hitachi U-2000 UV/VIS Spectrophotometer at a wavelength of 486 nm. At least three repeats were made for each point on the absorption isotherm curves.

Washing experiments demonstrated that HPC continued to desorb from particles grown with HPC even after repeated washing with anhydrous ethanol over a period of one week. Thus it was not possible to determine precisely the amount of HPC that was included in the TiO_2 particles. For the same reason, carbon analyses were not performed on the dried particles.

Water Segregation on TiO_2

The affinity of water for TiO_2 was measured by Karl-Fischer titration. Segregation in the particle pores and on the particle surface is believed to occur due to stronger hydrogen bonding between H_2O and TiO_2 than between ethanol and TiO_2. Suspensions consisting of $\approx$10 wt% TiO_2 were equilibrated at various concentrations of water. The samples were stored in glass bottles sealed with rubber septa to prevent water adsorption from the atmosphere. After agitation on the wrist-action shaker for 24 hours followed by centrifugation at 16,000 g-force for 20 minutes, the supernatant was removed from the septum-covered flask with a syringe and was filtered through a 0.2 micron filter in a septum covered glass vial which was first purged with dry nitrogen. Three water titrations were done for each sample with a Fisher Model 447 Karl-Fischer titrater.

Electrophoretic Mobility Measurements

Electrophoretic mobilities of the TiO_2 particles were measured as a function of water concentration and polymer concentration to determine the effects of electrostatic forces on particle growth. Electrophoresis measurements were made on the same suspensions used in the HPC adsorption experiments as well as on particles grown in the presence of HPC E using a Pen Kem Laser Zee Model 1500 instrument. Dilute TiO_2 suspensions were prepared by centrifuging the 10 wt% TiO_2 suspensions that had been equilibrated with HPC E at 16,000 g-force for 20 minutes. A drop of

original sample suspension was added to the resulting supernatant (mother liquor) giving a slightly turbid suspension. All of the electrophoresis measurements were made at 23.5°C. Conductivity was measured with a YSI model 32 conductance meter (Yellow Spring Instrument Co.) and pH was measured with an Orion SA 720 pH meter.

Results and Discussion

HPC Solution Properties

The solution properties of HPC affect the interactions of HPC with TiO_2 during particle growth and thus must be characterized. Table 2.1 summarizes the relevant structural parameters for HPC. The conformation of HPC in solution can be estimated with the wormlike chain theory in which the chain consists of N_k statistical segments, each with the length L_k known as the Kuhn length [32]. A polymer chain with degree of polymerization DP and monomer length L_{mon} has a contour length $L_c = DP \cdot L_{mon} = N_k \cdot L_k$. The Kuhn length L_k is the length along the backbone over which the backbone acts effectively as a stiff unit. A reasonable estimate of L_k for HPC is the Kuhn length for carboxymethylcellulose, a related cellulose derivative for which L_k = 10.8 nm [33]. This gives good agreement between the measured and calculated hydrodynamic diameter for HPC H in ethanol as shown in Table 2.1.

Table 2.1 - Structural Parameters for Hydroxypropylcellulose, HPC

Sample	M_w[a] kg mole^{-1}	DP[b]	L_c[c],nm	N_k[d]	R_{go}[e], nm	D_h[f],nm
HPC E	68.5	200	103	10	14	19
HPC H	≈1150	3340	1700	160	56	74

Monomer molecular weight = 0.344 kg mole^{-1}

HPC Kuhn length $L_k \approx$ 10.8 nm (from value for L_k for carboxymethylcellulose, from [33])
Monomer length L_{mon} = 0.515 nm

[a]Weight average molecular weight
[b]Degree of polymerization DP = M_w/(0.344 kg mole^{-1})
[c]Contour length of extended chain L_c = (0.515 nm)(DP)
[d]Number of Kuhn segments per chain $N_k = L_c/L_k$
[e] Theoretical unperturbed radius of gyration $R_{go} = (L_k L_c/6)^{0.5}$
[f]Hydrodynamic diameter calculated from $D_h = 1.33R_{go}$ for a nondraining coil from [30]

A chain with $N_k \geq 100$ typically has a random flight Gaussian coil conformation while a chain with $N_k \rightarrow 1$ behaves as a rigid rod. The values of N_k for HPC E and H in Table 2.1 show that HPC H should have a Gaussian coil conformation while HPC E lies between the coil and rod limit. The estimates of the unperturbed radius of gyration, R_{go}, are made assuming no excluded volume effects.

The effect of water concentration on the solubility of HPC in the reaction medium is a crucial issue as this will affect the extent of adsorption and the thickness of the adsorbed layer on TiO_2. The solubility was assessed qualitatively by DLS measurements of the hydrodynamic diameter D_h of HPC as a function of water concentration in ethanol. The results in Figure 2.2 show that D_h for HPC H increases with X_w indicating that HPC is more soluble in water than in ethanol. For example, the hydrodynamic diameter of HPC H in water is 201 nm compared to 70 nm in ethanol. The latter value compares well with the calculated value of $D_h = 74$ nm, shown in Table 2.1, for a non-draining Gaussian coil with no excluded volume effects. The larger value of D_h in water is presumably due to excluded volume effects which can lead to significant chain expansion in good solvents [34]. For HPC E in anhydrous ethanol, the scattering intensity was weak due to the low molecular weight. The measured hydrodynamic diameter was low, $D_h \approx 10$ nm and the effect of water concentration on D_h was not detectable. The effect of water concentration on TiO_2 stability will be discussed later.

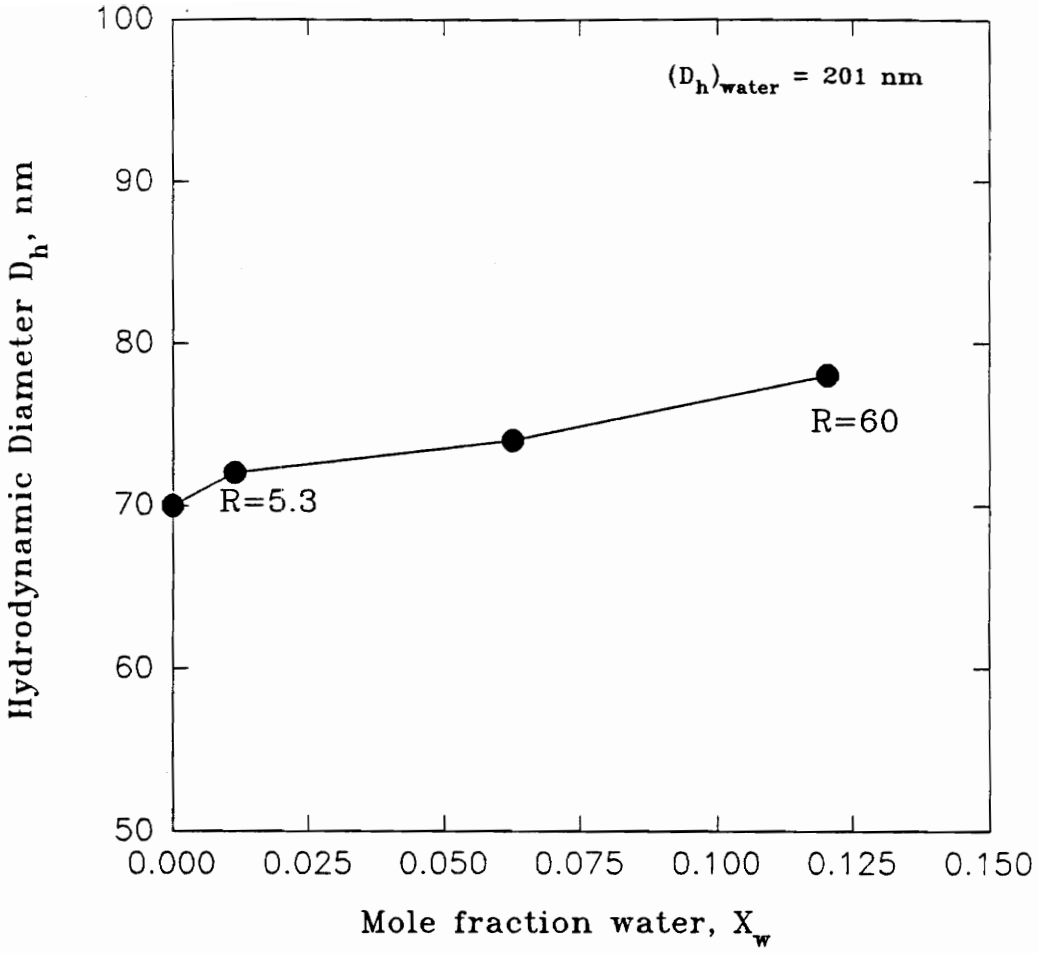

Figure 2.2. Hydrodynamic diameter of HPC H ($M_w \approx 1150$ kg mole^{-1}) as a function of mole fraction water X_w in an ethanol solution as determined by dynamic light scattering at a scattering angle of 90° and T = 25°C.

X-Ray Diffraction Analyses

X-ray diffraction results established the TiO_2 particles to be amorphous for samples grown with and without HPC at R = 5.3 and 60 as no crystalline peaks were detected in the diffraction spectra. This is consistent with the previous results of Edelson and Glaeser [35a,b] and more recent work by Wang, et al. [36] for TiO_2 made and handled at room temperature.

Particle Growth Rate

The objectives of the growth rate experiments were to probe the interactions of HPC with soluble and insoluble Ti species during the hydrolysis and condensation reactions and to determine the effect of silica contamination in HPC on particle growth. Particle growth rates and induction times were measured for TiO_2 suspensions made at [TEOT] = 0.04M and R = 6.2. Particle growth at higher water concentrations of R = 30-60 was very difficult to monitor by DLS due to the almost instantaneous onset of turbidity in the reaction mixture. Two methods of mixing HPC with TEOT were used:

Method 1- Solutions of HPC in ethanol and water were mixed with ethanolic TEOT using the method described earlier in the section on Experimental Procedures.

Method 2- Solutions of HPC in anhydrous ethanol were mixed with TEOT in ethanol and held for 105 minutes before adding water-ethanol mixtures by the equal volume method.

Modes of Interaction

There are three ways by which HPC can interact with soluble and insoluble Ti species:

Case 1-The hydroxyl groups on the polymer chain may react with the ethoxide groups of soluble $Ti(OC_2H_5)_4$ and undergo alcoholysis according the following reaction:

$$Ti(OC_2H_5)_4 \; + \; \mathit{HOC_3H_7\text{-}HPC} \rightarrow Ti(OC_2H_5)_3\text{-}\mathit{OC_3H_7\text{-}HPC} \; + \; C_2H_5OH$$

where $\mathit{HOC_3H_7\text{-}HPC}$ denotes the HPC chain with one of its hydroxypropyl groups. Related alcoholysis reactions occur in minutes at room temperature when TEOT is mixed with various alcohols other than ethanol as noted by Harris and Byers [23].

Case 2 - The hydroxyl groups on the HPC chain can hydrogen bond with the hydroxyl groups on soluble, partially hydrolyzed species, i.e. $Ti(OC_2H_5)(OH)_3$, $Ti(OC_2H_5)_2(OH)_2$, and $Ti(OC_2H_5)_3(OH)$

Case 3 - The hydroxyl groups on the HPC chain can hydrogen bond with the hydroxyl groups on the surface of fully condensed TiO_2 particles as shown in Figure 2.1(B).

Figure 2.3 shows the diameter versus time results for particles grown by both Methods 1 and 2. The growth curves can be divided into two regions: (i) the induction time, and (ii) the initial particle growth rate. These give qualitative insight into the interactions of HPC with Ti species.

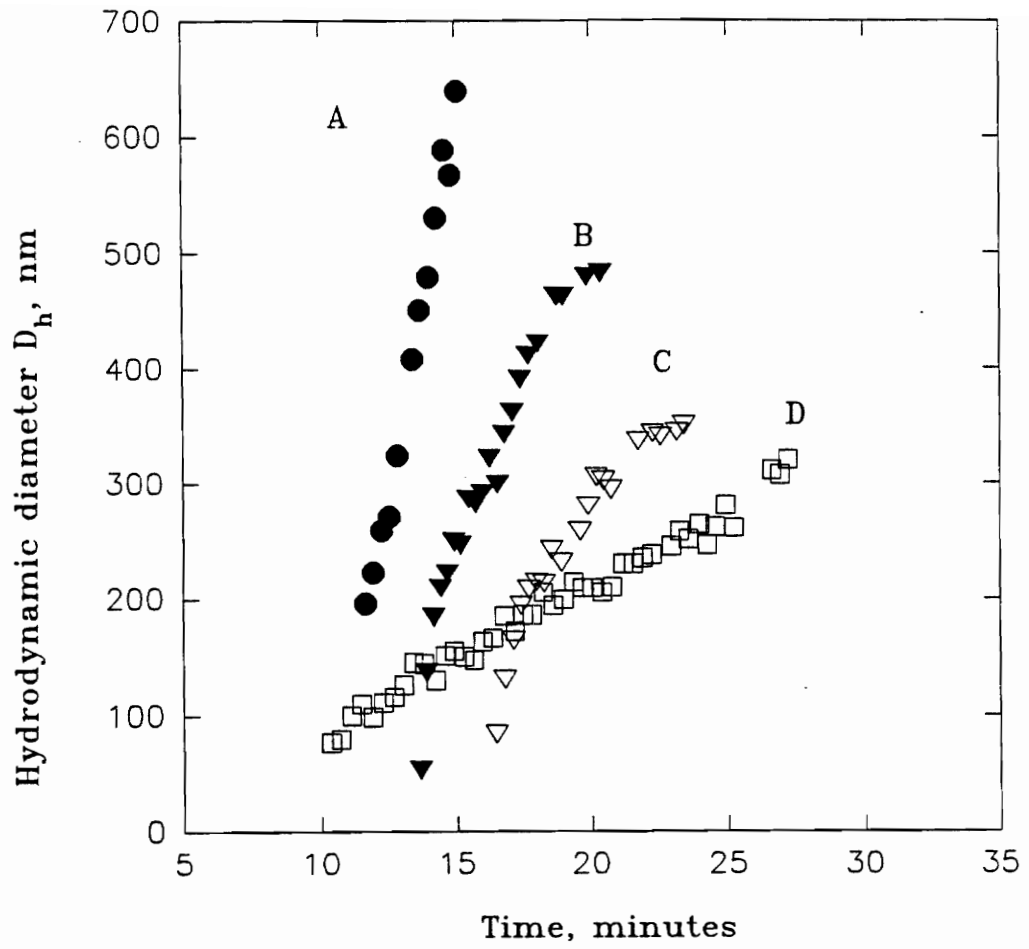

Figure 2.3. Hydrodynamic diameter versus reaction time for [TEOT] = 0.04 M and R = 6.2 and HPC E concentrations: (A) 0, (B) 0.85 x 10^{-3}, (C) 1.7 x 10^{-3} (D) 1.7 x 10^{-3} g cm^{-3}. Samples (A), (B), and (C) were grown by method 1, and sample (D) was grown by method 2. Dynamic light scattering measurements made at a scattering angle of 90° and T = 25°C.

Method 1 - Induction Time

With particles grown at C_p = 0, 0.85, and 1.7 g/l, the time of the onset of turbidity as determined visually was the same as the onset of particle detection in the DLS experiment, approximately 11-16 minutes. Given the rapid hydrolysis reaction as found by Harris and Byers [23], these induction times are the times required principally for the condensation reaction to form detectable particles. Two general observations were made for these experiments: (i) the scattering intensity increased from very low levels to levels readily detectable by DLS in an interval of $\approx$ 5-10 seconds which was the time between successive scans by DLS - this increase coincided with the onset of visual turbidity, and (ii) no particles were detected by DLS prior to the onset of turbidity even though DLS can measure particles as small as 3 nm. Similar observations have been reported for TEOT hydrolyzed in various alcohols. Growth experiments run at laser power > 10 mW failed to detect any scattering species before 11 minutes. These observations suggest that the hydrolysis reactions produce soluble, partially condensed, low molecular weight polymeric species which collapse at a critical concentration to form dense nuclei of the order of 2-3 nm which then grow within 5-10 seconds to the size first detected by DLS. The formation of 2-3 nm particles is consistent with the morphology of TiO_2 particles grown in the absence of HPC that will be discussed later. Look and Zukoski has proposed that nucleation occurs by a sol-gel phase transition like that proposed by Flory for polymer solutions [17]. In this scheme, swollen polymer gels form from the

condensation reaction which collapse rapidly upon reaching a critical molecular weight to form a nucleus. Scattering from the gels would be weak and undetectible if the refractive index of the gels was sufficiently close to that of the solvent. Bailey and MecCartney have observed gel-like species following the hydrolysis of TEOT in fast-freeze cryo-TEM experiments [25].

The induction time increased with HPC concentration from 11 minutes for C_p = 0 to 16 minutes for C_p = 1.7 g l^{-1}. Ring and Jean [19] reported a similar effect of polymer on the induction time. The increase in induction time with HPC concentration suggests HPC interactions according to Cases 1 and/or 2. It should be possible for HPC to form hydrogen bonds with the hydroxyl groups of hydrolysed Ti species according to Case 2. This would retard the diffusion of $Ti(OC_2H_5)(OH)_3$ and offer steric hindrance to its condensation to form 2-3 nm dense particles. Both effects would lead to a delay in the induction time. However, the hydrolysis of TEOT by water is much faster than the alcoholysis reaction between HPC and TEOT due to the higher reactivity of water molecules than the hydroxyl groups on the HPC chain and thus it is likely that this is not as important as Case 2.

Condensation after Induction

The initial growth rate, defined by the slope of the particle diameter versus time plot in the first two minutes after the onset of turbidity, varies only slightly for 0 $\leq C_p \leq$ 1.7 g l^{-1} i.e., 2.0 to 1.6 x 10^{-3} micron sec^{-1} suggesting the absence of any

significant HPC alcoholysis. If alcoholysis were occurring to a significant extent, then the initial slope should decrease markedly with increasing C_p for reasons discussed in the next section.

The growth rate of the particles grown with HPC decreased markedly after a particle size of about 250 nm was reached for C_p = 0.85 g l^{-1} and after a size of 220 nm was reached for C_p = 1.7 g l^{-1}, suggesting that HPC adsorption has occurred according to Case 3 to the extent to effect significant steric stabilization. Ring and Jean [19] reported a decrease in the growth rate from 7 x 10^{-4} micron/s for polymer free control to 1.3 x 10^{-4} micron/s for particles grown in the presence of HPC E at C_p = 3.4 g l^{-1}. However, these growth rates were derived from the slope of size versus time data over a much longer period of time, i.e. 20-30 minutes, than our experiments and so their data cannot be directly compared with ours.

Method 2 - Premixing HPC and TEOT

There were striking differences between the above results and particle growth in solutions where the HPC was premixed with TEOT prior to hydrolysis. The induction time for the premixed sample was 10 minutes compared to 16 minutes for the sample grown by Method 1 at C_p = 1.7 g l^{-1}. The particle growth rate was much slower, i.e., 3.3 x 10^{-4} micron/s, compared to particle growth of 1.6 x 10^{-3} micron/s when grown by Method 1. In these experiments at C_p = 1.7 g l^{-1} HPC, the ratio [initial molarity of $-OC_2H_5$ from TEOT]/[molarity of -OH from HPC] = 11. These

observations strongly suggest that HPC reacts with TEOT via alcoholysis as per Case 1. The bonding of these polymeric Ti-O-Ti species with HPC chains would reduce their diffusivity and hence reduce the condensation rate, and could conceivably retard the polymeric species collapse into 2-3 nm particles. Also, the bonded HPC would lead to slower growth rate due to steric forces. The occurrence of alcoholysis is further supported by the observation that the solution appeared clear although DLS could easily make size measurements. The solution became visually turbid only after the particle size of about 0.2 microns was achieved, i.e., about 20 minutes after the induction time. Recall that size measurements could be made by DLS for particles made by Method 1 only when the reaction mixture was noticeably turbid. The lack of visual turbidity in the premix case is consistent with the formation of a open network of polymeric Ti-O-Ti species linked together by HPC chains. Such a network should have a lower refractive index causing the solution to be more homogenous and hence should scatter visible light less strongly than denser TiO_2 particles. Microscopy experiments are planned to probe this point further.

Effect of Silica

If the silica contamination in HPC was causing a significant degree of heterogeneous nucleation, then the induction times for particles grown with HPC by Method 1 should decrease with increasing C_p and should be less than that for the polymer-free control, contrary to the results in Figure 2.3. However, the interactions of HPC with the particles might offset the effects of heterogeneous nucleation on the

induction time. Another way to estimate the effect of silica on particle growth is to compare the number concentration of silica particles with estimates of the TiO_2 nuclei number concentration. Assuming the silica density to be 2.32 g cm^{-3} [37] and a mean particle diameter of 10 nm, then the silica particle number concentration associated with 1.7 g l^{-1} HPC is 4 x $10^{10}cm^{-3}$. We estimate the TiO_2 nuclei number at 1% conversion of TEOT which, by comparison with Ring's data at [TEOT] = 0.075 M and [H_2O] = 0.5 M, occurs earlier than 10 minutes after the induction time [19]. The TiO_2 nuclei number concentration was 1.5 x $10^{14}cm^{-3}$ assuming an average nucleus diameter of 6 nm [35a], a nucleus density of 3.1 g cm^{-3} [14] and that the nuclei have not yet aggregated. Hence, the nuclei concentration due to homogeneous nucleation of TEOT is approximately 4 x 10^3 times the concentration of heterogeneous nucleation sites due to silica contamination and thus the presence of silica in HPC has a negligible effect on TiO_2 particle growth. Growth at higher water concentrations will have higher nucleation rates and hence will be even less affected by the silica.

Extent of Conversion of TEOT

HPC does not affect the percent conversion of TEOT grown by the conventional method of mixing HPC and water with the TEOT at the same time. The yield of TiO_2 after twenty four hours is virtually the same when the particles are grown with and without HPC E at [TEOT] = 0.075M as shown in Table 2.2. Ring et. al. [19] also found the yield to be independent of HPC concentration.

Table 2.2 - Extent of Conversion of Tetraethylorthotitanate, TEOT

R $[H_2O]/[TEOT]$	%Conversion No Polymer	%Conversion HPC E, C_p = 1.7 g l^{-1}
5.3	35	37
30	99	99
60	100	100

The extent of conversion, $\geq$ 99%, at R = 30 and 60 implies that even the fourth ethoxide group is hydrolyzed which is not the case at R = 5.3 after 24 hours as noted by Bowen and Barringer [13].

Particle Morphology

Polymer-free Control Particles

Figure 2.4 shows the TiO_2 particles grown in the absence of HPC stabilizer at R = 5.3 are highly agglomerated with the size ranging from 2 to 4 microns. Figure 2.5(A) is a high resolution (100,000 X) picture of particles in Figure 2.4. Note that the particle surface in Figure 2.5(A) is comprised of fine grains 2-10 nm in diameter and the dark spaces in between the grains presumably correspond to pores of similar dimension. The grainy morphology of the particle surface suggests a porous structure resulting from the collision and subsequent aggregation of many unstable nuclei in the size range of 2-10 nm. Similar surface morphologies were reported by Zukoski, et al. [16]

Particles grown in the presence of HPC

Figure 2.6(A) and (B) show that TiO_2 particles grown at R = 5.3 with both HPC E (M_w = 68.5 kg mole^{-1}) and HPC H ($M_w \approx$ 1150 kg mole^{-1}) are spherical, unagglomerated, and are about 0.3 microns in diameter which is quite similar to Ring's results at similar growth conditions [19]. The high resolution (100,000X)

micrograph of a particle grown with HPC E in Figure 2.5(C) was taken from the same sample shown in Figure 2.6(A). Note that the particle surface has a relatively rough texture compared to the particle surface of the particles grown without added HPC shown in Figure 2.5(A). Similar particle morphology is seen in Figure 2.5(D) for particles grown at R = 60 and for particles grown with HPC H (not shown). Surface roughness is not an artifact due to adsorbed HPC on the TiO_2 surface. Figure 2.5(B) is a high resolution picture of polymer free control particles grown at R=5.3 but equilibrated with HPC E for 24 hours after they were synthesized. The surface morphology of the particles is very similar to the surface texture observed for polymer free particles as shown in the Figure 2.5(A). Thus, the very different surface morphology observed in Figures 2.5(C) and (D) is due to a difference in the particle growth mechanism.

It appears that the particles made with HPC are formed due to the aggregation of particles having an average diameter of 20-25 nm which then collide to form the final aggregate. The dark regions correspond to pores of less than $\approx$ 20 nm size. This could explain why the particles synthesized in the presence of HPC are so porous, with the BET area $\sim$ 300 m^2g^{-1} as found by Edelson and Glaeser [35a,b]. Similar surface morphology was also observed by Edelson and Glaeser for amorphous TiO_2 particles made with HPC at R = 3 as well as for crystalline anatase TiO_2 obtained by sintering the amorphous particles [35b]. However, no mechanism was suggested to account for this morphology.

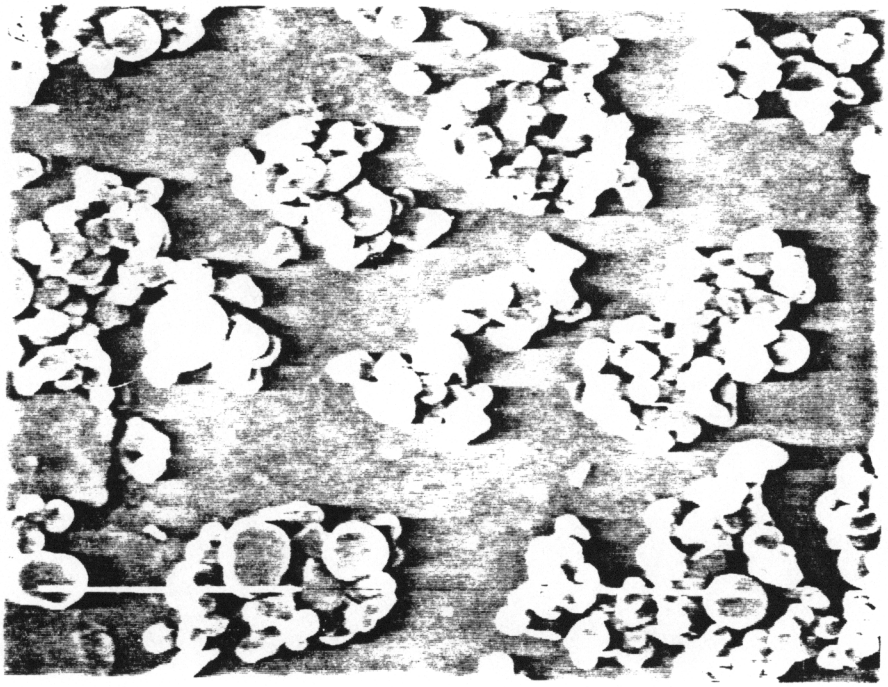

Figure 2.4. Scanning electron microscopy photograph of particles formed without HPC (bar = 5 μm) at [TEOT] = 0.075 M and R = 5.3.

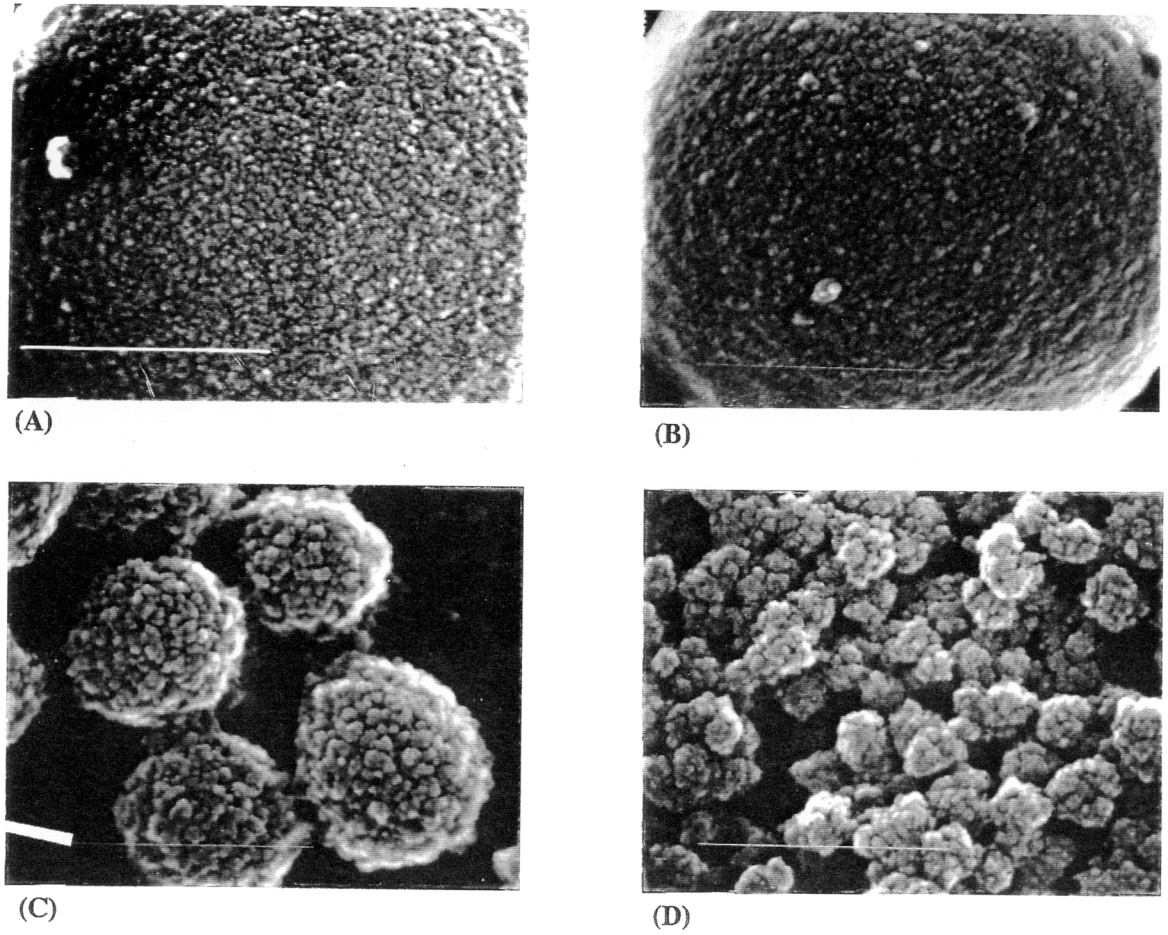

Figure 2.5. High resolution SEM photographs of surfaces of particles grown at [TEOT] = 0.075 M. (A) without HPC, (B) without HPC but equilibrated with HPC E, (C) and (D) HPC E at 1.7 x 10^{-3} gcm^{-3}. Samples (A), (B), (C) were grown at R = 5.3 and sample (D) was grown at R = 60.

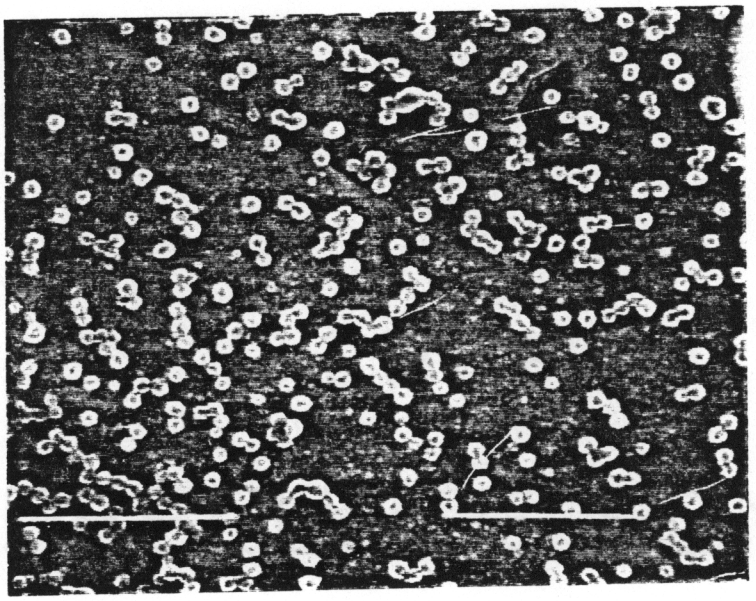

(A)

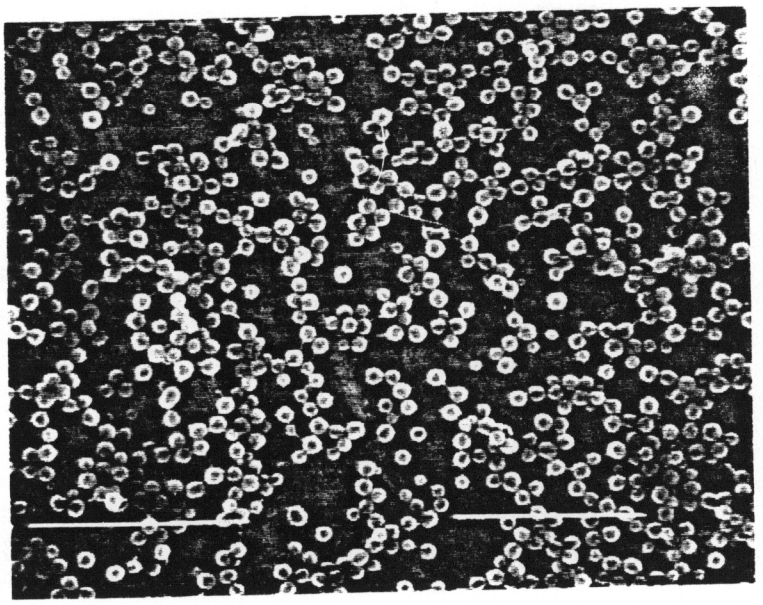

(B)

Figure 2.6. SEM photographs of particles grown with HPC (bar = 5 μm) at [TEOT] = 0.075 M, R = 5.3 and C_p = 1.7 x 10^{-3} gcm^{-3}. (A) HPC M_w = 68.5 Kg/mole, (B) HPC = 1150 Kg/mole.

The 20-25 nm size of the units comprising the aggregates proves that the HPC interacts with the TiO_2 very early in the growth process, most likely by a combination of the three cases discussed earlier. Assuming nuclei diameters in the range $\approx$2-6 nm, between 100-2000 nuclei would have to collide and aggregate to form a 25 nm aggregate. Given the estimated value of the Kuhn length for HPC, L_k= 10.8 nm, there are approximately 60 (-OH) binding sites per stiff segment. Given the chain dimensions of HPC E from Table 2.1, it is more accurate to describe the HPC-TiO_2 interactions at this stage in the growth process in terms of nuclei binding to parts of a polymer domain of length scale rather than in terms of classical polymer adsorption onto a macroscopic surface which would be more appropriate for describing adsorption later in the aggregation process. In any case, hydrogen bonding between HPC and TiO_2 is believed important at both length scales and were probed by measurements of HPC adsorption isotherms. These are presented in a later section and provide compelling evidence for hydrogen bonding between the hydroxyl groups on the HPC chain and surface Ti-OH groups.

A mechanism to account for the granular surface morphology seen in Figures 2.5(C) and (D) is suggested by the work by Look and Zukoski [16,17] who showed that electrostatically stabilized TiO_2 particles made in acidic conditions form in several steps. TiO_2 particles $\approx$ 2-20 nm in size precipitated initially and then quickly flocculated into a secondary minimum described by the DLVO theory. Subsequent condensation reactions due to the deposition of oligomeric species and nuclei formed

at later times fused the particles together to form permanent aggregates in the size range 100-1500 nm. The rough surface morphology of the TiO_2 particle in Figure 2.5(C) made with HPC is consistent with the hypothesis that $\approx$ 25 nm aggregates with some HPC adsorbed on their surfaces flocculated into a secondary minimum and then fused together to form larger, permanent aggregates. A rigorous proof of this hypothesis will require measurements of the rate and extent of HPC adsorption during particle growth along with accurate calculations of the steric repulsive energy for constructing the pair interaction energy curve with the DLVO theory.

Particle Size Analysis

Effects of Polymer Concentration and Molecular Weight

Figure 2.7 shows the effect of polymer concentration on the particle size when the particles are grown in the presence of HPC E and H at R = 5.3. The particle size decreased from 0.7 microns at C_p = 0.1 g l^{-1} to 0.33 microns at C_p = 1.7 g l^{-1} for particles grown with HPC E due to increasing HPC adsorption on the TiO_2 surface. The relative standard deviation shown in Figure 2.8 decreased from over 40% to 20% as HPC concentration increases at R = 5.3. These results agree well with Ring's results for HPC E where it was shown that the particle size does not change for C_p > 1.7 g l^{-1}, suggesting that the TiO_2 surface is effectively covered with HPC.

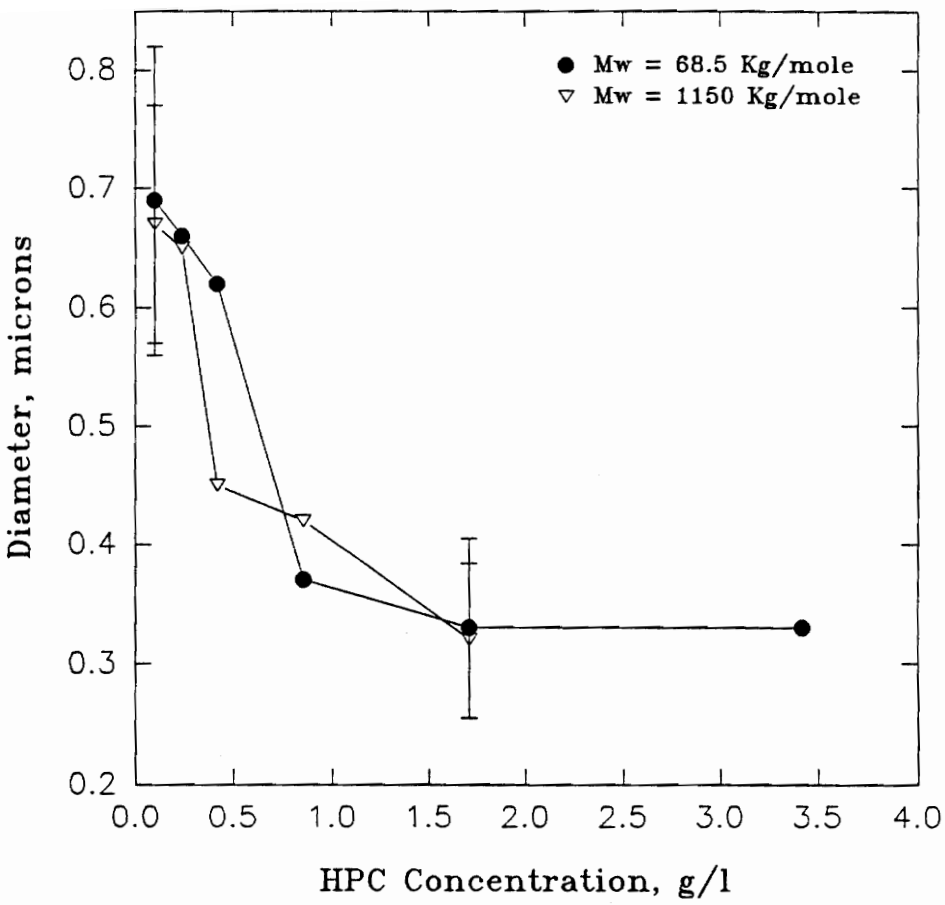

Figure 2.7. Mean diameter versus HPC concentration at [TEOT] = 0.075 M and R = 5.3. Mean diameter determined by transmission electron microscopy, TEM.

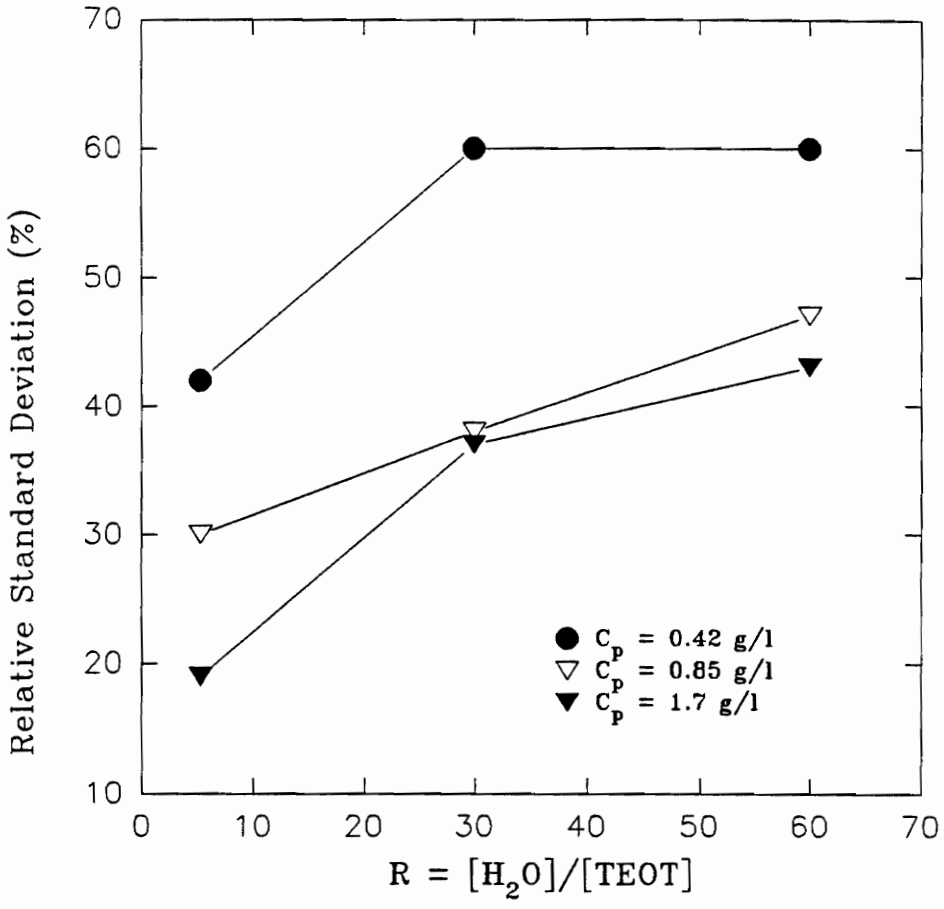

Figure 2.8. TEM standard deviation versus R at [TEOT] = 0.075 M at various HPC concentrations.

A similar trend of particle diameter with polymer concentration was observed with particles grown in the presence of the HPC H. At the higher HPC concentrations, HPC molecular weight in the range 68.5-1150 kg $mole^{-1}$ had relatively little effect on final particle diameter. This was found for all water concentrations 5.3 $\leq R \leq 60$. The stabilization of TiO_2 particles at $M_w \approx 1150$ kg $mole^{-1}$ was surprising since many polymers with molecular weights this high act as flocculants by bridging especially at low surface coverage by the polymer. However, Figure 2.7 shows that particles grown with HPC H at the lowest polymer concentration, C_p = 0.1 g l^{-1}, had virtually the same diameter as particles grown with HPC E.

Effect of Water Concentration

Polymer-free Control Particles

The water concentration in the reaction mixture has a profound effect on the morphology of the particles grown in the absence of polymer as evident from the TEM micrographs in Figure 2.9. The size of the subunits forming the aggregates decreases from 600 nm at R = 5.3 to 100 nm at R = 60 due to the rate of nucleation increasing markedly with water concentration. This is expected from the stoichiometry of the hydrolysis and condensation reactions. Increasing water concentration results in a higher number density of nuclei formed in the early stages of the reactions which leads to a higher number density of particles in the latter stage and a smaller average size of the subunits comprising the aggregates. The aggregated morphology is

identical to that seen in previous studies by Look and Zukoski [17] and Harris and Byers [23] and appears to be due to weak flocculation of the subunits followed by further condensation reactions that welded the particles to form the final aggregate [17].

Particles Grown with HPC

When the particles are grown in the presence of HPC, the particle diameter decreases dramatically with increasing water concentration as seen in the TEM micrographs in Figure 2.10. The particles grown with HPC E appear to be less spherically symmetric at the higher values of R = 30 and 60. This may be due to the limited number of collision and aggregation events these particles experienced before growth stopped. The irregular boundary observed may also be partly due to adsorbed HPC on the smallest particles. Image analysis of the particles grown at R = 60 showed a dense black core and a somewhat thicker gray periphery than for particles grown at R = 5.3. In the image analysis procedure, the gray peripheral area was rejected and only the dense black core was sized for particles grown at high R. When the gray area was considered as a part of the particle, the average diameter increased typically by 7% for particles grown at high R.

As seen in Figure 2.11, the particle diameter decreased to a minimum of approximately 70 nm when the particles were grown in HPC E at C_p = 1.7 g l^{-1} and R = 60.

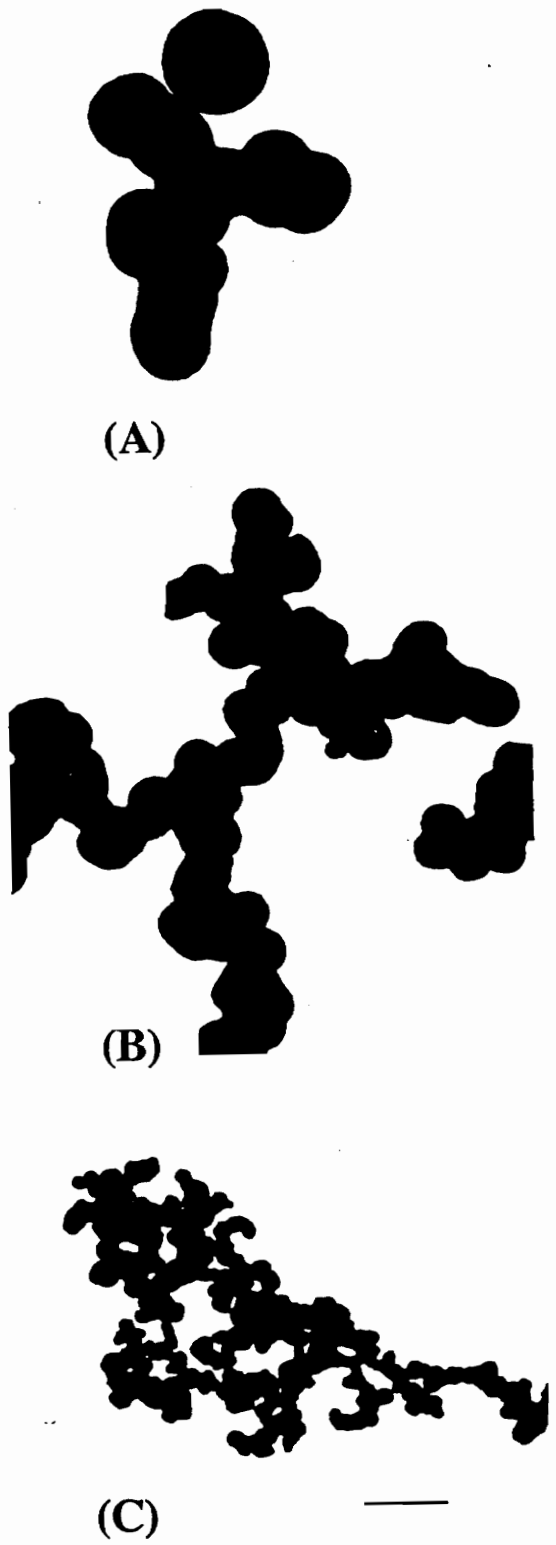

Figure 2.9. TEM photographs of particles grown without HPC (bar = 0.5 μm) at various R values at [TEOT] = 0.075 M

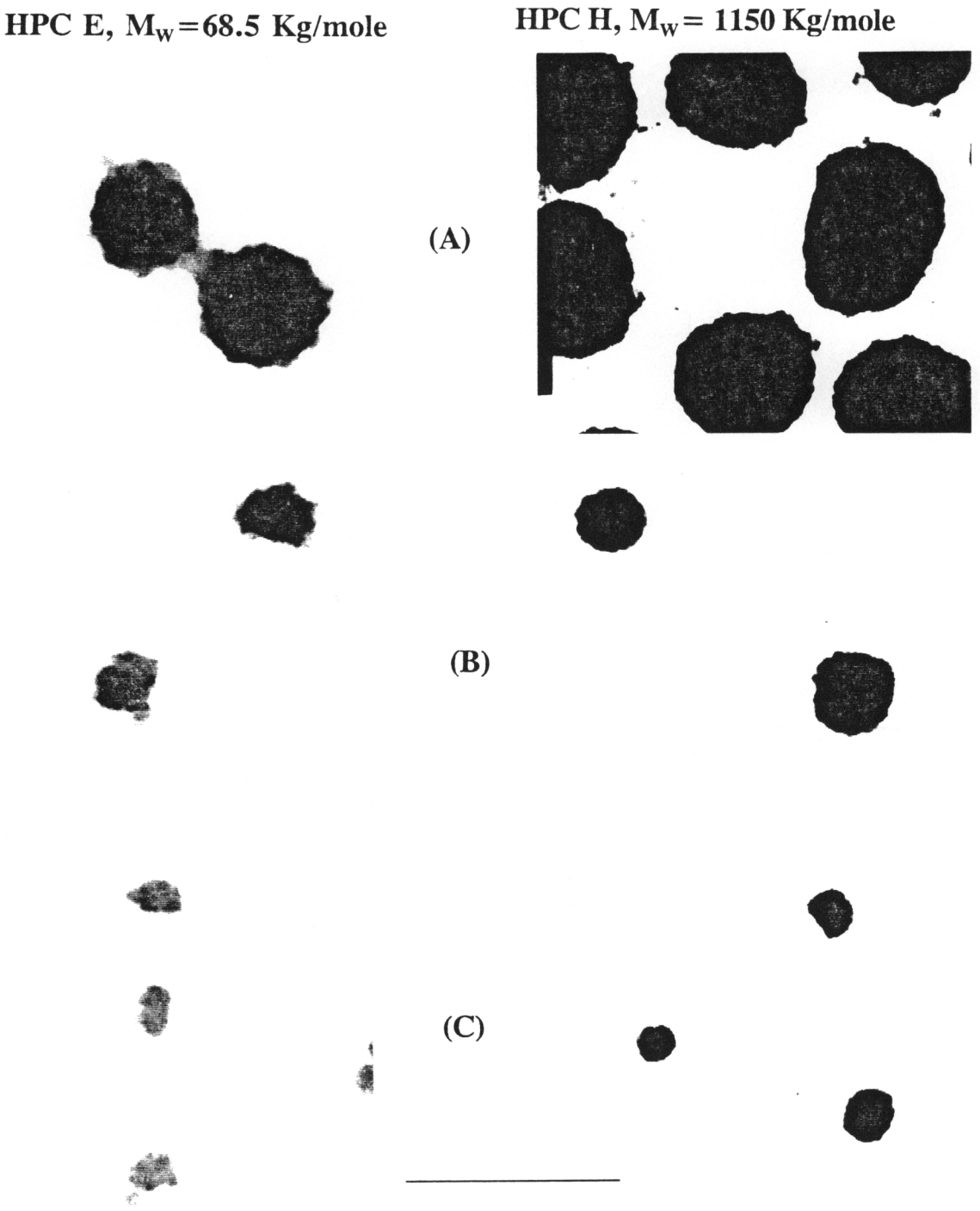

Figure 2.10. TEM photographs of particles grown with HPC (bar = 0.5 μm) at 1.7 x 10^{-3} gcm^{-3} at various R values at [TEOT] = 0.075 M.

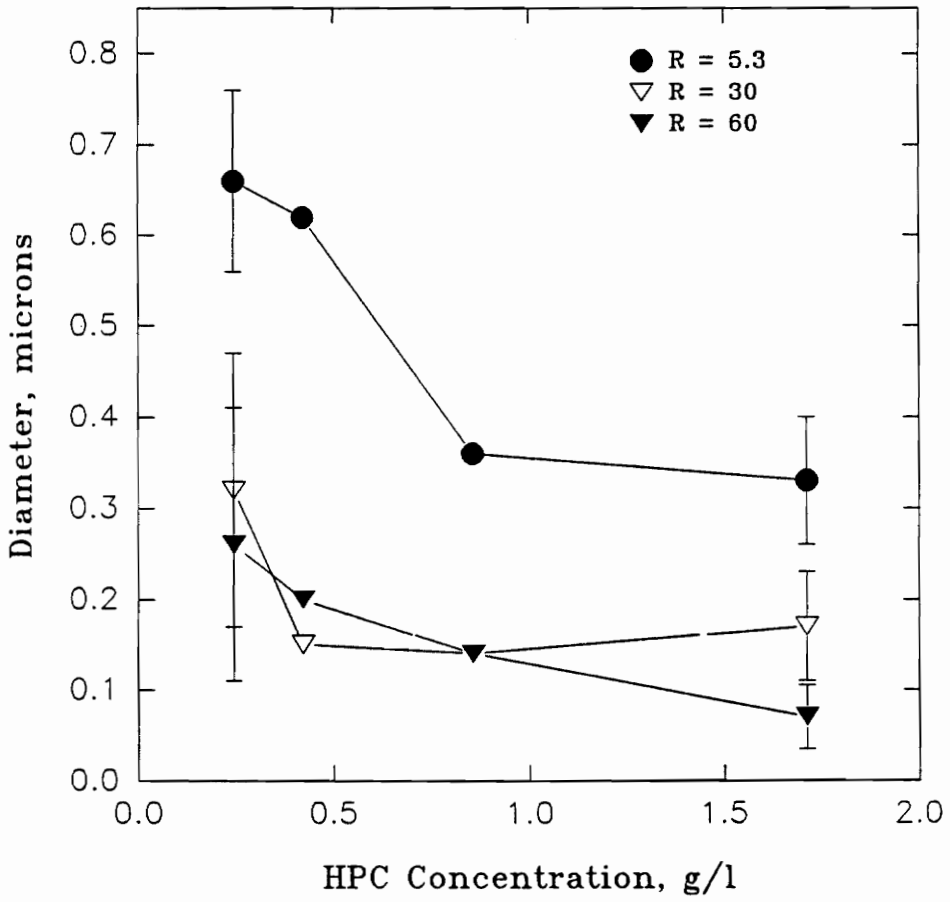

Figure 2.11. TEM mean diameter versus polymer concentration, g cm^{-3}, of HPC E at various R values.

Note that the relative standard deviation of the particle size shown in Figure 2.8 decreased from 65% to 42% with increasing HPC concentration. Similar trends were observed when the particles are grown in HPC H.

From Figure 2.12(A), the effect of HPC molecular weight on particle diameter at R = 60 is somewhat uncertain at low polymer concentration due to the large relative standard deviations. However, the effect of molecular weight is more pronounced at the high polymer concentration C_p = 1.7 g l^{-1} and high water concentration R = 60 as seen in Figures 2.12(A) and (B). The reduction in particle size with water concentration in the reaction mixture at a fixed polymer and TEOT concentration can be due to the effect of water concentration on: (i) the kinetics of the hydrolysis and condensation reactions discussed above, (ii) the adsorption of HPC on TiO_2, (iii) the interparticle electrostatic forces, and (iv) the solubility of HPC in the reaction medium. Factors (ii)-(iv) are discussed below.

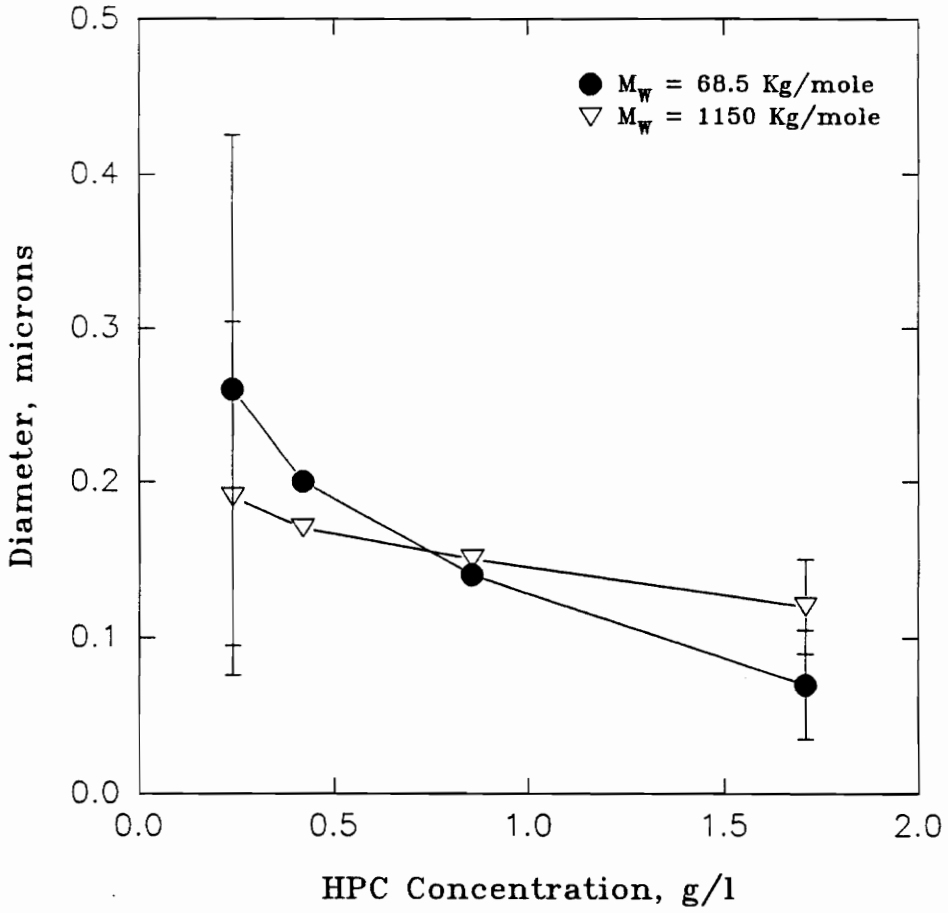

Figure 2.12. (A) TEM mean diameter size at R = 60 versus HPC E concentration at [TEOT] = 0.075 M.

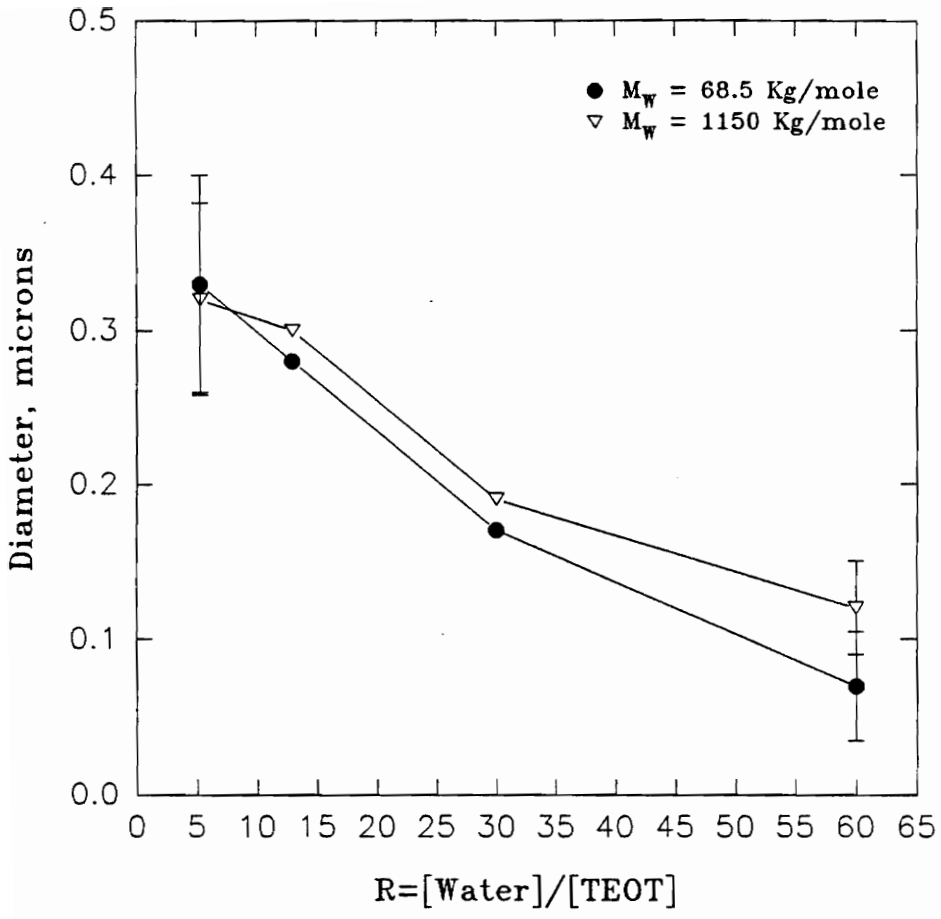

Figure 2.12. (B) TEM mean size versus R at $C_p = 1.7 \times 10^{-3}$ g cm^{-3}.

HPC-TiO_2-Solvent Interactions

HPC Adsorption Isotherms

A change in the solvent composition can affect the adsorption isotherm of a polymer which would necessarily affect steric stability [38]. Figure 2.13(A) shows that the mass of HPC adsorbed per gram of TiO_2, Γ, increases with water concentration at a fixed HPC molecular weight and concentration. The error bars represent 50 % confidence (2/3 σ) limits. The adsorbed amount Γ increases by about three-fold as the water mole fraction X_w increases from 0.01 (R = 5.3) to 0.12 (R = 60). Γ also increases with HPC molecular weight since the longer chains have more segments to adsorb onto the TiO_2 in keeping with previously reported studies of homopolymer adsorption and polymer adsorption theory [38,39]. The adsorption of HPC E at C_p = 1.7 g l^{-1} is significantly less than reported by Ring and coworkers at similar conditions. For example, at X_w = 0.01, the amount of HPC E adsorbed is 5 x 10^{-4} gm/gm TiO_2 which is ten times lower than reported by Ring et al. [19]. The discrepancy could be due to the difference in the powder preparation technique.

Ring and coworkers used TiO_2 powders which were dried at 100°C in nitrogen for 8 hours whereas the powder in the present study was never dried in an effort to replicate as closely as possible the in-situ adsorption of HPC on the growing TiO_2 particles. The surface chemistry of TiO_2 powder can change significantly depending upon the washing and the drying conditions to get the dry powders which in turn would have a significant affect on the polymer adsorption isotherm.

(A)

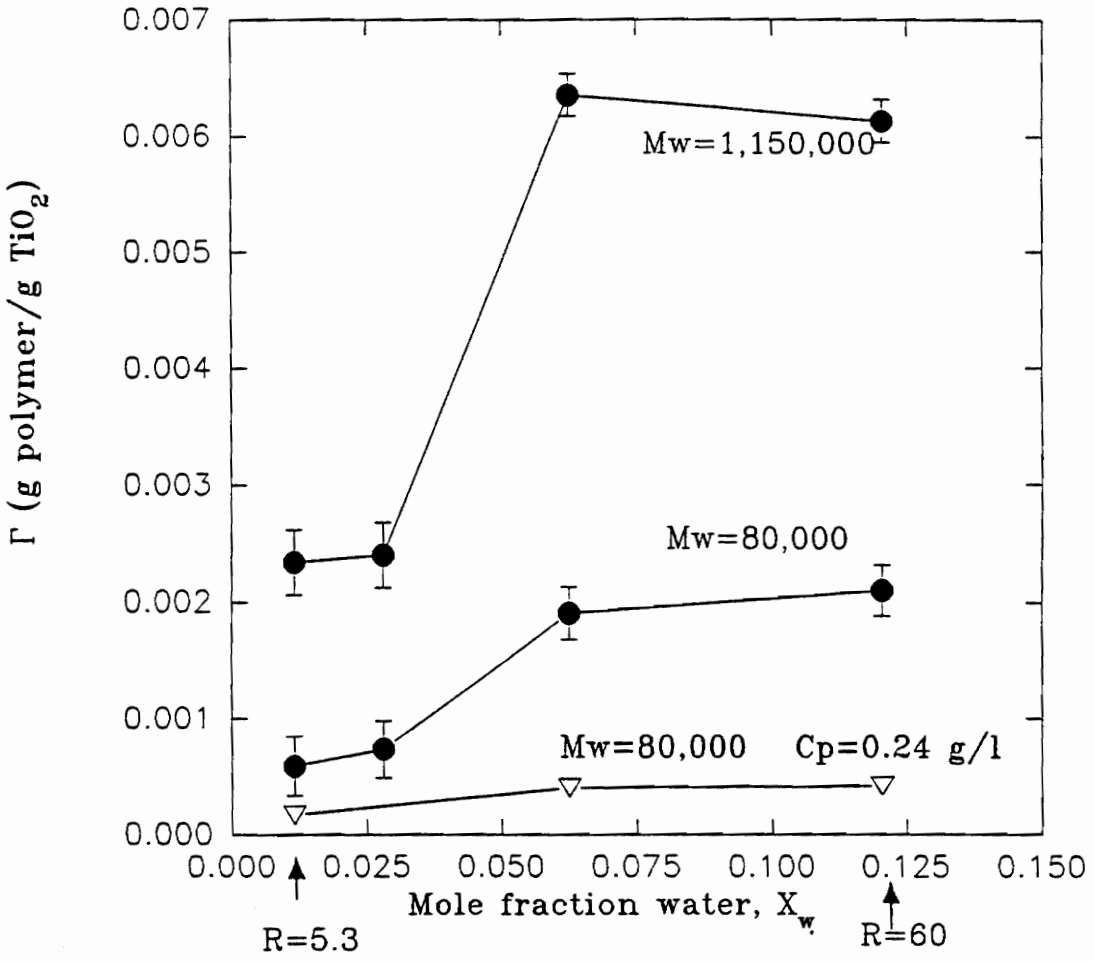

Figure 2.13. (A) HPC adsorption isotherm, versus mole fraction water at C_p = 1.7 x 10^{-3} g cm^{-3}.

Hence, it is reasonable to expect the difference in adsorption isotherms in the two cases.

Calculations by Ring and coworkers [19] of the pair interaction energy from the DLVO theory for TiO_2 particles with adsorbed HPC were made assuming that the HPC molecules were terminally adsorbed, i.e. only one point along the chain was attached to the TiO_2 surface. This led to values of the primary maximum V_{max} as high as 90 KT units which would mean extremely high stability. Since HPC has an average of 3 hydroxyl groups per repeat unit which can adsorb on TiO_2 by hydrogen bonding, it is highly probable that it adsorbs in the form of trains, loops and tails [39]. Hence the assumption that the polymer is terminally attached is probably not valid. Precise calculations of the pair interaction energy curve requires accurate measures or estimates of the adsorbed layer thickness and of the segment density profile as a function of distance from the particle surface [40]. The titanium particles produced by in-situ steric stabilization are so polydisperse that it is not possible to use dynamic light scattering to measure the effective thickness of the absorbed HPC layer. Thus, the estimates of the absorbed layer thickness for HPC are necessarily crude and rather uncertain.

Water Segregation on TiO_2

The Karl-Fischer titration results in Figure 2.14 show that water segregates at the TiO_2 surface and possibly in the pores of the particles. Segregation of water in

and on the TiO_2 particle is favored thermodynamically since water forms a more polar and hence stronger hydrogen bond with Ti-OH than does ethanol. These results suggest that water facilitates HPC adsorption through the formation of hydrogen bonds between the Ti-OH surface and the hydroxyl groups on the HPC, as depicted in Figure 2.13(B). By contrast, ethanol cannot participate in hydrogen bond formation between the Ti-OH surface and the HPC. Note that the plateau in the water adsorption curve in Figure 2.14 occurs at approximately the same water concentration as does the plateau in the HPC adsorption isotherm in Figure 2.13(A). This segregation effect may be related to the short range repulsive hydration force proposed by Look and Zukoski to account for the morphology of TiO_2 particles [16,17]. They proposed that water molecules formed ordered layers at the surface of TiO_2 particles, thus generating a repulsive force with a range of $\approx$1-2 nm.

Electrophoretic Mobility

Water concentration also affects the surface charge of TiO_2. As shown in Figure 2.15, the electrophoretic mobilities of the polymer-free control TiO_2 particles increased with water concentration, reaching a plateau at approximately the same concentration at which the water segregation curve in Figure 2.14 reached a plateau. The suspension conductivity, also shown in Figure 2.15, decreased from 0.5 to 0.3 x 10^{-6} mhos cm^{-1} with increasing water concentration. This decrease was most likely due to the solvent viscosity which increased by 7% as R increased from 5.3 to 30 as

(B)

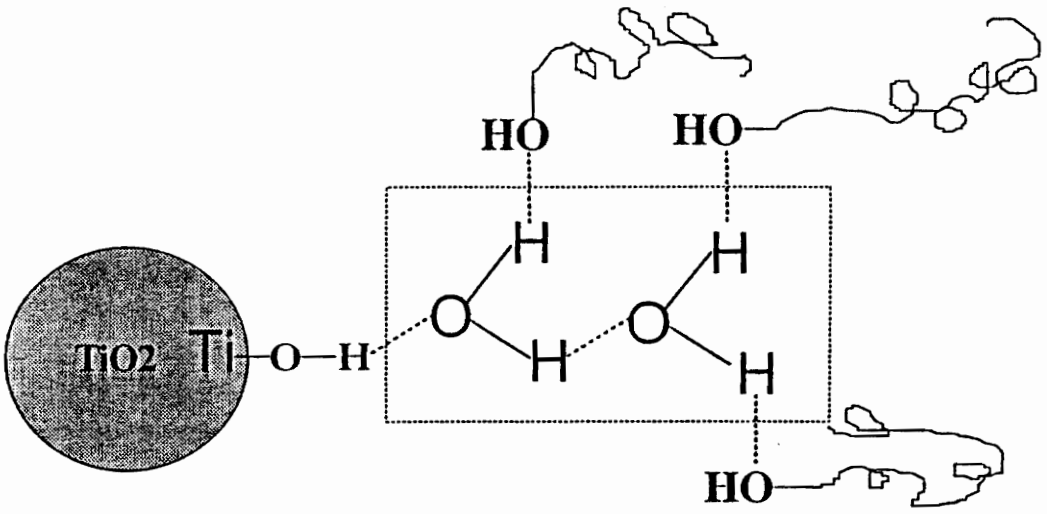

Figure 2.13. (B) Water bridging between the TiO_2 surface and HPC via hydrogen bonding.

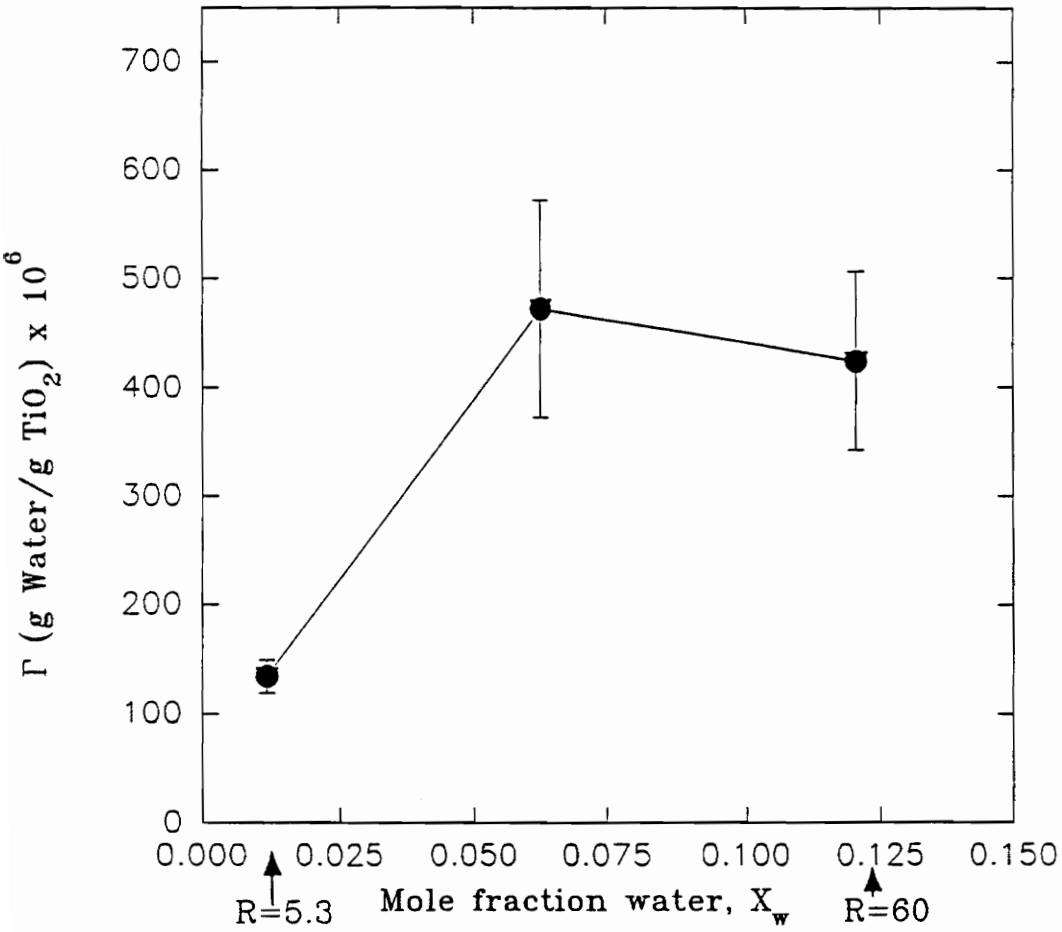

Figure 2.14. Water adsorption isotherm, versus mole fraction water without HPC.

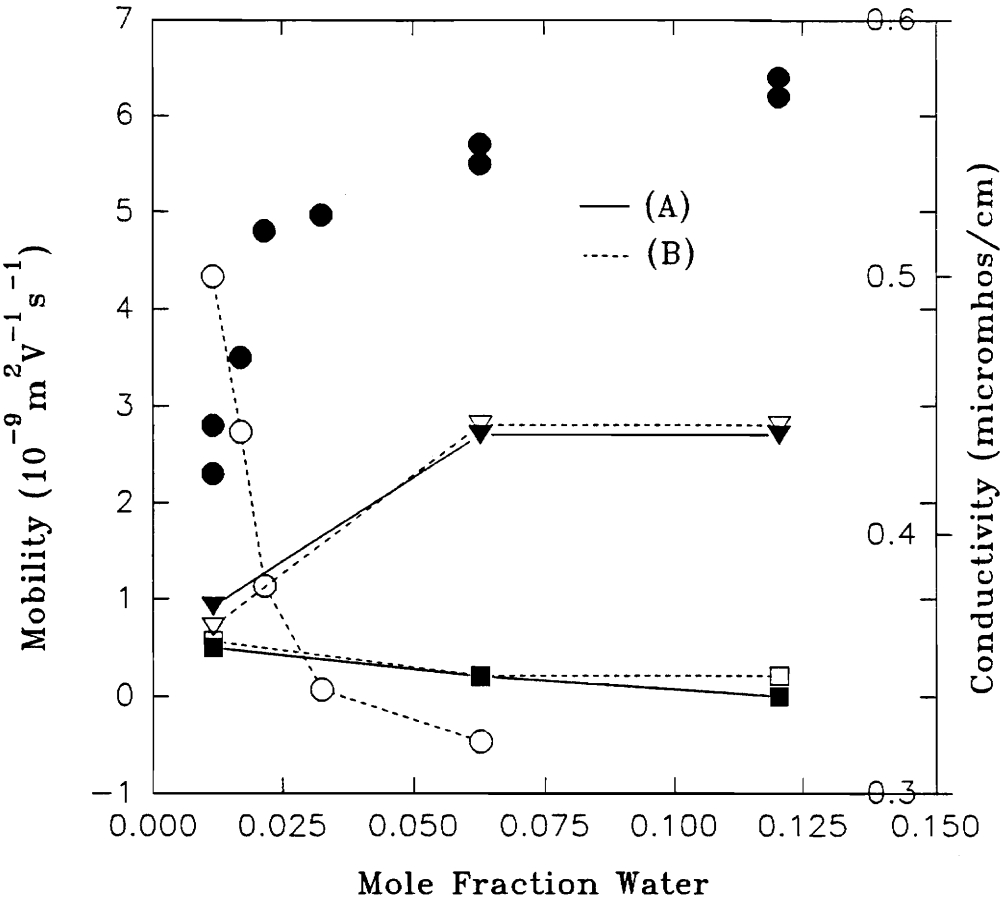

Figure 2.15. Electrophoretic mobility, versus $[H_20]/[TEOT]$, R, of the particles grown with and without HPC E and conductance versus R of particles grown without HPC; ● mobility of polymer free control particles; ○ conductivity of polymer free control particles; (A) ____, particles grown in HPC, (B) ----, polymer free control particles equilibrated with HPC.

measured by capillary viscometry. At these low ion concentrations, the conductivity varies directly with the ion mobility at infinite dilution, μ^0, which can be related to the ion's solvated radius r and solvent viscosity η by a generalized form of Walden's rule [41]

$$\mu^0 r\eta = \text{constant.}$$

Measurements of the suspension pH were somewhat erratic with pH $\approx 6 \pm 1$ due to the very low suspension conductivity. The slightly acidic conditions were most likely due to the absorption of atmospheric CO_2 in the water. The slightly acidic pH accounted for the protonation of the Ti-OH surface and thus the increase in electrophoretic mobility with R. The isoelectric point, IEP, of TiO_2 in water is 6.2 [14]. However, it is not known if the IEP shifts in an ethanol-water solution.

The method of O'Brien and White [42] was used to estimate the zeta potential ζ by assuming the effective ionic strength was 10^{-6} M and that the effective size of the particles "a" was that of the subunit making up the aggregate as determined from the TEM micrograph in Figure 2.9. These assumptions gave values of $a\kappa$ in the range 3.5-0.6. The resulting values of ζ were +20 mV at R = 5.3 and +40 mV at R = 60 for the polymer-free control samples. Look and Zukoski [16] reported a decrease in the mobility of the TiO_2 particles from 2.0 to -1.6 10^{-9} $m^2v^{-1}s^{-1}$ with increasing water concentration in the range R = 5-10. Mobilities for R > 10 were not reported. The

reason for this discrepancy with our data is not clear at present.

Electrophoretic mobilities of particles grown with HPC at C_p = 0.24 and 1.7 g l^{-1} were virtually identical to those of the polymer-free particles equilibrated with HPC at equivalent concentrations. This confirms that keeping the polymer-free particles in ethanol prior to adsorption isotherm and electrophoresis experiments replicates well the surface chemistry of the in-situ stabilized particles. The trends in the curves at C_p = 0.24 and 1.7 g l^{-1} are due to the adsorbed polymer which shifts the shear plane from the TiO_2 surface, reducing the zeta potential at the slip plane relative to the C_p = 0 case [43]. The increase in mobility at C_p = 0.24 g l^{-1} in Figure 2.15 is consistent with the HPC adsorbing in a relatively flat train configuration since the particle surface is not completely covered. At the higher concentration C_p = 1.7 g l^{-1} where the particle surface is completely covered, the HPC chains very likely form tails and loops which would extend the shear plane from the surface and hence reduce the mobility. This is consistent with a previous study of the adsorption of poly(vinyl alcohol) on AgI particles [44]. Note that the mobility curve reaches a plateau at water concentrations corresponding to the plateaus in the HPC adsorption isotherm and water segregation curves in Figures 2.13 and 2.14, respectively. The very low mobility at R = 60 and C_p = 1.7 gl^{-1} proves the absence of significant electrostatic stabilization effects precisely at the conditions that result in the smallest particle sizes.

HPC Solubility Effects

The increasing solubility of HPC with water concentration as shown by Figure 2.2 should lead to increased steric repulsive forces, particularly since HPC adsorbs more at higher R. However, the relatively slight increase of the hydrodynamic diameter of HPC H by only 10% as R increases from 5.3 to 60 suggests that the increasing solubility may be only a secondary effect compared to the increase in HPC adsorption and the increasing nucleation rate with R.

Conclusions

This study details the effects of water concentration on the formation of TiO_2 particles from the hydrolysis and condensation of tetraethylorthotitanate, TEOT, in the presence of the polymer hydroxypropylcellulose, HPC. The polymer provides in-situ steric stabilization of the TiO_2 particles. Water was shown to segregate at the TiO_2 surface and to promote HPC adsorption through enhanced hydrogen bonding. The scaled water concentration R = $[H_2O]/[TEOT]$ ranged from 5.3-60. The particle size decreased by ten-fold upon the addition of HPC at high water concentrations due to the combined effects of increased HPC adsorption and increased nucleation rates. Mean particle diameters as small as 70 nm were obtained. The particles grown with added HPC had surface morphologies that suggest the particles aggregated by flocculating initially into a secondary energy minimum followed by condensation reactions that welded the aggregates together. Particle growth rate studies indicate that

HPC can undergo an alcoholysis reaction with TEOT when mixed in the absence of water. HPC in the molecular weight range $68.5 \leq M_w \leq 1150$ kg mole^{-1} has a relatively slight effect on the mean particle size. Electrophoresis measurements show the absence of any significant electrostatic stabilization effects under conditions giving the smallest particle sizes.

Future work will consist of efforts to directly measure the presence of Ti-O-(polymer) bonds formed by the alcoholysis reaction. It may be possible to design polymers with reactive groups which would react rapidly with a particle surface, leading to more effective steric stabilization in the earliest stages of particle growth. The effect of polymer on the internal structure of TiO_2 particles will be also be addressed in future work. Finally, any model for particle growth in the presence of a stabilizing polymer must account for the relative kinetics and extent of polymer adsorption. Validation of such a model can only be done with a system where the repulsive steric forces are well-defined.

References

1. Intelligent Processing of Materials, Report of an Industrial Workshop Conducted by the National Institute of Standards and Technology, Gaithersburg, MD, August 31-September 1, 1988. NISTIR 89-4024, (January, 1989), US Department of Commerce, p.38.

2. Chestnoy, N., Hull, R., and Brus, L.E., J. Chem. Phys., 85(4), 2237 (1986).

3. Wagner, W., Averback, R.S., Hahn, H., Petry, W., and Wiedenmann, A., J. Mater. Res., 6, 2193 (1991).

4. Brinker, C.J. and Scherer, G.W., 'Sol-Gel Science: The Physics and Chemistry of Sol-Gel Processing', Academic Press, San Diego, (1990).

5. Matijevic, E., Ann. Rev. Mater. Sci., 15, (1985) 483.

6. Ring, T.A., MRS Bulletin, 15(1), 34 (1990).

7. Livage, J., MRS Bulletin, 15(1), 18 (1990).

8. Matijevic, E., in 'Science of Ceramic Chemical Processing', eds. Hench, L.L. and Ulrich, D.R., Wiley, New York, 1986, 463-481.

9. Barringer, E., Jubb, N., Fegley B., Pober, R.L., and Bowen H.K., Ultrastucture Processing of Ceramics, Glasses, and Composites, eds. Hench, L.L., and Ulrich, D.R., Wiley, New York, 1984, 315-333.

10. Matijevic, E., Acc. Chem. Res., 14, 22 (1981).

11. Matijevic, E., Chapter 27 in 'Ultrastucture Processing of Ceramics, Glasses, and Composites', Hench, L.L., and Ulrich, D.R. (eds), Wiley, New York, (1984).

12. Sugimoto, T., Adv. Colloid Interface Sci., 28, 65 (1987).

13. Barringer, E.A., and Bowen, H.K., Langmuir, 1, 414 (1985).

14. Barringer, E.A., and Bowen, H.K., J. Am. Ceram. Soc., 65, C-199 (1982).

15. Look, J-L., Bogush, G.H., and Zukoski, C.F., Faraday Discuss. Chem. Soc., 90, 345 (1990).

16. Look, J-L., and Zukoski, C.F., J. Am. Ceram. Soc., 75(6), 1587 (1992).

17. Look, J-L., and Zukoski, C.F., Colloidal Stability and TiO_2 Precipitate Morphology: Influence of short Range Repulsions, to be published.

18. Mates, T.E., and Ring, T.A., Colloids and Surfaces, 24, 229 (1987).

19. Jean, J.H., and Ring, T.A., Colloids and Surfaces, 29, 273 (1988).

20. Jean, J.H., and Ring, T.A., Mat. Res. Soc. Symp. Proc., 73, 85 (1986 MRS).

21. Jean, J.H., and Ring, T.A., Langmuir, 2, 251 (1986).

22. Look, J-L., and Zukoski, C.F., Shear Induced Aggregation During the Precipitation of Titanium Alkoxides; to be published.

23. Harris, M.T., and Byers, C.H., J. Non-Crystalline Solids, 103, 49 (1988).

24. Harris, M.T., Byers, C.H., and Brunson, R.R., 'Hydrolysis and Condensation Kinetics for Liquid-Phase Tetraethylorthosilicate Reactions in Alkaline-Alcohol Solvents', AICHE Annual Meeting in New York (November 15-20, 1987).

25. Bailey, J.K., and Mecartney, M.L., Mat. Res. Soc. Symp. Proc., 180, 153 (1990).

26. Dislich, H., and Hussman, E., Thin Solid Films, 77, 129 (1981).

27. Brinker, C.J. and Scherer, G.W., 'Sol-Gel Science: The Physics and Chemistry of Sol-Gel Processing', Academic Press, CA, Chapter 14, (1990), 839 (Chapter 14).

28. Yau, W.W., Chemtracts - Macromolecular Chemistry, 1, 1, (1990).

29. "KLUCEL, Hydroxypropyl Cellulose, Physical and Chemical Properties",

Aqualon Company, subsidiary of Hercules, Inc. (1981). In a personal communication, it was revealed that the silica powder size was 10 nm.

30. Nagpal, V.J., and Davis, R.M., "A Dynamic Light Scattering Study of Micelle Formation in Solutions of Poly(2-ethyl-2-oxazoline-dimethylsiloxane) in Water-Isopropanol Mixtures", submitted to Langmuir.

32. Yamakawa, H., Modern Theory of Polymer Solutions, Harper and Row, New York (1971).

33. Davis, R.M., Macromolecules, 24, No.5, 1149 (1991).

34. Hiemenz, P.C., Polymer Chemistry, Marcel Dekker, New York (1984).

35. (a) L.H. Edelson and A.M. Glaeser, J. Am. Ceram. Soc., 71, (1988) 225. (b) L.H. Edelson and A.M. Glaeser, J. Am. Ceram. Soc., 71, C-198, (1988).

36. Wang, Q.J., Moss, S.C., Shalz, M.L., Glaeser, A.M., Zandbergen, H.W., and Zschack, P., Physics and Chemistry of Finite Systems: From Clusters to Crystals, Vol II, Kluwer Academic Publishers, The Netherlands, 1287, (1992).

37. 'Lange's Handbook of Chemistry', J.A. Dean, (ed), McGraw Hill, New York, (1985).

38. Cohen Stuart, M. A., Fleer, G. J., and Scheutjens, J. M. H. M., Journal of Colloid and Interface Science, 97, 515 (1984).

39. Buscall, R. and Ottewill, R.H., 'Polymer Colloids', edited by R. Buscall, T. Corner, and J.F. Stageman, Elsevier Applied Science Publishers, London, Chapter 5, (1985).

40. Napper, D.H., 'Polymeric Stabilization of Colloidal Dispersions', Academic Press, (1983).

41. O'M Bockris, J. and Reddy, A.K.N., 'Modern Electrochemistry', Volume 1, Plenum Press, New York, (1970).

42. O'Brien, R.W. and White, L.R., Trans. Faraday Soc. II, 74, 1607, (1978).

43. Hunter, R.J., 'Zeta Potential in Colloid Science, Principles and Applications', Academic Press, San Diego, (1981).

44. Koopal, L.K. and Lyklema, J., Disc. Faraday Soc., 59, 230, (1975).

Chapter 3

The Effects of Solvent Composition on the Growth of Titania Particles by a Sol-Gel Process.

Introduction

Solvent Effects

Sol-gel reactions of metal alkoxides can be carried out in a variety of solvents for the purpose of making metal oxide gels and powders. The properties of the resulting metal oxides, i.e., morphology and domain size, depend to some extent upon the solvents in which the reactions are performed. Solvent effects on the reactions of titanium alkoxides have been reported by several investigators [1-3]. These studies report the effect of alcoholic solvents on the chemical modification of titanium alkoxides due to alcoholysis. Alcohol interchange reactions occur when alkoxides are dissolved in alcohols other than the parent one [4]. Alcohol interchange strongly affects hydrolysis and condensation reactions. For instance, titanium isopropoxide $Ti(OPr^i)$ forms $Ti(OAm^t)_4$ when it is dissolved in tertioamylic alcohol ($OHAm^t$). Hydrolysis of $Ti(OPr^i)$ is very rapid, giving polydispersed powder whereas $Ti(OAm^t)$ leads to stable sols [3]. Alcohol interchange also occurs when tetraethylorthotitanate, TEOT, is dissolved in alcohols other

than ethanol. For instance, Harris *et al.* [1] studied the formation of titania particles due to the hydrolysis and condensation of TEOT in ethanol, 1-butanol, and tert-butyl alcohol. Spherical particles were formed in ethanol and 1-butanol whereas titania precipitates formed in tert-butyl alcohol had no regular shape due to gel formation.

The addition of a nonreactive, non-alcoholic solvent does not affect the structure of the titanium alkoxide but can affect the particle growth by changing the solvent environment in which the hydrolysis and condensation reactions occur. There are no reported studies on the effect of non-alcoholic solvents on the hydrolysis and condensation of titanium alkoxides. The purpose of this paper is to study the effect of an organic additive on particle formation when TEOT undergoes hydrolysis and condensation in a mixture of ethanol and tetrahydrofuran, THF. Particles were grown in the presence and absence of a soluble polymer, hydroxypropylcellulose, HPC, that served as an in-situ steric stabilizer and limited final particle size. THF was chosen as an organic additive since it is miscible with ethanol and water and dissolves HPC readily, a prerequisite for steric stabilization which will be discussed in more detail after a review of solvent effects on the hydrolysis and condensation reactions of metal alkoxides.

Some studies have been reported on the effect of solvent composition on the reactivity of silicon alkoxides [5-8]. The work most relevant to the present study was reported by Artaki *et al.* who investigated the effect of organic additives on the hydrolysis and condensation of silicon tetramethoxide, TMOS, under neutral conditions [6]. These reactions involve nucleophilic substitution as shown below in scheme I for a

alkoxide in a figure taken from [5]:

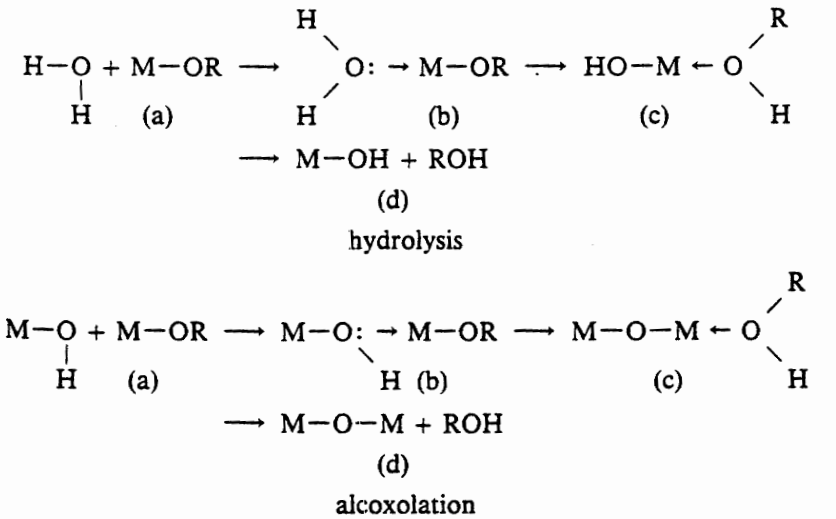

Scheme 1

The reactions in the work by Artaki *et al.* were carried out in 1:1 volume

of methanol/organic solvents. The presence of organic diluent had a dramatic effect on the hydrolysis and condensation on TMOS due to hydrogen bonding and electrostatic interactions between the solvents and the hydrolyzed species. Particle growth was fastest in the presence of weakly hydrogen bonding solvents like dioxane and acetonitrile and slowest in the strongly hydrogen bonding solvents like methanol. Since the reaction scheme of TEOT in presence of water is also nucleophilic substitution [5b], the findings of Artaki's work may also be applied to TEOT reactions.

Steric Stabilization

Steric stabilization occurs due to the mutual repulsion of colloidal particles covered with adsorbed polymer. This is accounted for in the modified DLVO theory of colloid stabilization [9,10]. To prevent coagulation into the primary minimum, steric repulsive forces, in combination with repulsive electrostatic forces if present, must generate a kinetic barrier to flocculation caused by attractive van der Waals forces. For a given set of particle growth conditions, a secondary minimum may form leading to secondary flocculation that can affect TiO_2 particle formation if the minimum occurs when reactive species are still condensing onto the particles' surfaces. In such a case, the weakly flocculated particles may become welded together by partially condensed species that adsorb and subsequently condense. This was demonstrated by Look and Zukoski who studied TiO_2 particle formation where electrostatic stabilization was dominant [11].

For effective steric stabilization against coagulation, the particle surface must be

sufficiently covered with adsorbed polymer. In addition, the adsorbed layer must be sufficiently thick and the polymer solubility must be sufficiently high to generate repulsive steric forces. Ring *et al.* first demonstrated that HPC was an effective in-situ steric stabilizer for TiO_2 particles grown in ethanol by the reactions shown above. The polymer adsorbs onto the TiO_2 particles as they nucleate and aggregate, ultimately limiting the aggregate size [12, 13]. Ring established that HPC adsorbed and reached saturation on the TiO_2 particle surface at a plateau polymer concentration of 1.7 g l^{-1} for HPC with a nominal molecular weight of 60 kg/mole. This concentration gave a minimum particle size.

The work described in Chapter 2 demonstrated that the water concentration had a dramatic effect on the rate of formation and ultimate size of TiO_2 particles formed in ethanol in the presence of HPC [14]. For particles grown at a fixed TEOT concentration of 0.075M and at neutral pH, the size decreased drastically with increasing water concentration, defined as R = [water]/[TEOT]. For example, at C_p = 1.7 g l^{-1} of HPC E, the average particle size decreased from 350 nm at R = 5.3 to 70 nm at R = 60. The principal effects of water concentration were two-fold. Water was shown to segregate at TiO_2 surface and to promote HPC adsorption through enhanced hydrogen bonding. The greater amount of adsorbed HPC led to increased steric repulsion between TiO_2 particles, yielding smaller particle sizes. Secondly, the overall nucleation rate increased markedly with increasing water concentration as can be seen from reactions 1 and 2 above. It is generally observed that an increasing nucleation rate, when coupled with sufficient

particle stabilization, leads to smaller final particle size. Charge effects on the TiO_2 particles and the effect of water concentration on the solubility of HPC played a relatively minor role in particle stabilization. Particles grown in the presence of HPC had a granular surface morphology strongly suggesting that TiO_2 particles initially 20-30 nm in size flocculated into a secondary minimum and were then welded together to form permanent aggregates due to subsequent condensation reactions. Detailed calculations of the DLVO potential energy curves are precluded by the lack of a model that accounts for the kinetics of the HPC adsorption rate and the establishment of a steric layer during reactions 1 and 2.

In all of this previous work with HPC, the liquid phase composition was changed with the addition of water which was one of the reactants. The purpose of the present work is to study particle formation when the liquid phase composition is affected by the addition of the inert diluent THF which does not directly take part in the chemical reaction. This diluent profoundly affects particle growth and, in the presence of HPC, leads to dispersed particles where the smallest size observed had mean diameters of 50 nm.

Experimental

Materials

Tetraethylorthotitanate, TEOT, (95 weight % TEOT, 5% ethanol) was obtained from the Alfa Chemical Company and was used as received. Anhydrous ethanol, 200

proof, was obtained from the Aaper Alcohol and Chemical Company. Anhydrous tetrahydrofuran (water < 50 ppm) was obtained from Aldrich Chemical Company in a Sure/Seal™ bottle. Hydroxypropylcellulose, HPC, was kindly donated by the Aqualon Company, a subsidiary of Hercules Incorporated. The nominal molecular weight used in this study was 60 kg $mole^{-1}$ (lot # 6684) with the designated grade E. This was the same sample used in a previous study [14] where the molecular weight distribution was analyzed by gel permeation chromatography giving the following: number average molecular weight M_n = 40 kg $mole^{-1}$, weight-average M_w = 68.5 kg $mole^{-1}$, intrinsic viscosity $[\eta]$ = 82 $cm^3\ g^{-1}$. The HPC samples were dried in a vacuum oven at room temperature for about 4 hours and then at 100°C for about 20 hours prior to their use in the particle growth experiments. Homogeneous, gel-free stock solutions of HPC in anhydrous ethanol were prepared with typical concentrations of 0.2 g l^{-1} by stirring at room temperature for twenty four hours. Deionized water with a resistivity of 16-18 x 10^6 ohm-cm was used in all of the experiments. Fisher-certified 50% hydrogen peroxide and concentrated sulfuric acid (~ 36 N) were obtained from Fisher Scientific and were used as received to study the conversion of TEOT to TiO_2. All glassware was cleaned first with a detergent and then soaked in a saturated solution of alcoholic KOH for 24 hours followed by soaking in 2 M HCl solution for another 24 hours. This was followed by washing thoroughly with tap water and finally washed 4 times with deionized water. The glassware was then dried thoroughly in air in a laminar flow hood for at least two days before being used for experiments.

Mixing Procedures

For particle synthesis, equal volumes of solutions of TEOT in ethanol, denoted as solution A, and a solution of HPC in ethanol, THF, and water, denoted as solution B, were mixed rapidly and shaken for 5 seconds and were then allowed to sit quiescently for 24 hours before the particles were analyzed. Solution A consisted typically of a 5 ml mixture of TEOT and anhydrous ethanol mixed in a nitrogen glove bag to prevent premature hydrolysis of the TEOT by atmospheric moisture. Solution B consisted typically of a mixture of an HPC stock solution, water, and varying amounts of THF such that the volume of solution B was constant at 5 ml. Hence, solution B consisted of 0-5 ml THF and, correspondingly, 5-0 ml ethanol - volume of the water was insignificant. The maximum THF concentration, 5 mls THF + 5 mls ethanol, is expressed as 1:1 THF:ethanol on a volume basis. Henceforth, "pure ethanol" will refer to ethanol/water mixtures without any THF. THF was withdrawn from the Sure/Seal bottle using a glass syringe. Before the withdrawal, some dry nitrogen was first injected into the bottle to maintain a positive pressure within the bottle to avoid air contamination. Both solutions A and B were filtered through a 0.2 micron Gelman Acrodisc™ PTFE filter. For the purpose of measuring particle growth by dynamic light scattering, the reaction mixture was filtered again through a 0.2 micron filter just after mixing solutions A and B. The polymer-free control samples were grown at a water concentration $R(=[H_2O]/[TEOT]) = 4.5$ and at a TEOT concentration of 0.041 M. The samples grown in the presence of HPC were grown at water concentration of $R = 5.5$ and at a TEOT

concentration at 0.04 M. Prior to making stock solutions and samples, all glassware was purged 4 or 5 times with dry nitrogen in a glove bag.

Electron Microscopy

The TiO_2 particles size and state of agglomeration were determined by transmission electron microscopy, TEM, with a Philips 420T Scanning Transmission Electron Microscope. Samples were prepared by taking a drop of suspension on a copper grid coated with carbon. Suspension consisting of particles grown in 1:1 THF/ethanol mixture in HPC was first diluted in ethanol (about 10 times) and a drop of this diluted suspension was taken on a copper grid.

Dynamic Light Scattering

The TiO_2 particle growth rate was measured by dynamic light scattering as a function of HPC and THF concentrations. The effect of solvent composition on the hydrodynamic diameter of HPC was also measured to determine the qualitative effect of solvent composition on the solubility of HPC. The hydrodynamic diameter, D_h, was measured with a Brookhaven model 2030AT variable angle dynamic light scattering machine equipped with a digital correlator with 136 channels and a Lexel 95-2 argon ion laser operated at a wavelength of 514.5 nm. Measurements were made at a scattering angle of 90° and a temperature of 25.0 $\pm$ .1°C. The hydrodynamic diameters were calculated using the second cumulants method described elsewhere [15]. For the particles

grown in HPC, the measurements were conducted at a fixed polymer concentration of C_p = 1.7 g l^{-1}. Refractive index of THF/ethanol mixtures were measured using a Bellingham & Stanley Abbe refractometer model 60/ED. The viscosities were measured using a Cannon Ubbelohde capillary viscometer in a water bath at 25°C.

Extent of Conversion of TEOT

The extent of conversion of the TEOT after 24 hours was determined by measuring the amount of soluble titanium species in solution by a spectrophotometric method using hydrogen peroxide [16]. Titanium ions form a yellow complex with hydrogen peroxide $[TiO.H_2O_2]^{2+}$ which can be detected by spectrophotometry at a wavelength of 410 nm. The soluble species was separated from the particles by centrifugation at 26,000 g for 10 minutes. The clear supernatant containing HPC was filtered through a 0.2 micron filter whereas the polymer free control samples were filtered through an Gelman Acrodisc PTFE 0.02 micron filter.

Results and Discussion

Polymer-Free Control

Final Particle Size

In the absence of any stabilizing HPC, large agglomerates of TiO_2 were obtained as seen in the TEM micrographs in Figure 3.1 of particles grown in ethanol (a) and in a 1:1 THF:ethanol mixture (b) after 24 hours.

(a)

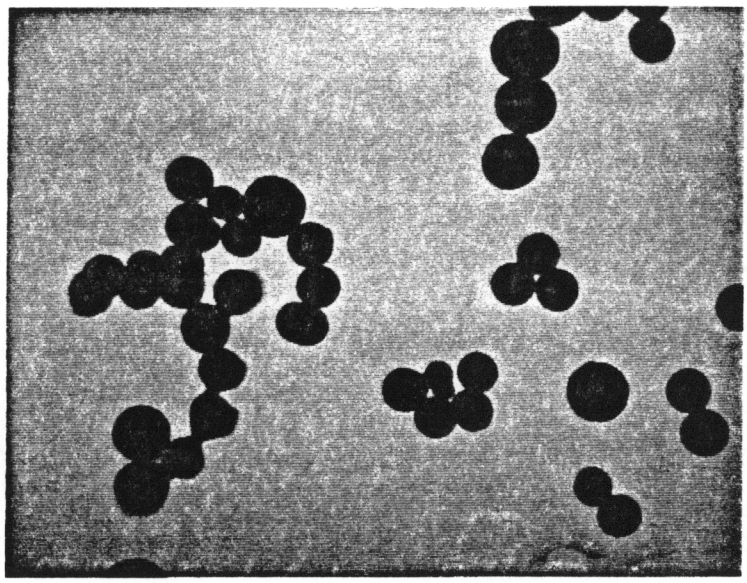

2 μm

(b)

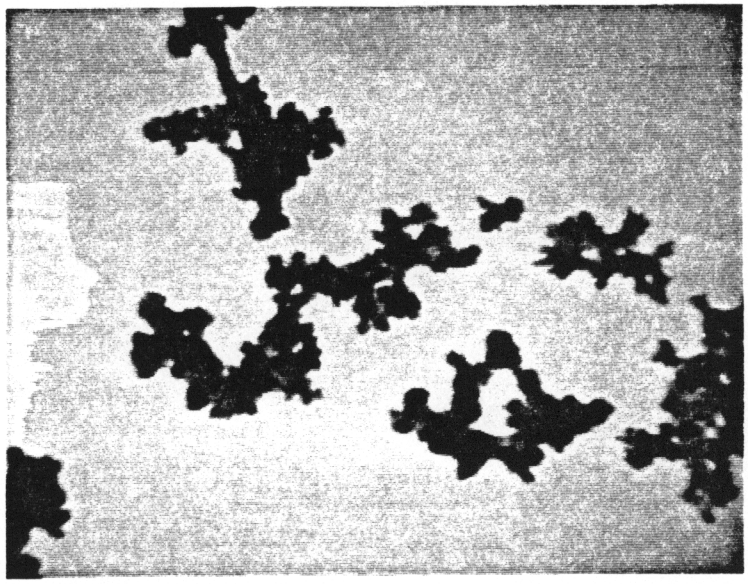

2 μm

Figure 3.1. Transmission electron micrographs of TiO_2 particles grown without HPC at [TEOT] = 0.041 M, and R (=[Water]/[TEOT]) = 4.5 : (a) particles grown in ethanol; and (b) particles grown in a 1:1 THF:ethanol volume mixture.

(c)

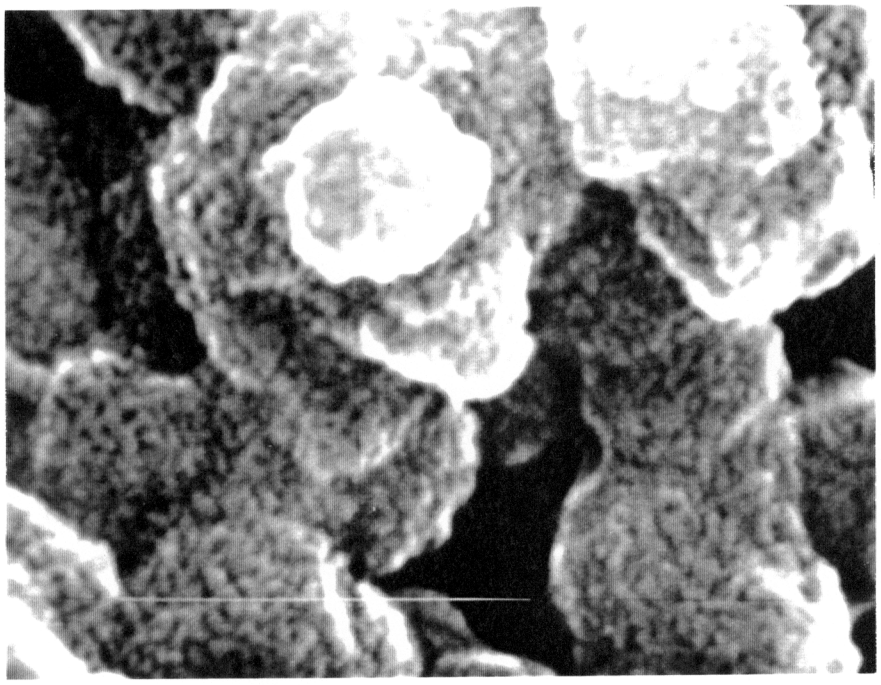

Figure 3.1. (c) Scanning electron micrograph of TiO_2 particle surface grown without HPC at [TEOT] = 0.041 M, R = 4.5, and 1:1 THF:ethanol volume mixture.

The size of the primary particles forming the aggregates was smaller when the particles were grown in the presence of THF. For instance, the size of primary particles range between 500 to 1000 nm when grown in ethanol whereas they range between 60 to 80 nm when grown in a mixture of 1:1 THF:ethanol. The primary particle sizes obtained with added THF are smaller because they formed at a higher nucleation rate which is discussed in the next section. A high resolution micrograph of the surface of the particles grown in 1:1 THF:ethanol, shown in Figure 3.1(c), shows the same type of slightly grainy morphology as was observed earlier for particles grown just in ethanol in the absence of HPC [14]. The aggregated particles reflect the balance of attractive Van der Waals forces and repulsive electrostatic forces acting between the particles. Both of these forces depend upon solvent properties which are affected by the concentration of THF. The most important solvent properties affecting colloid stability are the refractive index and dielectric constant.

The magnitude of attractive Van der Waals forces between the suspended TiO_2 particles is governed by the Hamaker constant which increases with the difference between the refractive index of solvent and particles [17]. The THF:ethanol solvent system has a refractive index (1.373 for the 1:1 THF:ethanol system) closer to that of TiO_2 (between 1.62-2.1 from [14]) than does pure ethanol as listed in Table 3.1. Thus, TiO_2 particles in the THF:ethanol mixtures experience weaker Van der Waals attractive forces than in pure ethanol. This raises the primary maximum in the potential energy diagram given by the modified DLVO curve and suppresses coagulation. However,

secondary flocculation may still occur as discussed previously.

The dielectric constant ϵ can affect the interparticle electrostatic forces by affecting both the degree of charge at the particle surface and the range of electrostatic forces given by the Debye length, κ^{-1}, which is proportional to $\epsilon^{0.5}$ [18]. The dielectric constant of THF is less than that of ethanol as seen in Table 3.1 and thus the addition of THF to the reaction medium should reduce the Debye length and suppress electrostatic effects. In our earlier electrophoresis studies [14], TiO_2 particles were found to be positively charged when grown at R = 5.3 in ethanol with no THF due to protonation of the Ti-OH surface groups. However, the particle zeta potential in the absence of HPC, $\sim$ +20 mV corresponding to an electrophoretic mobility of 1 x 10^{-9} m^2 v^{-1} s^{-1}, was not sufficient to prevent the formation of large, irregular aggregates as is clear from Figure 3.1(a). While the effect of THF on the degree of protonation of the Ti-OH groups was not measured, it is clear from Figure 3.1(b) that electrostatic effects alone were not sufficient to prevent the formation of permanent aggregates in the presence of THF.

Table 3.1

Solvent Properties

Solvent	Refractive Index* n	dielectric constant* ϵ	δ_h**, $Mpa^{1/2}$
Ethanol	1.361	24.3	19.4
THF	1.405	7.3	8.0
1:1 THF:ethanol	1.373[a]		
Water	1.332	78.3	42.3

[a] Experimentally measured by Abbe Refractometer

* From reference [19b]

** Hansen solubility parameter for hydrogen bonding effects [19a]

Growth Rate

Figure 3.2 shows that THF had a dramatic effect on the growth of particles as measured by dynamic light scattering. The growth curves are marked 0, 1, 2, 3, 4, and 5 corresponding to the amount of THF in mls present in the reaction mixture. The particle growth rate was slowest for pure ethanol system and the growth rate increased with THF concentration. For example, the growth rate for curves 0, 2, and 5 were 13,

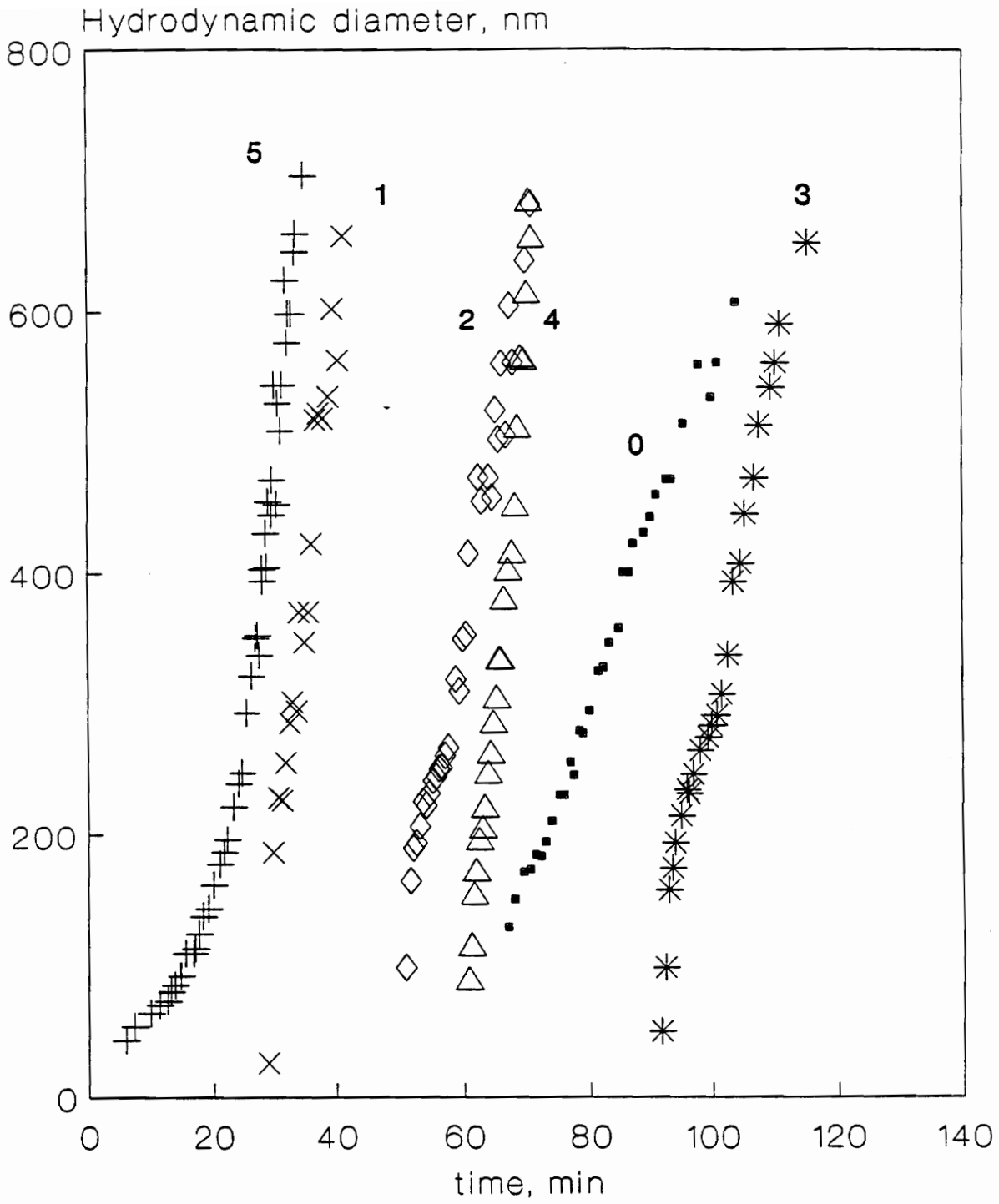

Figure 3.2. Growth rate study by dynamic light scattering of the particles grown in the absence of HPC and varying THF concentration; [TEOT] = 0.041 M, and R = 4.5: curves 0, 1, 2, 3, 4, and 5 are the growth rate curves when the particles were grown in 0, 1, 2, 3, 4, and 5 ml of THF and rest ethanol for the total volume of 10ml.

29, and 49 nm/min, respectively. In curves 2 to 4, the initial growth regime shows a non-linear behavior which was highly reproducible.

The growth curve in Figure 3.2 for 1:1 THF:ethanol (curve 5) has two regimes, similar to those observed by Harris *et al.* [1] when particle growth occurred from TEOT in tert-butanol. The initial slow growth regime was caused by a very high initial nucleation rate caused by the added THF. This generated a high concentration of relatively small aggregates (20 nm) early in the reaction (induction time about 6 minutes) as seen in curve 5. Conversely, for no added THF the minimum observable size by DLS was ~ 129 nm and the induction time was ~ 67 minutes as seen in curve 0. The small aggregates in curve 5 were colloidally unstable and thus the growth rate increased markedly after about 25 minutes due to aggregation enhanced by high particle concentration, i.e. the collision frequency was high. Another factor leading to higher growth rates with added THF is the lower viscosity of the THF:ethanol system compared to ethanol as seen in Table 3.2. This led to an increase in the diffusion rate of the condensing species and unstable aggregates [5].

Table 3.2

Solution Properties of Hydroxypropylcellulose, HPC, and Extent of Conversion of Tetraethylorthotitanate, TEOT

THF:Ethanol Volume Ratio	HPC Concentration g l^{-1}	Viscosity (mPa s)[1]	HPC Hydrodynamic diameter[2], nm	% Conversion of TEOT[3]
0:10	0	1.078	---	49
5:5	0	0.58	---	99
0:10	1.7	1.32	30	48
5:5	1.7	1.08	20	99

[1] measured by an Ubbelohde capillary viscometer at 25°C

[2] from second cumulants method by dynamic light scattering at a scattering angle of 90° at 25°C

[3] measured by the H_2O_2 method after 24 hours at room temperature

The increase in nucleation rate with added THF is primarily due to the changes in the hydrogen bonding capability of the solvent which is best characterized by the Hansen solubility term for hydrogen bonding, δ_h [19a]. Table 3.1 lists value of δ_h for

ethanol, THF, and water. Ethanol is a protic solvent capable of forming strong hydrogen bonds with water and partially hydrolyzed TEOT species Ti-OH. As a result of this hydrogen bonding, the nucleophilicity (activity) of water is reduced which retards both the hydrolysis and condensation reactions in scheme's 1 and 2. Also, the effective network of strong intermolecular hydrogen bonding could provide a network which shields or sterically hinders the reactant molecules, thereby reducing their ability to diffuse and participate in the condensation reaction [6].

On the other hand, aprotic THF forms considerably weaker hydrogen bonds than ethanol. Hence, the effective hydrogen bonding of water in the THF:ethanol system would be less than in pure ethanol. This leads to an increased nucleophilicity (activity) of water. The reduction in the extent of hydrogen bonding would also lead to a reduction in the steric hindrance of the reacting species. Hence, the diffusion of the condensing species through the bulk on the surface would be facilitated which ultimately would lead to an increase in the particle growth.

Further evidence for the increase in the forward reaction rates in the hydrolysis and condensation comes from the conversion data as seen in Table 3.2. The conversion was measured after 24 hours of the reaction by the hydrogen peroxide method [16]. Zukoski *et al.* [20] have shown that the conversion of TEOT in pure ethanol after 24 hours of reaction is close to equilibrium conversion for [TEOT] = 0.05 M and R = 5. The increase in conversion in the case of a 1:1 THF:ethanol system implies that THF acts as a catalyst in the reaction by increasing the activity of water. HPC had no effect

on the equilibrium conversion which is consistent with earlier findings in ethanol [14]. Finally, given reaction scheme's 1 and 2, Le Chatelier's principle implies that replacement of ethanol with THF promotes the forward reactions.

Another reason for the increase in growth rate in THF:ethanol system is the likely effect of THF concentration on the solubility of partially hydrolyzed and condensed species from the reactions of TEOT. Since ethanol has a considerably higher value of δ_h than does THF, it is very likely that a THF:ethanol mixture is not as good a solvent as is ethanol for the low molecular weight, partially hydrolyzed and condensed soluble species. Lower solubility means that these soluble species would more readily phase separate from a THF:ethanol mixture, leading to a lower critical nuclei size and concentration at which the nucleation occurs. These low molecular weight species should precipitate out of solution earlier than in the ethanol system. This is supported by the observation in Figure 3.2 that particles as small as 20 nm were measured in the 1:1 THF:ethanol mixture whereas the smallest size measured in pure ethanol system was about 129 nm.

The time of onset of detectable particles for curves 2 to 4 does not vary with the THF concentration in a regular pattern. The scattering intensity, I, which must have a certain minimum value for detection by the photomultiplier, varies as $\sim N_p R^6$ for spherical particles at a fixed wavelength and scattering angle where N_p is the number concentration of scattering particles and R is the particle radius [21]. The lack of a consistent trend in onset time reflects the complex interplay between the factors discussed

above that change N_p and R as the THF concentration changes. The non-linear initial growth regime seen in curves 2 to 4 could also be due to these complex changes. However, when the particle growth occurs in the presence of HPC, steric forces dominate particle growth and consistent trends in both onset time and growth rate are seen as discussed in the following section.

Particles grown in the presence of HPC.

Figure 3.3 shows that particles grown in the presence of HPC in ethanol and in 1:1 THF:ethanol mixture are much more dispersed and have a much smaller size than particles grown without HPC. At an HPC concentration of 1.7 g l^{-1}, the particle size was ~ 350 nm when grown in pure ethanol whereas it was ~ 50 nm (some agglomerates of ~ 100 nm size were also observed) when grown in the 1:1 THF:ethanol mixture. Figure 3.4 shows hydrodynamic diameter D_h versus time curves when the particles were grown solutions of HPC with a concentration of 1.7 g l^{-1}. The curves are labelled as 0p, 2p, 3p, 4p, and 5p corresponding to 0, 2, 3, 4, and 5 ml THF in the presence of HPC. The curve for 1 ml added THF was deleted for the sake of clarity. All the curves in Figure 3.4 have two regimes: the linear initial growth regime after which the growth curve bends and plateaus. The bend in the linear growth curve marks the onset of significant colloid stabilization due to the steric forces generated by adsorbed HPC at the particle surface. This shape of the growth curve was consistent with the one observed in our earlier work [14] when the particles were grown in HPC in ethanol. It is also observed

(a)

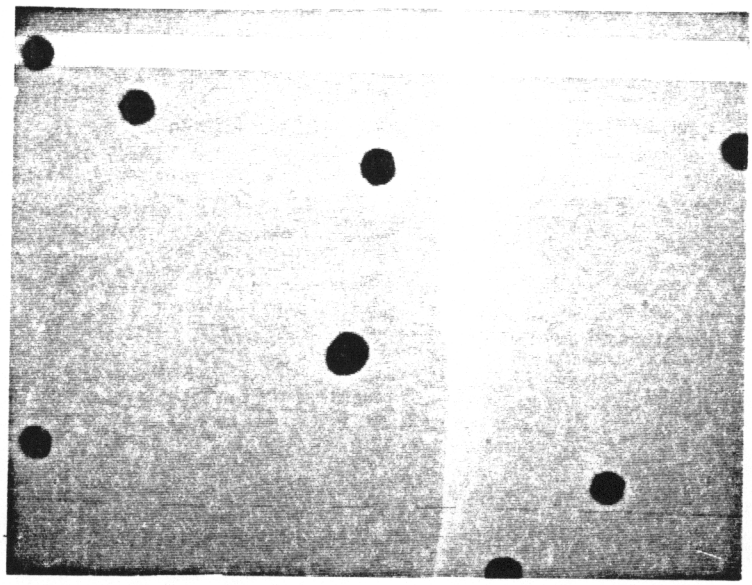

(b)

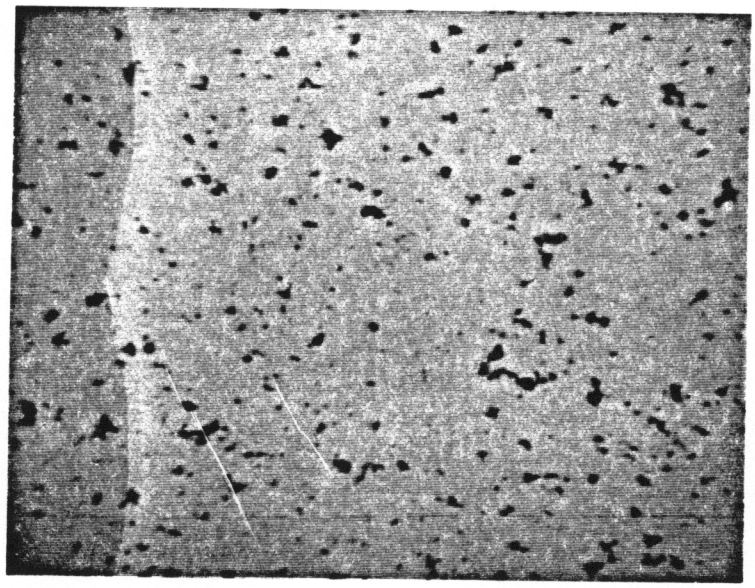

Figure 3.3. Transmission electron micrographs of TiO_2 particles grown in the presence of HPC at C_p = 1.7 g/l, [TEOT] = 0.04 M, and R = 5.5 : (a) particles grown in ethanol; and (b) particles grown in 1:1 THF:ethanol volume mixture.

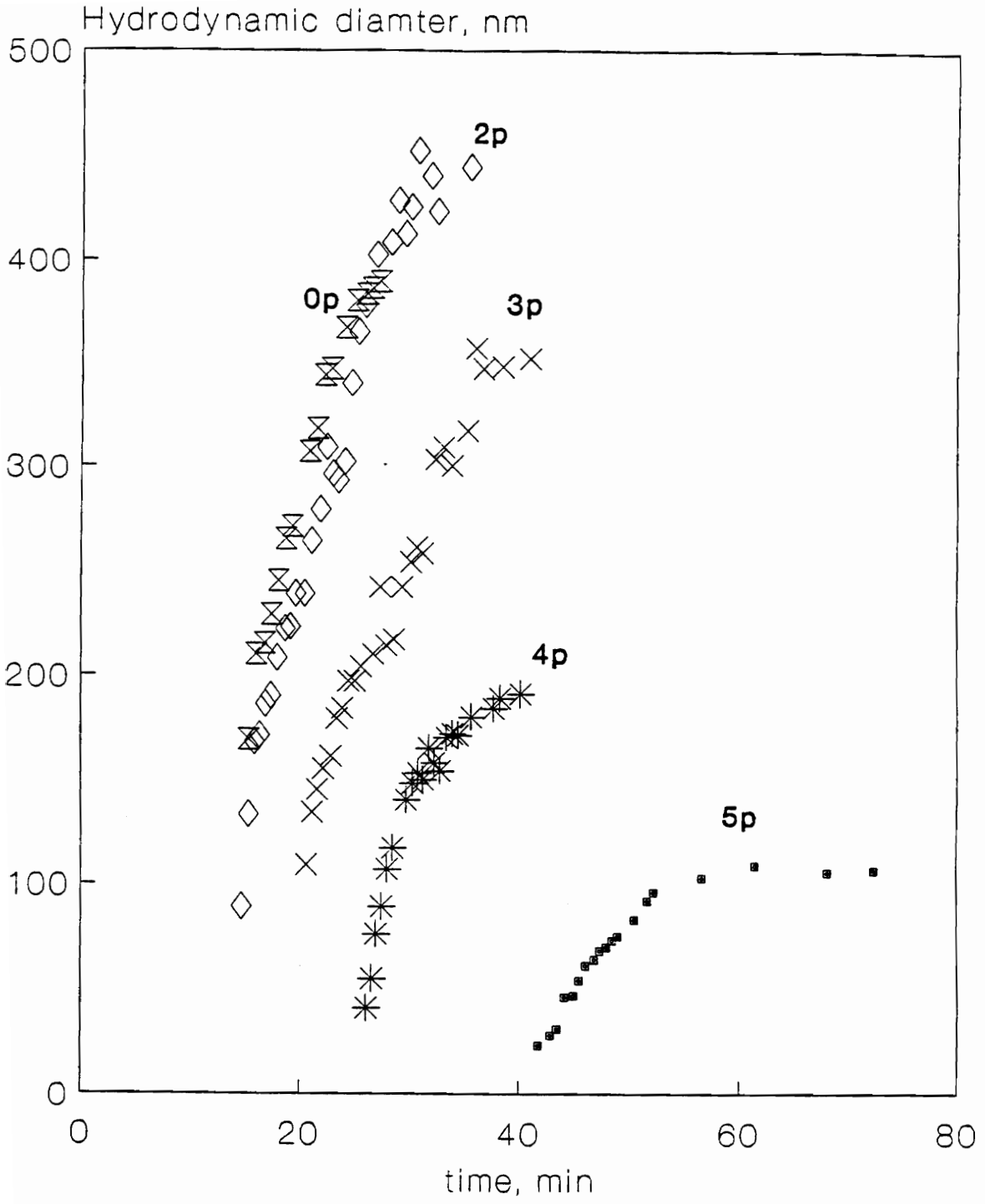

Figure 3.4. Growth rate study by dynamic light scattering of the particles grown in the presence of HPC and varying THF cocentration; [TEOT] = 0.04 M, and R = 5.5: curves 0p, 2p, 3p, 4p, and 5p are the growth curves when the particles were grown in 0, 2, 3, 4, and 5 ml THF and C_p = 1.7 g/l.

that the bend occurs at smaller particle size with increasing THF concentration, e.g. the bend occurs at $D_h \sim 380$ nm in ethanol whereas it occurs at $D_h \sim 100$ nm in the 1:1 THF:ethanol mixture. In general, the growth rate in HPC solutions was slower than in the polymer-free cases. For the 1:1 THF:ethanol mixture, the growth rate in the polymer-free case was 49 nm/min after 25 minutes whereas it was 7 nm/min (linear regime) in the presence of HPC.

From Table 3.2, the hydrodynamic diameter of HPC is less in the 1:1 THF:ethanol mixture than in ethanol which implies that HPC is less soluble in mixtures of THF:ethanol. This reduction in HPC solubility should lead to an increase in HPC adsorption at the particle surface [22]. Evidence for this comes from Figure 3.4 where the bend in the growth curve occurs at a lower particle size with increasing THF concentration as seen in curves 3p, 4p, and 5p. Greater HPC adsorption with increasing THF concentration would lead to greater steric stabilization at a smaller particle size. Also, the higher adsorbed amounts of polymer would shield the particle surface from the condensing species, thus decreasing the overall particle growth rate with increasing THF concentration. This would also explain the increase in the time of onset of detectable particles (induction time) increased when the THF:ethanol ratio was greater than 2:8. For example, the induction time was 15, 21, 26, and 42 minutes for volumes of added THF of 0, 3, 4, and 5 mls, respectively.

Conclusions

The addition of tetrahydrofuran, THF, to reacting solutions of tetraethylorthotitanate, TEOT, in water and ethanol had a significant affect on the growth of TiO_2 particles. This is seen both in the presence and absence of the polymer hydroxpropylcellulose, HPC, which served as an in-situ steric stabilizer. In the absence of HPC, no colloid stabilization was observed. In the presence of HPC and THF, dispersed particles with a typical diameter of 50 nm were obtained. Particle growth rates were markedly higher in a 1:1 volume mixture of THF:ethanol than in pure ethanol. The primary reason for this increase is the decrease in the hydrogen bonding capability of the solvent system with the addition of THF. This increased the activity of the water leading to faster hydrolysis and condensation rates which yielded higher nucleation rates. The addition of THF to the reaction medium also resulted in a decrease in the solvent viscosity which promoted the diffusion of oligomeric species and a decrease in the magnitude of the attractive Van der Waals forces. The addition of THF may also have resulted in a decrease in the solubility of partially hydrolyzed and condensed oligomeric species which would also contribute to an increase in the nucleation rate. Particle growth in HPC was significantly slower than in the polymer-free cases due to polymer adsorption on the particle surface. Stabilization was greatly enhanced with increasing THF concentration. These results suggest that the proper choice of solvent medium and a stabilizing polymer may provide a practical route to the synthesis of sub-100 nm metal

oxides from alkoxide precursors.

References

[1]. M. T. Harris and C. H. Byers, J. Non-Crystalline Solids, 103 (1988) 49-64.

[2]. M. Nabavi *et al.*, J. Non-Crystalline Solids, 121 (1990) 31-34.

[3]. Livage *et al.*, MRS Bulletin, XV(1) (1990),18-25.

[4]. J. Livage, M. Henry, and C. Sanchez, Prog. Solid State Chem. 18 (1988) p.259.

[5]. Brinker, C.J. and Scherer, G.W., 'Sol-Gel Science: The Physics and Chemistry of Sol-Gel Processing,' Academic Press, CA, 1990, (a) Chapter 3; (b) Chapter 2.

[6]. I. Artaki, T.W. Zerda, and J. Jonas, J. Non-Crystalline Solids 81 (1986) 381-395.

[7]. G. Orcel and L.L. Hench, J. Non-Crystalline Solids 79 (1986) 177-194.

[8]. L.L. Hench *et al.*, in Better Ceramics Through Chemistry II, eds. C.J. Brinker, D.E. Clark, and D.R. Ulrich (Mat. Res. Soc., Pittsburgh, Pa., 1986).

[9]. Polymeric Stabilization of Colloidal Dispersions, edited by Napper, D.H., Academic Press, 1983.

[10]. R. Buscall, and R.H. Ottewill, in Polymer Colloids, edited by R. Buscall, T. Corner, and J.F. Stageman, Elsevier Applied Science Publishers, London, Chapter 5, (1985).

[11]. J-L. Look, and C.F. Zukoski, Colloid Stability and TiO_2 Precipitate Morphology: Influence of Short Range Repulsions, to be publihed.

[12]. J.H. Jean, and T.A. Ring, Mat. Res. Soc. Symp. Proc. 73 (1986 MRS) 85.

[13]. J.H. Jean, and T.A. Ring, Colloids and Surfaces 29 (1988) 273.

[14]. V.J. Nagpal, R.M. Davis, and J.S. Riffle, "In-Situ Steric Stabilization of Titanium Dioxide Particles Synthesized by a Sol-Gel Process", submitted to Colloids and Surfaces.

[15]. V.J. Nagpal, R.M. Davis, J.S. Riffle, "Dynamic Light Scattering Study of Micelle Formation in Solutions of Poly(2-ethyl-2-oxazoline-dimethylsiloxane) in Water-Isopropanol Mixtures", Submitted to Langmuir.

[16]. Instrumental Methods of Analysis, edited by Willard, H.H., L.L. Merritt, and J.A. Dean, 4th ed., Van Nostrand, Princeton, (1968) p.106.

[17]. Intermolecular and Surface Forces, edited by Jacob N. Israelachvili, Academic Press, CA (1985) Chapter 6.

[18]. R.J. Hunter, Zeta Potential in Colloid Science, Academic Press, CA (1981) p. 364.

[19]. Handbook of Solubility Parameters and Other Cohesion Parameters, edited by A.F.M. Barton, CRC Press, Boca Raton, FL 1983.

[20]. Look, J-L., Zukoski, C.F., J. Am. Ceram. Soc. 75(6) (1992) p. 1587.

[21]. M. Kerker, The Scattering of Light and Other Electromagnetic Radiation, Academic Press, New York (1969).

[22]. Cohen Stuart, M.A., Fleer, G.J., and Scheutjens, J.M.H.M., Journal of Colloid and Interface Science 97 (1984) p.515.

Chapter 4

Chemical Modification of Poly(propylene oxide) Based Polymers For Steric Stabilization

Introduction

Submicron powders find applications in the ceramic industry when high performance materials are required [1]. Monosized spherical particles are precursors for making dense ceramic bodies. Smaller particles lead to close packing and approach the theoretical density of the green body. Sintering time and temperature of the green body can be significantly reduced as the particle size reduces [2]. Synthesis of ceramic particles can be broadly classified as: particles produced in solution (sol-gel technique), and particles produced from solution which includes techniques like aerosols and evaporative decomposition of solutions, and vapor-phase reactions (by flame, plasma, or laser). These techniques have been reviewed by Matijevic and Gherardi [3,4,5]. Sol-gel techniques include particle synthesis from aqueous metal salts and alkoxide precursors. One important advantage of sol-gel process over other processes is it's ability to transform completely from the molecular precursor to the solid material. This permits better control of the entire process and allows the synthesis of tailor-made powders [5]. Bowen and Barringer showed that discrete spherical particles of titanium dioxide can be

synthesized via the hydrolysis and condensation of titanium ethoxide [6,7]. These reactions can be shown as follows:

$$Ti(OC_2H_5)_4 + 4H_2O \rightarrow Ti(OH)_4 \qquad \text{(Hydrolysis)}$$

The condensation reaction can occur by either removal of water (oxolation) or ethanol (alcoxolation). These condensation reactions can be shown as follows:

$$TiOH + TiOH \rightarrow Ti\text{-}O\text{-}Ti + H_2O \qquad \text{(Oxolation)}$$

$$TiOH + TiOR \rightarrow Ti\text{-}O\text{-}Ti + C_2H_5OH \qquad \text{(Alcoxolation)}$$

The resulting TiO_2 precipitates were ultrasonicated to break the floccs into primary particles. The primary particles were then stabilized by washing them with water at pH = 10 to achieve electrostatic stabilization. The mean size of TiO_2 particles achieved was 0.5 microns. Zukoski et al. [8] showed that in-situ electrostatic stabilization can be achieved by growing TiO_2 particles under alkaline conditions. The particles synthesized had mean diameters ranging between 0.15-0.7 microns depending upon the pH and electrolyte concentrations. Electrostatic stabilization is sensitive to any changes in pH or salt concentration since the electrical double layer is compressed at high ion concentrations. Steric stabilization on the other does not suffer from these disadvantages and hence can have wider applications. Ring et al. [9,10] showed that hydroxypropylcellulose (HPC) can be used as an in-situ steric stabilizer to grow dispersed

TiO_2 particles from TEOT by alkoxide chemistry. The lowest average particle diameter was ~ 0.3 microns.

Our previous work [11] in Chapters 2 and 3 built upon Ring's findings and addressed several key issues concerning polymer-particle-solvent interactions during the synthesis of TiO_2 particles. The concentration of water in the reaction medium had a profound effect on the particle size. The nucleation rate, HPC adsorption, and HPC hydrodynamic diameter increased with water concentration. By carefully controlling the HPC and water concentration in the reaction mixture, an average particle size of 0.07 microns was achieved. The effects of the two extreme molecular weights of HPC i.e., Mw=68 Kg/mole and 1150 kg/mole on the particle size were studied. It was found that at low water concentration R(=[TEOT]/[water]) = 5.3, the molecular weights of the HPC studied had no appreciable effect on the particle size suggesting that effective stabilization might be realized with even lower molecular weight. Since relatively pure HPC with molecular weight lower than 68 kg/mole is commercially not available, there was a need to investigate other low molecular weight polymers which could act as steric stabilizers. Our data indicated that the primary mode of HPC adsorption was due to the hydrogen bonding between the hydroxyl groups along the HPC backbone and at the TiO_2 surface. In the case of HPC, this happens because there are on an average 3 hydroxyl groups per repeat unit along the HPC chain and each hydroxyl group has the tendency to hydrogen bond with the hydroxyl group at the surface. The adsorption of homopolymers like HPC at the surface is random, i.e., the adsorption occurs in the form

of trains, loops, and tails [12,13] as shown in Figure 4.1(a). Only the tail and loops of the chain, which stay in solution, contribute to steric stabilization. Since only a fraction of the chain is in the tail and loop form, more efficient use of stabilizing polymer is desirable where the fraction of segments attached as loops or tails is maximized. If the polymer chain has adsorbing groups only at the end of the chain then the adsorption occurs at the particle surface at the chain end. Such an adsorption is termed as terminal attachment [12] and is shown in Figure 4.1(b). In this case, most of the polymer chain remains unadsorbed and stays in solution to form the steric layer. This makes the most efficient use of the polymer and hence relatively low molecular weight homopolymers may be used as steric stabilizers. In general, low molecular weight polymers (Mw $<$ 10 kg/mole) have higher solubility than their higher molecular weight homologues. Hence low molecular weight steric stabilizers can be used in a variety of solvents and therefore have wider applications. In addition, low molecular weight polymers do not affect the suspension viscosity significantly and hence are easy to process.

Vincent et al. [14] stabilized silica dispersions by grafting the triethoxy-terminated poly(ethylene oxide) chains to silica particles having a mean diameter of 162 nm. Silica particles were first grown by the Stober Process and then triethoxysilane terminated poly(ethylene oxide) PEO (Mw = 18000) was added to prevent aggregation. The polymer concentration in the reaction mixture was approximately 0.8 g/l. It was assumed that triethoxysilane terminated PEO chains grafted at silica surface via a condensation reaction between the ethoxy group on PEO and the hydroxy group at silica surface under

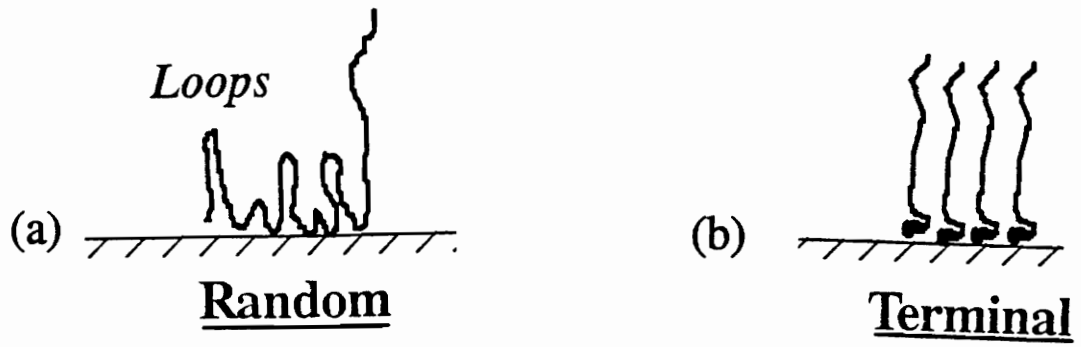

Figure 4.1. Modes of polymer adsorption at the surface.(a) Random adsorption characteristic of homopolymer adsorption. (b) Terminal adsorption occurs as point attachment characteristic of end-functionalized polymer where the adsorption occurs at the end of the chain.

basic conditions. The amount grafted per unit area was significantly higher than physically adsorbed PEO (Mw = 5 x 10^6) on silica particles from aqueous solution and hence it was concluded that a significant fraction of the PEO end grafted.

This work concerns in-situ stabilization of TiO_2 particles where a low molecular weight polymer, commercially known as Jeffamine D2000 with an average molecular weight of 2000, was end-functionalized and used used as a steric stabilizer. The stabilizing polymer adsorbs onto the aggregating particles, ultimately establishing a steric layer that generates repulsive forces that stop aggregation. In-situ steric stabilization is a complex process and is governed by the polymer-particle-solvent interactions which affect the kinetics and thermodynamics of polymer adsorption. Unlike equilibrium adsorption on fully developed surfaces, the adsorption of polymer in this case has to be within the time scales of particle growth which makes the process a challenging one.

The structure of Jeffamine D2000 is shown in Figure 4.2(a). It has a poly(propylene oxide) backbone and carries reactive primary amine groups at each ends which makes it difunctional [15]. A monofunctional form M2000 is also available and is terminated with primary amine at one end. A trifunctional form was also tested structure of which is shown in Figure 4.2(b).

(a)

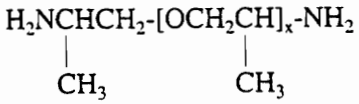

(b)

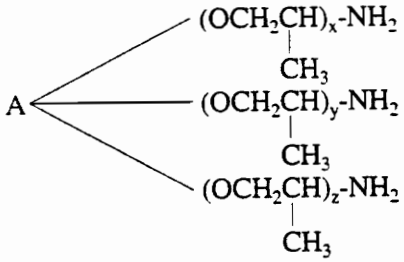

Figure 4.2. Structure of (a) Jeffamine D2000, x = 33; (b) Jeffamine T5000, A = glycerine, (x + y) = 85 mole% poly(propylene oxide).

The amine groups were reacted with isocyanatopropyl triethoxysilane (i-CPTS) to obtain tri-ethoxy silane groups at the chain ends. This is shown in the reaction scheme 1 as follows:

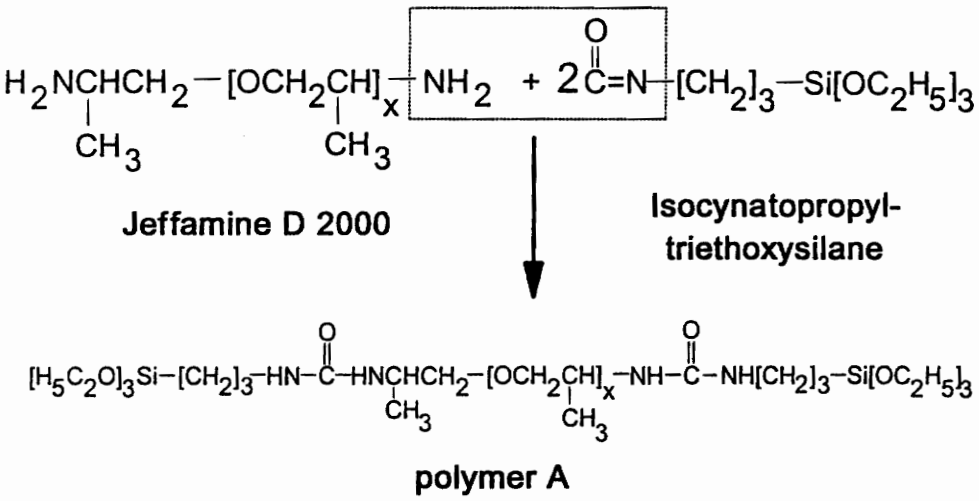

Scheme 1

In the presence of water, the ethoxy silane Si-OC_2H_5 group hydrolyzes to Si-OH which is shown in the reaction scheme 2 as follows:

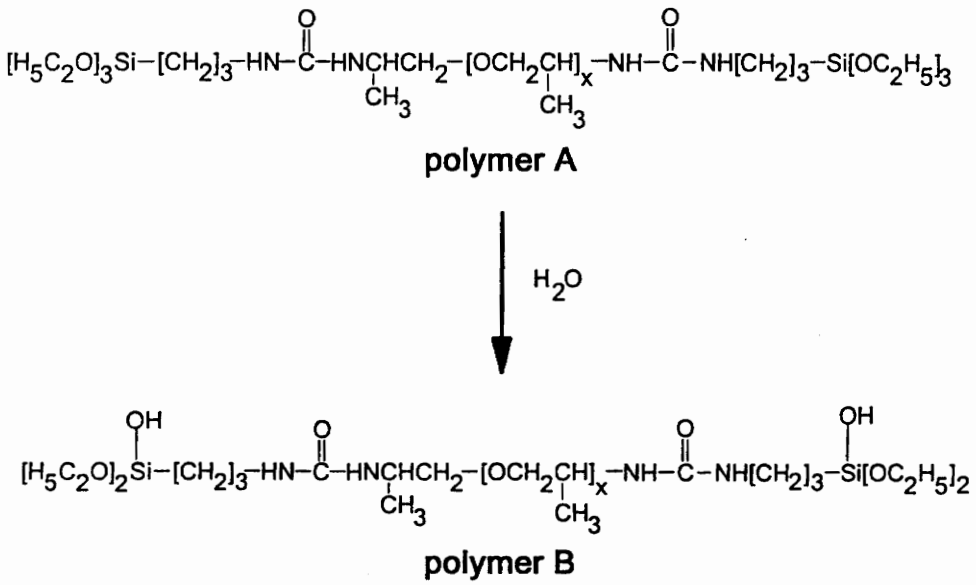

Scheme 2

The Si-OH group can then adsorb and possibly react with Ti-OH groups on the surface of TiO_2 particles. This technique offers a novel approach in designing steric stabilizers.

The outline of this paper is as follows. The end-functionalization of the PPO is described, followed by the characterization of the end-functionalization and subsequent

hydrolysis reaction by FT-IR and ^{29}Si NMR respectively. This is followed by results and discussions on particle growth and finally calculations for steric stability by DLVO theory are described.

Experimental Procedure

Materials

Samples of Jeffamine polymers were kindly donated by Texaco Chemical Company. Well defined poly(propylene oxide) polymers of molecular weight 2, 3.9, and 13 kg $mole^{-1}$ were kindly donated by the Olin Corporation. Isocynato propyl triethoxysilane (95%) was obtained from Huls America. Anhydrous ethanol (200 proof) was obtained from the Aaper Alcohol and Chemical Company. Titanium ethoxide (95 weight%, 5% ethanol) was obtained from the Alfa Chemical Company.

All glassware was cleaned first with a detergent and then soaked in a saturated solution of alcoholic KOH for 24 hours followed by soaking in 2M HCl solution for another 24 hours. This was followed by washing with tap water and finally washed 4 times with deionized water. The glassware was then dried in air in a laminar flow hood for at least two days before being used for experiments.

Procedure

End-functionalization of Jeffamine D2000

The Jeffamine samples were dried in a vacuum oven at room temperature for about 4 hours and then at 60°C for about 20 hours prior to their use. Two moles of i-CPTES are needed for every of mole Jeffamine D2000 as seen in reaction scheme 1. Typically, 10 gm of Jeffamine were dissolved in 8 gm of ethanol in 50 ml erlenmeyer flask and 2.6 gm of i-CPTES was added to this mixture to obtain polymer A. The concentration of polymer A in the stock solution was 61% by weight. Prior to the addition of any reactants, the flask was purged with dry nitrogen in a glove bag and was sealed by a rubber septum. The reactants were then added into the flask using a plastic syringe tipped with a needle.

Infra-Red Analysis

The reaction was carried at room temperature and the completion was monitored after 24 hours by taking a drop of this mixture between KBr pellets and placing them in a Nicolet 510 FT-IR Spectrometer. The addition reaction of amine group with the isocynato group was detected by the transmission scan in the infra-red region. The O=C=N- group in i-CPTES absorbs strongly at 2270 cm^{-1} wavenumber before the reaction [16]. This peak vanished at the end of the reaction due to the conversion of O=C=N- to the -OC-NH- group as seen in the reaction scheme 1. The presence and

absence of the absorption peak at 2270 cm^{-1} before and after the reaction is seen in Figure 4.3(a) and (b) respectively. Figure 4.3(a) is the FT-IR spectra just after the addition of the reactants and Figure 4.3(b) is the spectra after 24 hours of the reaction.

Hydrolysis of polymer A

Polymer A was hydrolyzed with water to obtain -Si-OH- groups at each end of the polymer chain to obtain polymer B as shown in the reaction scheme 2. For this purpose, about 0.13 gm of end-functionalized Jeffamine was taken from the stock solution containing 60% polymer A by weight in 5 ml ethanol and 0.08 gm water was added to this solution. The hydrolysis reaction was monitored by ^{29}Si NMR. The hydrolysed polymer mixture was designated solution B and was used for particle growth as discussed below in the section on particle growth.

^{29}Si NMR analysis

^{29}Si NMR analysis was done with a Varian Unity 400 NMR Spectrometer to monitor the hydrolysis and condensation of triethoxysilane end-groups in polymer A. A 60° pulse was used and t1 was determined as 13.5 seconds. A delay time of 20 seconds was used per scan. Chemical shifts were determined by using tetramethylsilane (TMS) externally. About 4 gm of a 61 wt% polymer solution in ethanol was hydrolyzed with 0.03 gm of water at 25°C without any acid or base catalyst. Figure 4.4 shows the ^{29}Si NMR spectra of polymer A. The unhydrolysed peak due to triethoxy silane species

$CH_2Si(OEt)_3$ occurs at -44.93 ppm which is in accordance with the findings of Surivet et al. [17]. Due to hydrolysis, this peak vanishes with time and a new peak at -44.7 ppm evolves as seen in Figure 4.5 within 45 minutes the hydrolysis is complete. This new peak is due to the $CH_2Si(OEt)_2(OH)$ species resulting from the hydrolysis of one ethoxy groups. The absence of peaks between -40 and -44 ppm imply the absence of tri and di hydroxy silane species [17]. Thus in the absence of any acid or base catalyst, only one ethoxy group hydrolyzes. Also, the absence of any peaks between -44.9 and -64 ppm implies that no condensation occurred between the Si-OH groups to form Si-O-Si linkages [17]. Hence, the hydrolysis of polymer A produced only $CH_2Si(OEt)_2(OH)$ species which remained stable for 3 days. On the fourth day, the solution became noticeably viscous and finally gelled and NMR analysis could not be done.

An attempt was made to further hydrolyze the remaining two ethoxy groups by adopting the following strategies: (a) heating polymer A in ethanol and water mixture at 70°C for 6 hours (the mixture gelled when heated for more than 6 hours); (b) since ethanol is released when a Si(OEt) group hydrolyses to Si-OH, it was anticipitated that hydrolysing polymer A with water in an inert diluent like THF and dimethylformamide might result in an increased extent of hydrolysis. However, ^{29}Si NMR revealed that even in cases (a) and (b) only one ethoxy group hydrolysed. The use of an acid catalyst to promote the hydrolysis reaction was avoided so as to minimize the electrostatic effects and achieve stabilization due to the adsorbed polymer only.

(a)

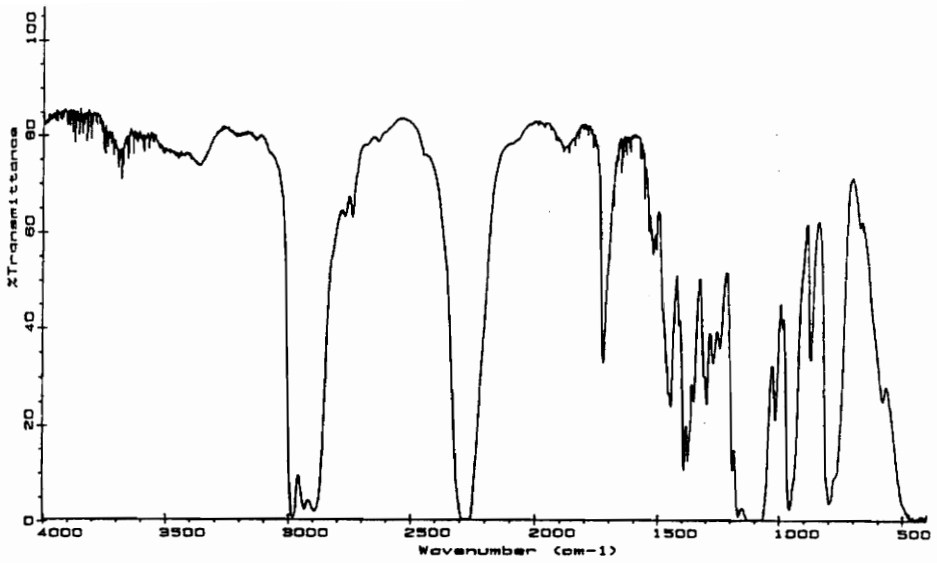

(b)

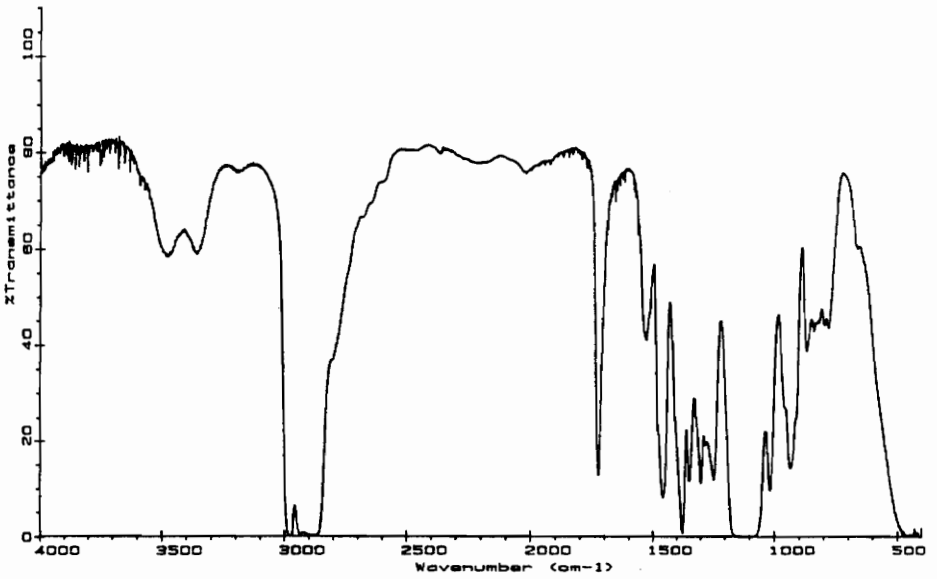

Figure 4.3. FT-IR transmission spectra of polymer A; (a) at the begining of the reaction, large peak at 2270 cm^{-1} due to isocyanate group; (b) 24 hours after the reaction, no peak at 2270 cm^{-1} due to the consumption of C=N in the isocyanate group.

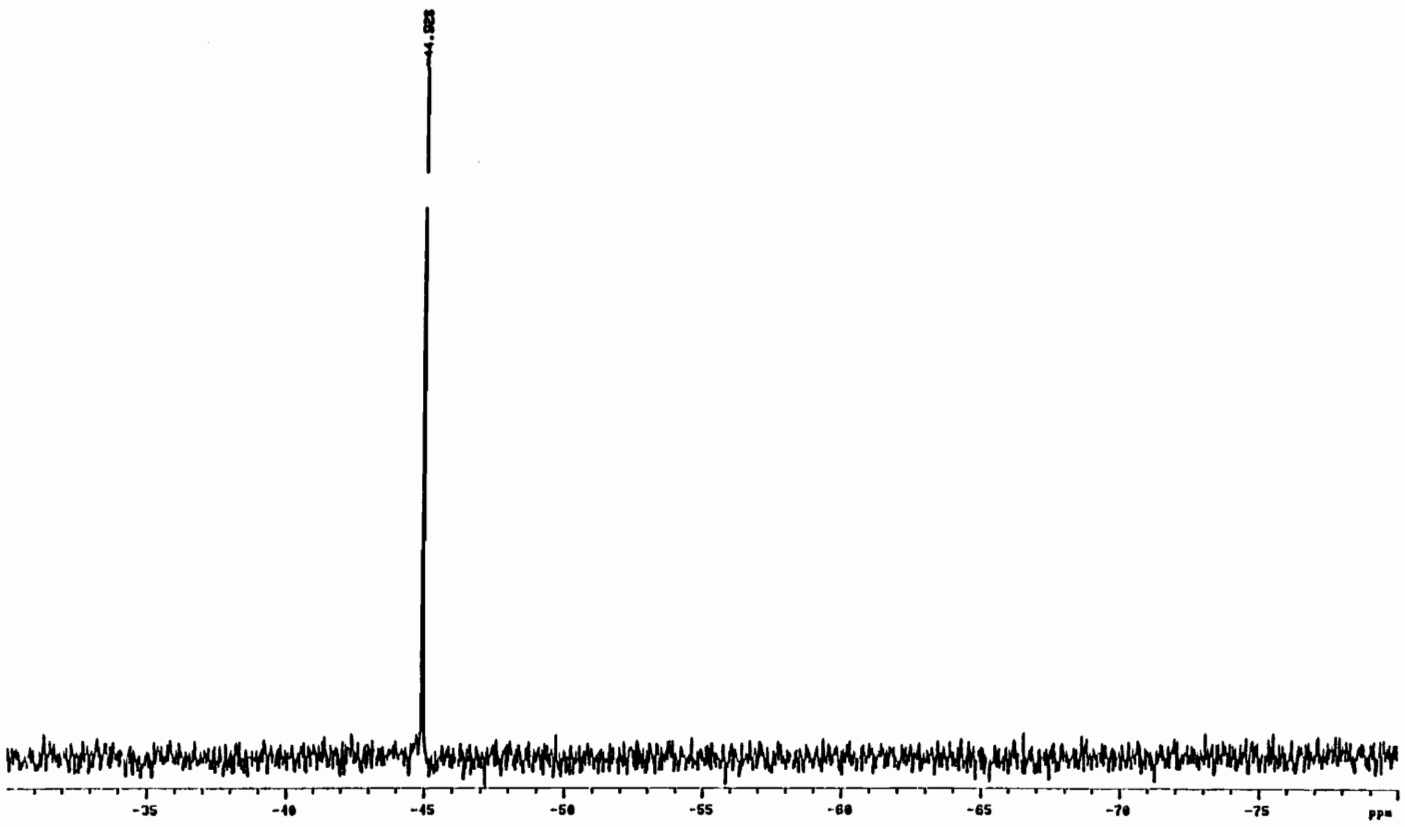

Figure 4.4. ^{29}Si NMR spectra of unhydrolyzed polymer A. The peak at -44.93 ppm is due to the triethoxysilane group.

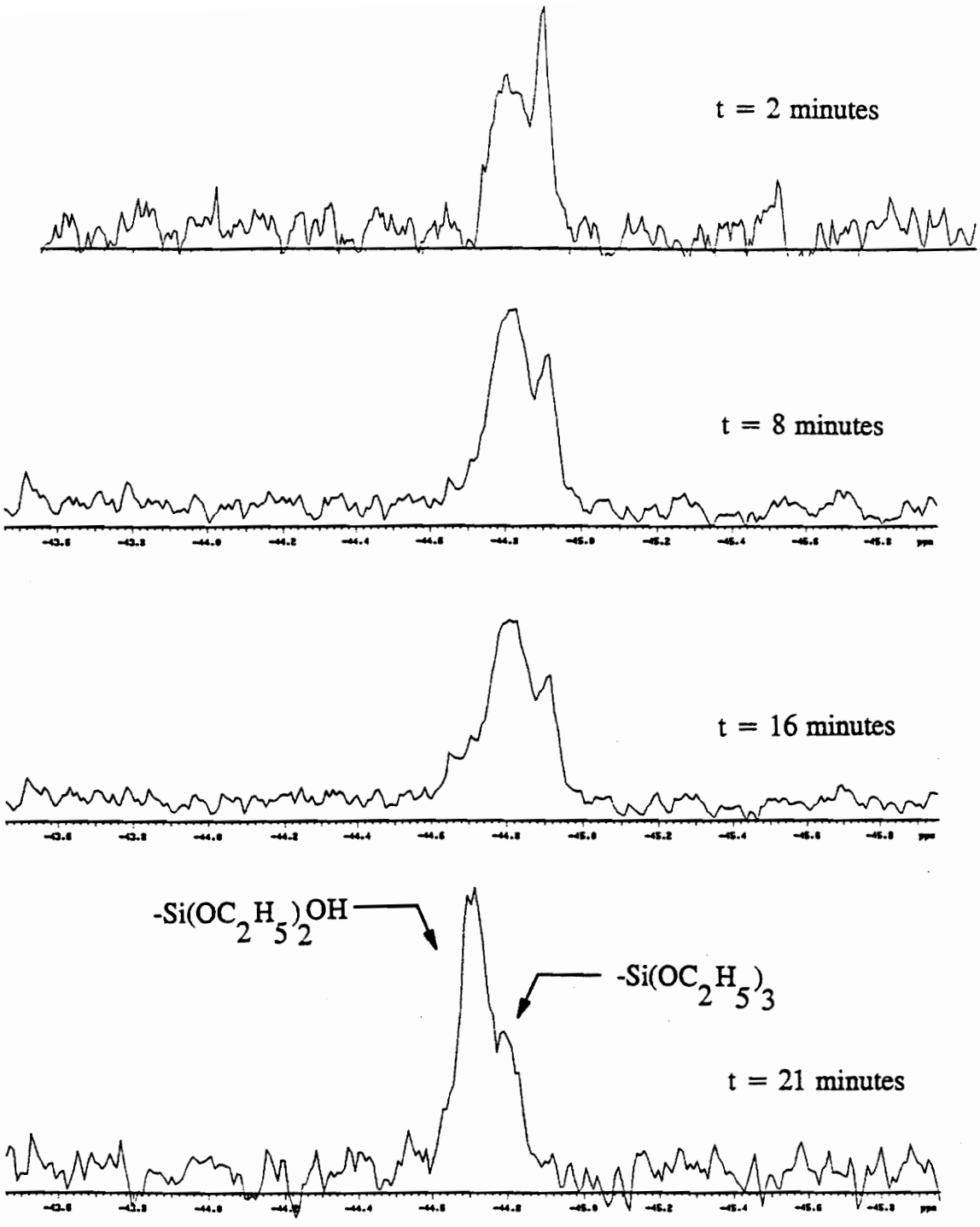

Figure 4.5. Evolution of hydrolysis peak at -44.7 ppm due to $Si(OC_2H_5)_2OH$ group by ^{29}Si NMR. The unhydrolyzed peak at -44.93 ppm reduces in intensity with time.

End-Functionalization of well defined poly(propylene oxide) polymers

Jeffamines poly(propylene oxide)s terminated with primary amines. Hence it was anticipated that a 2000 molecular weight poly(propylene oxide) end-capped with i-CPTS should give stability results similar to that obtained by end-functionalized Jeffamine D2000. Well-defined di-hydroxy terminated poly(propylene oxide) of 3 different molecular weights, 2, 3.9, and 13 kg/mole were end-capped with i-CPTS. Since the hydroxy groups are far less reactive than amine groups (at Jeffamine chain ends) towards the isocyanato group at room temperature, the end-functionalization was done at 70°C under nitrogen for 24 hours. For this purpose, neat PPO (all three molecular weights) was reacted with stochiometric amounts of i-CPTS with constant stirring. Use of ethanol was avoided since ethanol would react with i-CPTS at elevated temperatures. The end-functionalization was complete at the end of 24 hours as determined by the FT-IR spectra. ^{29}Si NMR of the end-functionalised PPO's at the end of 24 hours gave two peaks at -45 ppm and -46.35 ppm. The peak at -46.35 ppm is a condensation peak presumably due to $CH_2(OEt)_2Si\text{-}O\text{-}Si(OEt)_2CH_2$ species. This is possible to the fact that hydrolysis and subsequently condensation of ethoxysilane group can occur due to trace amounts of moisture at 70°C in spite of a nitrogen blanket. The molar ratio of these two peaks was 12:1, respectively, from peak integrals.

Particle Growth

For particle synthesis, equal volumes of solutions of TEOT in ethanol, denoted

as solution A, and a solution of polymer B in ethanol and water, denoted as solution B, were mixed rapidly and shaken for 5 seconds and were allowed to sit quiescently. Solution A consisted typically of a 5 ml mixture of titanium ethoxide and anhydrous ethanol mixed in a nitrogen glove bag to prevent early hydrolysis of the ethoxide by atmospheric moisture. Both solutions were filtered with a 0.2 micron Gelman Acrodisc PTFE filter. Solution B consisted of polymer B, ethanol and water as discussed in the section describing hydrolysis of polymer A. All particle growth experiments were performed at a fixed initial TEOT concentration of 0.04M. The polymer concentration of polymer A was varied between 3.9 to 16 g/l and the water concentration, described as R = $[H_2O]/[TEOT]$ was 11. To determine the effect of polymer molecular weight and functionality, particles were also grown with i-CPTS end-capped Jeffamine M2000 (at C_p = 3.9 to 16 g/l), D4000 (at C_p = 3.9 to 32 g/l), D400 (at 3.9 to 8 g/l), and T5000 (at 3.9 to 8 g/l). The end-functionalization and the subsequent hydrolysis of these polymers was done in the same manner as done for D2000 mentioned in the procedure section. All of these polymers have the poly(propylene oxide) repeat unit but they differ in functionality and molecular weight. For instance, M2000 has an average molecular weight of 2000 but is monofunctional, i.e., it has amine termination only at one end, D400 and D4000 are difunctional but have molecular weights of 400 and 4000 respectively, and T5000 is trifunctional with a 5000 molecular weight. Particles were also grown with Jeffamine D2000 (no end-functionalization) and with polymer A (without prehydrolysis with water). Particle growth with the prehydrolysed end-functionalized

PPO's was done at polymer concentration between 3.9 to 8 g/l.

The particle size was determined by transmission electron microscopy (TEM) using a Philip 420T Scanning Transmission Electron Microscope.

Results and Discussion:

Particle Size

Jeffamine D2000

Figure 4.6(a) shows the TEM micrograph of particles grown without the polymer B. The particles are in the form of large agglomerates of the sizes of 5-10 microns. Similar particle morphology was observed when the particles were grown with Jeffamine D2000 (non end-functionalized with i-CPTS) and polymer A (i.e., no prior hydrolysis of polymer A to polymer B). Figure 4.6(b) shows the TEM micrograph of particles grown with polymer B at C_p = 8 g/l. Discrete, spherical TiO_2 particles of mean size 0.35 microns are observed in this figure. These results establish that end-functionalization with i-CPTS and its pre-hydrolysis before particle growth was essential to achieve in-situ steric stability. The hydrolysis and condensation of TEOT is much faster than that of triethoxysilane in the absence of any acid or base catalyst [4b]. Hence, if polymer A is not pre-hydrolysed, then hydrolysis and adsorption of polymer A does not occur within the time scale of particle growth and hence no steric stability is achieved.

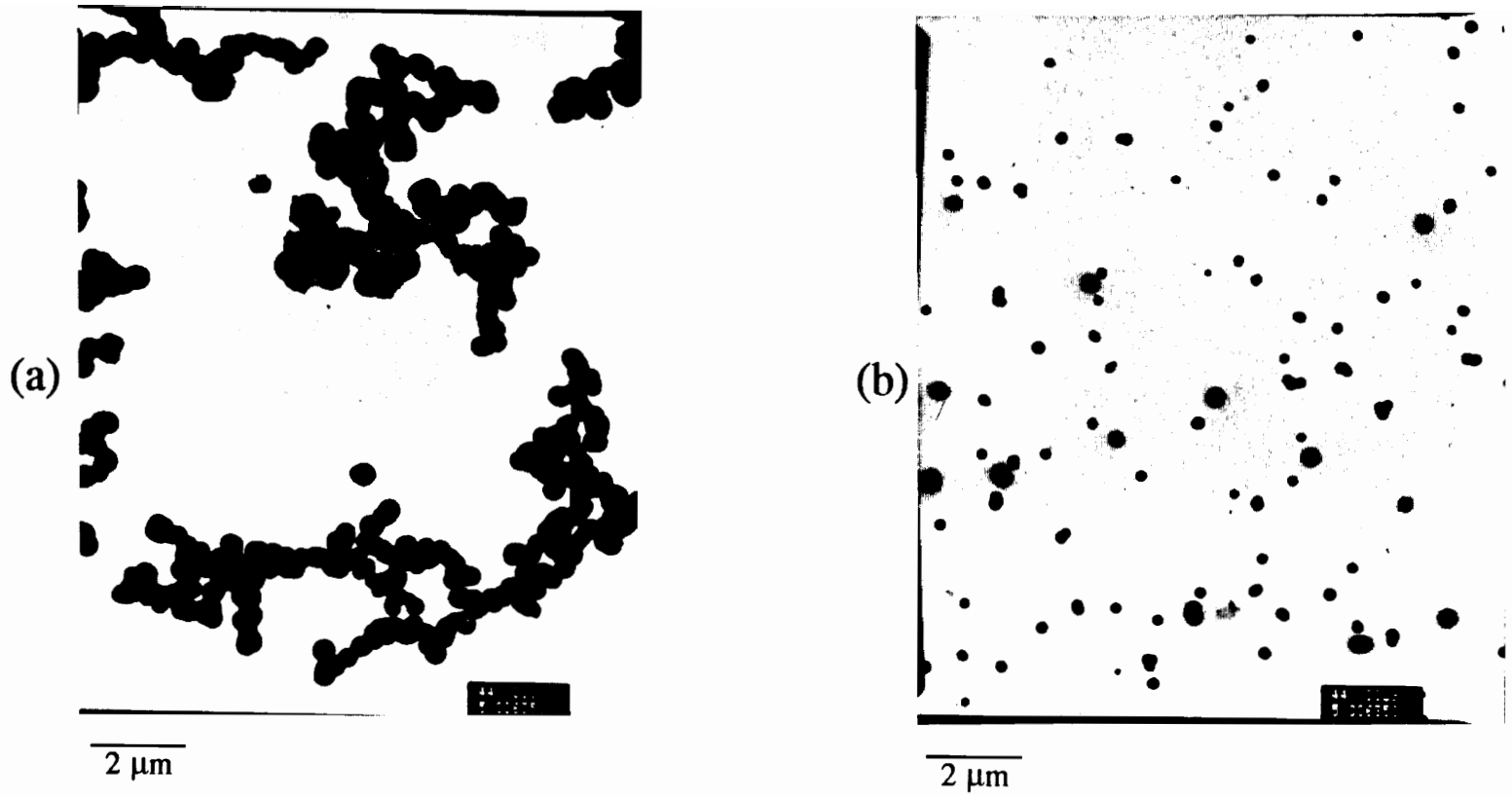

Figure 4.6. TEM micrographs of TiO_2 particles grown at [TEOT] = 0.04 M and R = 11; (a) polymer free control; (b) C_p = 8 g/l.

When the particles were grown in the presence of polymer B at C_p = 3.9 g/l, no steric stability was observed. At C_p = 8 g/l, some large background particles of the sizes of 0.5 to 0.6 microns were also observed along with the small 0.35 micron size primary particles as seen in Figure 6(b). At C_p = 16 g/l, the size of the primary particles decreased to 0.2 microns. Even at this polymer concentration, larger background particles were observed but their size was approximately 0.4 microns. The formation of large particles in both cases could be due to the bridging flocculation caused due to the difunctionality of polymer B which will be discussed in the polymer adsorption section.

Jeffamine D2000 from three different batches were end-functionalized and particle growth was carried out as mentioned above. However, end-functionalized Jeffamine D2000 from one of the batches did not give any steric stability. Hence, samples of Jeffamine D2000 from all the three batches were analyzed for metal impurities by inductive coupling plasma (ICP) technique. No metal impurity was detected in any of the three samples within the detection limit of 0.01 ppm of ICP. The chemical structure of the three samples were compared by ^{13}C NMR analysis and were found to be the same. Hence, at this point, it is not clear why one batch of Jeffamine D2000 failed to give steric stability.

Effect of Molecular weight of D series of Jeffamine

In order to determine the effect of molecular weight on particle size, TiO_2 particles were grown in the presence of D400 and D4000 which were terminated with

i-CPTS and prehydrolysed as mentioned in the procedure section. In both cases, the particles obtained were large agglomerates as in the case of the polymer-free control as seen in Figure 4.6(a). The lack of steric stabilization from D400 could be due to an insufficient steric layer thickness due to its low molecular weight. It is not clear why D4000 failed to impart steric stabilization. One reason could be that the long polymer chain of D4000 with reactive end-groups at both the chain ends lead to bridging flocculation where one end of the chain adheres to the surface of one particle and the other end adheres to the surface of the neighboring particle.

Effect of polymer functionality

In order to determine the effect of functionality on steric stabilization, particles were grown in the presence of i-CPTS end-functionalised M2000 (monofunctional) and T5000 (trifunctional). Both polymers were unable to impart in-situ steric stability to the growing TiO_2 particles. In this case, either bridging flocculation or lack of a sufficient steric layer thickness would lead to agglomeration of TiO_2 particles. The lack of steric stability due to M2000 even at a polymer concentration as high as 16 g/l suggests that the stability seen due to the difunctional polymer B is due to the adsorption of polymer B at the particle surface occurs in the form of loops which anchor the polymer strongly.

Particle growth in i-CPTS end-functionalized Poly(propylene oxide)

When the particles were grown with the pre-hydrolysed end-functionalized

PPO's, no steric stability was observed. This could be due to the fact that the partial condensation which occurred during the end-functionalization reaction reduced the polymer solubility in ethanol to an extent where sufficient steric layer thickness was not achieved.

Mechanism of Polymer Adsorption

The adsorption of the PPO on the titania surface could be due to the following reasons:

(i) Hydrogen bonding between the OH groups at the end of the chain polymer B and the TiO_2 surface. However, when particles were grown with hydroxyl-terminated poly(propylene oxide) having a mean molecular weight of 2000, no in-situ steric stabilization was observed. This strongly suggests that hydrogen bonding alone is not causing the adsorption of polymer B at the titania surface.

(ii) At neutral pH, the Si-OH group on the chain end deprotonates [4b] so that the chain ends of polymer B have a partial negative charge. Previous work [11] has shown that TiO_2 surface had a slight positive charge as evident from the electrophoretic mobility of $+2.8 \times 10^{-9}$ m^2 V^{-1} s^{-1} at R = 11. Hence the adsorption of polymer B could be due to the electrostatic attraction between the negatively charged $[Si\text{-}O]^-$ species and the positively charged TiO_2 surface which would lead to the terminal adsorption of the polymer.

(iii) Based on work by Yoldas [19], the adsorption of Polymer B could also be due to the

formation of Si-O-Ti bonds at the titania surface. The Si-OH group at the end of polymer B chain could react with Ti-OR group during particle formation and graft itself at the titania surface by forming a Si-O-Ti covalent linkage leading to the terminal grafting of the polymer. In order to test this, a large batch of particles (about 600 ml) were grown according to the procedure mentioned in the particle growth section. This batch was then concentrated at 25°C in vacuum to increase the polymer and TiO_2 concentration to 18 and 7 wt% approximately. ^{29}Si NMR (scanned for 4 hours) conclusively established the absence of Si-O-Ti condensation since only one peak was observed at -44.7 ppm which corresponded to $CH_2Si(OEt)_2(OH)$ species. Hence the mode of polymer adsorption can be due to either (i) or (ii) mechanism or both acting simultaneously. The fact that the difunctional chain gives steric stability and the monofunctional does not, suggests that both ends are required to adsorb to cause a net decrease in free energy which is required for adsorption. The polymer chain loses entropy when adsorbed and hence it would adsorb only if the decrease in enthalpy of adsorption would offset the loss in entropy, i.e., the adsorption is enthalpy driven [20]. Hence, for the adsorption to occur these conditions should be met:

$$\Delta H_{ads} < 0, \text{ and } |\Delta H_{ads}| > |T\Delta S_{ads}|$$

In the case of monofunctional low molecular weight polymer B, the decrease in enthalpy due to adsorption at one end may not be enough to offset the loss in entropy and

hence the polymer does not adsorb to impart steric stability.

PPO Chain Statistics

The chain dimensions of PPO in solution are estimated from the equation for R_g for a wormlike chain [21] which is given as:

$$R_g^2 = L^2\left[\frac{1}{6N_k} - \frac{1}{4N_k^2} + \frac{1}{4N_k^3} - \frac{1-e^{-2N_k}}{8N_k^4}\right] \quad (1)$$

where N_k is the number of Kuhn segments per chain, L is the contour length.

The Kuhn length L_k is estimated from values of characteristic ratio $C_\infty = \langle r^2 \rangle_0 / M^{0.5}$ according to :

$$L_k = (M_{mon} / L_{mon}) \langle r^2 \rangle_0 / M \quad (2)$$

For PPO in methanol at 25°C [22],

$$\langle r \rangle_0 / M^{0.5} = 0.075 \text{ nm} \quad (3)$$

where $\langle r \rangle_0$ is the unperturbed root mean square end to end distance in nm, M is the

molecular weight in g/mole, n is the number of monomer units forming the chain, and l is the length of each monomer unit. For n = 34 (for PPO molecular weight = 2000, and monomer molecular weight = 58) and L_{mon} = 0.38 nm, equations (2) and (3) give L_k = 0.87 nm. Therefore the number of Kuhn segments N_k can be given as:

$$N_k = nL_{mon}/\text{Kuhn length} = 15 \quad (4)$$

According to the N_k value from equation (4) the 2000 molecular weight PPO is not in a Gaussian coil regime. Hence according to equations (1) and (4), R_g = 1.3 nm.

In-Situ Steric Stabilization due to Polymer B

For a polymer to act as an effective in-situ steric stabilizer it must adsorb sufficiently quickly and to such an extent that the primary maximum in the total interparticle energy V_T becomes ~ 10 kT. At this point, particle aggregation into the primary minimum slows significantly. The parameters affecting the steric potential energy V_S are described in the following equation for $h < 2\delta$ [12]:

$$\frac{V_s}{kT} = \frac{4}{3}\pi A_2 C_i^2 (\delta - \frac{h}{2})^2 (3r + 2\delta + \frac{h}{2}) \quad (5)$$

where A_2 is the second virial coefficient in mole cm^3/g^2, N_{Av} is Avagadro's number, C_i is the polymer concentration in the adsorbed layer in g/cm^3, δ is the steric layer thickness in nm, r is the radius of particle in nm, and h is the surface-to-surface distance of separation between the particles. In order to calculate the steric potential energy due to adsorbed polymer, δ, C_i, and A_2 have to be known or approximated.

Steric layer thickness δ

In the case of terminally attached polymer at one end, it is well known that the adsorbed chains undergo chain extension at full surface coverage [23-28]. In the present case, polymer B has two reactive end groups and hence it is very likely that the polymer is adsorbed in the form of a loop. Toprakciaglou et al. [27] studied the adsorption of PEO-PS-PEO triblock copolymer (Mw = 129 kg/mole) on mica where PEO blocks were the sticking ends of the polymer. They concluded that the triblock copolymer with two sticking ends adsorbed in a mixed mode, forming loops and tails. Due to the lack of measurements of the steric layer thickness and due to complexities in estimating loop dimensions, it is assumed in the calculations that the steric layer thickness is equal to $2R_g$, i.e., the adsorbed polymer coil has the same dimensions as in solution and that the polymer adsorbs so that the chains form a packed layer at the particle surface. Hence, $\delta = 2R_g = 2.6$ nm is assumed. This is a worst case since in actuality there should be some chain extension. It is significant that DLVO theory predicts steric stability even in this worst case scenario.

Calculation of C_i

Assuming that the polymer chains adsorb in a close-packing fashion the concentration of polymer B in the adsorbed layer can be given as:

$$C_i = \frac{M}{N_{AV}\frac{4}{3}\pi R_g^3} \tag{6}$$

where M is the molecular weight, N_{AV} is Avagadro's number and R_g is the radius of gyration of the polymer. Substituting M = 2000 and R_g = 1.3 nm the value of C_i as 0.36 g/cc is obtained.

Calculation of A_2

Jeffamine D2000 readily dissolved in ethanol. Hence, assuming a conservative χ value of 0.48, the second virial coefficient can be calculated as [29]:

$$A_2 = \frac{(0.5-\chi)}{\rho_2^2 V_1} \tag{7}$$

where ρ_2 is the density of polymer (ρ_{PPO} = 1.07 g/cm^3)[21] and V_1 is the molar volume of ethanol. This gives a conservative minimum value of A_2 as 3 x 10^{-4} mole cm^3/g^2.

Van der Waal's attractive potential V_A

If it is assumed that the interparticle electrostatic effects are negligible (which is a safe assumption in this case since no acid or base is added) then the total potential V_T is the sum of V_s and V_A. The Van der Waal's attractive potential energy V_A between the approaching particles is given by the equation:

$$V_A = -\frac{A}{12}\left[\frac{1}{x^2+2x} + \frac{1}{x^2+2x+1} + 2\ln\frac{x^2+2x}{x^2+2x+1}\right] \qquad (8)$$

where A is the composite Hamaker constant defined by :

$$A = (\sqrt{A_{11}} - \sqrt{A_{22}})^2 \qquad (9)$$

where A_{11} is the Hamaaker constant of TiO_2 and A_{22} is the Hamaaker constant of ethanol, and $x = h/2r$.

According to equations (8) and (9) Van der Waal's attractive potential can be calculated for a given a particle size when the Hamaker constants of TiO_2 A_{11} and ethanol A_{22} are known. These values are 4.2×10^{-22} J and 3.563×10^{-20}J [30] respectively which give the composite $A = 2.83 \times 10^{-20}$ J.

Total Potential Energy V_T

Figure 4.7 is a plot of potential energy versus distance of separation between the particles of radius 175 nm which was the smallest dispersed size observed for D2000 at C_p = 8 g/l. In this plot it is observed that both V_A and V_s increase in magnitude as the particles approach and the attached polymer layers interpenetrate, i.e., $h < 2\delta$. However, the magnitude of V_s increases more rapidly than does V_A and hence the total potential energy V_T is positive at $h < 3.8$ nm. To achieve colloidal stability for the duration of about a month at room temperature, V_{max} should be greater than 15 kT [12]. In the present case this occurs at $h < 3.5$ nm. At $h = 1$ nm, V_T has a maximum positive potential which is equal to 134 kT and is termed as V_{max}. Hence, the DLVO calculations support steric stabilization by polymer B even when the conservative values of A_2 and δ are assumed. As mentioned before, the actual values of both A_2 and δ may be greater which would further increase V_s and hence colloid stability.

A better understanding on the effect of functionality and molecular weight can be obtained by comparing the adsorption isotherms and the chain conformations of end-functionalized Jeffamines, e.g., D2000, D4000, M2000 and T5000, at the titania particle surface. Adsorption isotherms can be studied by detecting the change in polymer concentration after adsorption by UV absorption since the carbonyl group at the chain end absorbs in the UV region. The fraction of segments adsorbed as trains may be studied by ^1H NMR as done by Van der Beek et al. [18]. Terminal attachment should result in little or no detectable trains.

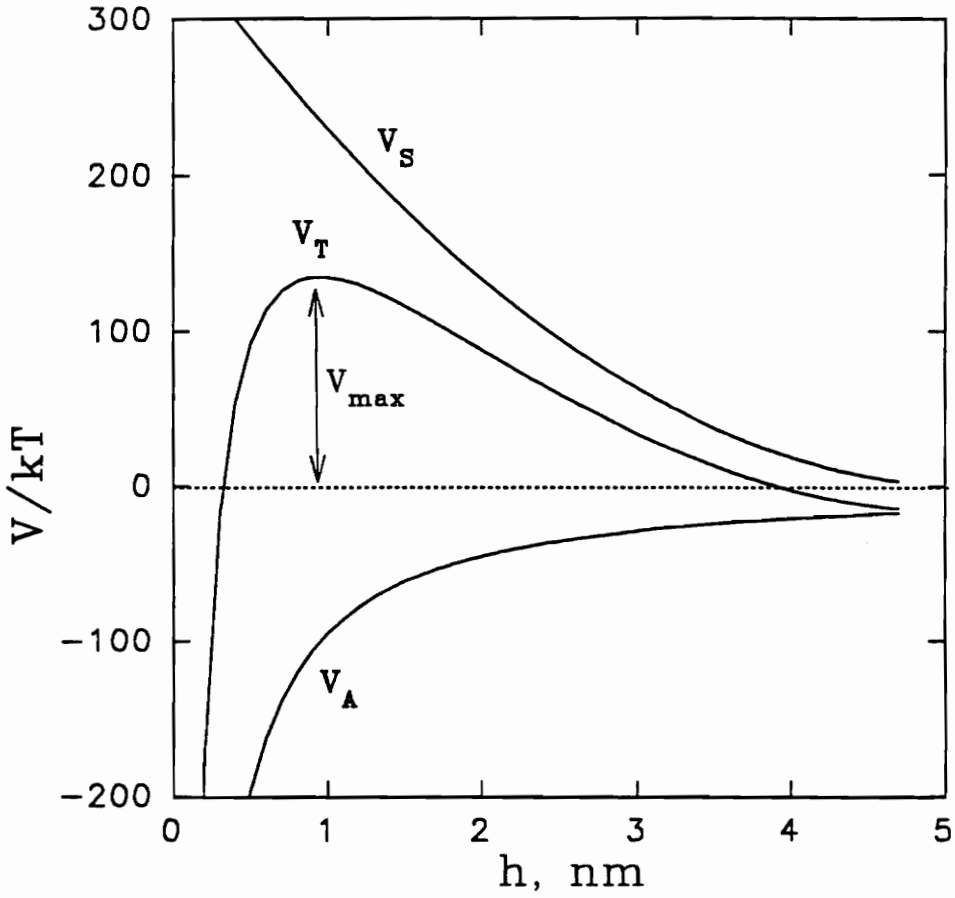

Figure 4.7. Potential energy V/kT versus distance of separation h between two spherical particles of radius 175 nm by DLVO calculations; V_A is Van der Waal's attractive potential, V_S is steric repulsion potential, and $V_T = V_A + V_S$ assuming the absence of electrostatic effects.

Conclusions

This work clearly shows that end-functionalized polymers can be used effectively as in-situ steric stabilizers. The polymer concentration needed to achieve steric stability with the end-functionalized PPO D2000 was much higher (8 g/l) than the plateau concentration of HPC (1.7 g/l). This was due to the fact that the polymer chain had only 2 adsorbing groups in the case of polymer B whereas HPC has 3 hydroxy groups per repeat unit. Theoretical predictions by DLVO calculations also support this assuming complete surface coverage by the polymer and that the steric layer thickness was twice the radius of gyration. This work suggests that if a polymer chain has a few adsorbing groups (compared to only 2 in this case) at the chain end then it will be possible to achieve in-situ steric stability at polymer concentrations much lower than 8 g/l.

References

1. Livage J. MRS Bulletin, 15(1) (1990) 18.
2. E. Barringer, N. Jubb, B. Fegley, R.L. Pober, and H.K. Bowen in Ultrastructure Processing of Glasses, Ceramics, and Composites, eds., L.L. Hench, and D.R. Ulrich, Wiley, New York, 1984, p. 315.
3. E. Matijevic and P. Gherardi, Transformation of Organometallics into Common and Exotic Materials: Design and Activation, NATO ASI series E, no. 141, ed. R.M. Laine (Martinus Nijhoff, Dordrecht, 1988), p.279.
4. Sol-Gel Science: The Physics and Chemistry of Sol-Gel Processing, edited by C.J. Brinker, and G.W. Scherer, Academic Press CA, 1990, (a) Chapter 4, (b) Chapter 3.
5. J. Livage, M. Henry and C. Sanchez, Prog. Solid St. Chem. 18 (1988) p. 259-341.
6. Barringer E. A., and Bowen, H.K., Langmuir, 1 (1985) p. 414.
7. Barringer, E.A., and Bowen, H.K., J. Am. Ceram. Soc., 65 (1982) C-199.
8. Look, J-L., and Zukoski, C.F., Faraday Discuss. Chem. Soc., 90 (1990) p. 345.
9. Mates, T.E., and Ring, T.A., Colloids and Surfaces, 24 (1987) p. 229.
10. Jean, J.H., and Ring, T.A., Colloids and Surfaces, 29, (1988) p. 273.

11. Nagpal, V.J., Davis, R.M., and Riffle, J.S., In-Situ Steric Stabilization of Titanium Dioxide Particles Synthesized by a Sol-Gel Process, submitted to Colloids and Surfaces.

12. Polymeric Stabilization of Colloidal Dispersions, edited by D.H. Napper, Academic Press, 1989.

13. T.F. Tadros in Polymer Colloids, edited by R. Buscall, T. Corner, and J.F. Stageman, elesevier 1985.

14. K. Bridger and B. Vincent, European Polymer Journal, 16 (1980) p.1017-1021.

15. The JEFFAMINE Polyoxyalkyleneamines, Texaco Chemical Company, subsidiary of Texaco Incorporated.

16. Spectrometric Identification of Organic Compounds, eds. Robert M. Silverstein, G. Clayton Bassler, and Terence C. Morrill, John Wiley & Sons (1981) p.130.

17. Francoise Surivet, Thanh My Lam, Jean-Pierre Pascault, and Quang Tho Pham, Macromolecules 25 (1992) p.4309-4320.

18. G.P. van der Beek and M.A. Cohen Stuart, Langmuir, 7(1991) 327-334.

19. B.E. Yoldas, J.Non Crystalline Solids 38-39 (1980) p.81-86.

20. Cohen Stuart, M.A. Fleer, and J.M.H.M. Scheutjens, J. Colloid Interface Sci., 97 (1984) p.515.

21. H. Yamakava, Modern Theory of Polymer Solutions, Harper and Row, New York 1971.

22. Polymer Handbook, edited by J. Bandrup and E.H. Immergut, Wiley, New York

(1975).

23. Intermolecular and Surface Forces, edited by Jacob N. Israelachvili, Academic Press CA, 1985.

24. S. Patel, and M. Tirrell, M. Annu. Rev. Phys. Chem. 1989, 40.

25. David Guzonas, D. Boils, and M.L. Hair, Macromolecules, 24 (1991) p.3383.

26. H.J. Taunton, Chris Toprakcioglu, L.J. Fetters, and Jacob Klein, Macromolecules, 23 (1990) p.571-580.

27. S.T. Milner, Science, 251 (1991) p.905.

28. Liming Dai, and Chris Toprakciaglu, Macromolecules, 25 (1992) p.6000-6006.

29. Polymer Chemistry, edited by P.C. Hiemenz, Marcel Dekker, New York (1984).

30. J. Visser, in Surface and Colloid Science, edited by E. Matijevic, Wiley-Interscience, New York, 1976, Vol.8, p.21.

Chapter 5

A Dynamic Light Scattering Study of Micelle Formation in Solutions of Poly(2-ethyl-2-oxazoline-dimethylsiloxane) in Water-Isopropanol Mixtures

Introduction

Diblock copolymers in selective solvents, i.e. solvents where only one block is soluble, can form a variety of structures including spherical, cylindrical, and lamellar micelles as well as clusters of micelles. When adsorbed at interfaces, they can form well-organized layers which makes diblock copolymers particularly useful for colloid stabilization as well as surface tension control and emulsification [1,2]. There are numerous studies of diblock adsorption from solutions of selective solvents [3-5] as well as of diblock copolymers in solutions [6-11, 13-15]. Many solution studies have focused on relating block length ratio and block-solvent interactions to micelle formation, structure, and properties. Static light scattering studies have provided measurements of micelle radius, second virial coefficients, and aggregation number while dynamic light scattering studies have provided measurements of hydrodynamic radii and micelle shape with depolarized light scattering [12]. Small angle x-ray scattering studies [10] have

probed micelle structure at smaller length scales, while small angle neutron scattering studies [13,14] have probed structural features in the cores and coronas of micelles. In addition, viscometry has been used to characterize micellar hydrodynamic properties [15]. The effect of block length and solvent interactions in selective solvents on micelle size and the critical micelle concentration, cmc, has been modelled with some success with scaling laws [16] and mean field theories [9] although considerable work remains to be done.

Diblock solution behavior in mixtures of selective and nonselective solvents poses additional complexities due to the partitioning of the nonselective solvent between the micelle core and the liquid phase. Since applications of copolymers may involve mixtures of solvents, it is important to understand the effect of solvent composition on micelle formation. There is particular interest in diblock copolymers for use as colloid stabilizers where at least one block is water-soluble. Interactions between polymer chains and water are still poorly understood due to the complex structure of water and hydrogen bonding between polymer and water.

Work in this chapter presents the first study of the micellar properties of a novel diblock copolymer consisting of poly(2-ethyl-2-oxazoline-dimethylsiloxane), designated as PEOX-PDMS, in mixtures of water and isopropanol, IpOH. The polymer structure is shown in Figure 5.1. This work focuses on the effect of solvent composition and polymer concentration on the formation and structure of micelles characterized by dynamic light scattering.

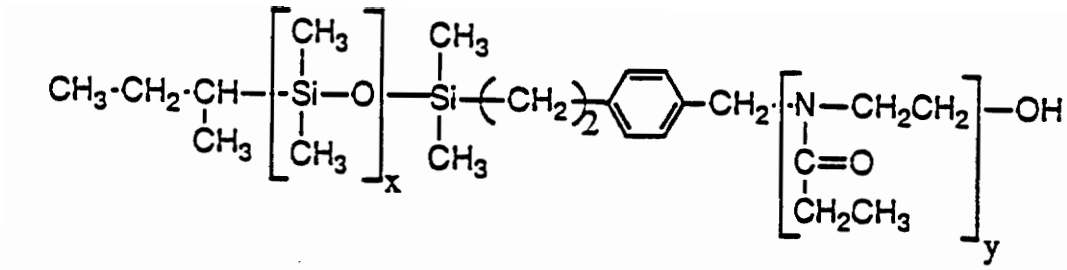

Figure 5.1. Structure of Poly(2-ethyl-2-oxazoline-dimethylsiloxane) diblock copolymer.

PEOX is soluble in both water and isopropanol whereas PDMS is soluble only in isopropanol. Hence, water is the selective solvent for PEOX which will be shown to form the corona of micelles whose shapes vary from spherical to ellipsoidal in mixed solvents with relatively low concentrations of isopropanol. At higher concentrations of IpOH, the copolymer exists as isolated chains in a nonselective solvent environment. Results for a PEOX-PDMS diblock copolymer at very low molecular weights show anomalously high hydrodynamic diameters which are interpreted as micelle aggregation due to strong hydrogen bonding between the PEOX corona chain segments. This study was motivated by the need to understand better the solution behavior of diblock copolymers in aqueous media as a prerequisite for developing model water soluble diblock steric stabilizers and by the relative lack of experimental studies on diblock copolymers in mixtures of a selective and a nonselective solvent.

A review of the literature shows few previous studies of diblock solution properties in mixtures of selective and nonselective solvents. Mandema [7] et.al. used static and dynamic light scattering to observe dramatic changes in the size and shape of micelles of hydrogenated poly(styrene-isoprene) in mixtures of trans-decalin, a solvent for both the blocks, and decane, a non solvent for polystyrene. In pure trans-decalin, the copolymer existed as a single chain whereas, in pure decane, small compact structures with hydrodynamic radius of 30 nm were observed. In a 60/40 v/v trans-decalin/decane mixture at 25°C, large structures with hydrodynamic radii of 180 nm were observed. Light scattering gave large dissymmetry ratios which were attributed to the formation of

ellipsoidal micelles.

Anomalous micelle sizes have also been reported for micelles formed by hydrophilic-hydrophobic type block copolymers in selective solvents. Tuzar et al.[8] observed large micelle sizes in a polystyrene-b-poly(2-vinylpyridine) while varying temperature in toluene which is selective for polystyrene. The present work was done at a fixed temperature, but an analogy can be drawn between the temperature dependence and the mixed solvent composition dependence of the micelle structures in the sense that both affect the thermodynamic quality of the solvent for the either blocks. Duval and Picot [17] studied the micelle formation of a polystyrene-poly(methyl methacrylate) (PS-PMMA) diblock copolymer in dioxane/1-chloro-n-hexane mixtures where the quality of the solvent was varied by varying the temperature and by varying the composition of mixtures of dioxane, a good solvent for both blocks, and 1-chloro-n-hexane, a non-solvent for PMMA at room temperature. At $T < 30°C$, micelles with hydrodynamic radius $R_h = 35$ nm formed at dioxane weight fractions $\Phi < 0.1$ while unassociated molecules existed for $\Phi > 0.4$. In the intermediate weight fractions, $0.1 < \Phi < 0.4$, anomalously large micelles were observed which were believed to be ellipsoidal structures. Similar results were obtained when the experiments were conducted at different temperatures and at fixed Φ.

Large micelle structures have also been reported by Cogan et al. in a system consisting of polystyrene-poly(ethylene oxide), PS-PEO, in cyclopentane, a selective solvent for polystyrene [18,19]. In dry cyclopentane, the hydrophilic poly(ethylene oxide)

core crystallized, resulting in hydrodynamic radii ranging from 40-110 nm as determined by dynamic light scatering using the program CONTIN to measure micelle size distributions. Upon the addition of trace amounts of water, the crystalline PEO dissolved but remained confined in the micellar core. The structures were identified as starlike polymeric micelles. This system differs from the present copolymer PEOX-PDMS in that the hydrophobic PDMS that forms the micellar core is amorphous and the solvent mixture water-IpOH is completely miscible.

There are at present no rigorous theories for diblock micelle formation in mixed solvents. However, the mean field theory of Munch and Gast for diblocks in a purely selective solvent provides some qualitative guidelines for understanding micellization in mixtures of selective and nonselective solvents where the solvent composition, and hence incompatibility with the insoluble core, varies [9]. It was shown that the incompatibility parameter $\chi_{BS}N_B$, where χ_{BS} is the Flory-Huggins interaction parameter of the core block B with the solvent S and N_B is the degree of polymerization of the core block, controlled various aspects of micellization. As incompatibility $\chi_{BS}N_B$ increased, the critical micelle concentration, cmc, and the micelle aggregation number decreased while the corona thickness increased. At a fixed level of incompatibility, a spherical micelle regime was predicted for relatively small ratios of N_B/N_A and for when the solvent size N_S was small with respect to the total degree of polymerization N ($= N_A + N_B$), characterized by large values of the ratio N/N_S. By contrast, a lamellar micelle regime was predicted to occur for $N_B/N_A \simeq 1$ and for relatively low values of N/N_S.

In a related study for copolymers in highly selective solvents, Halperin proposed a model for spherical micelles with a small core formed by a diblock with an insoluble block with degree of polymerization N_B and an extended corona formed by a soluble block with degree of polymerization N_A [16]. For such systems where $N_A >> N_B$, the Daoud-Cotton model [20] for star polymers can be applied to describe the micellar structure [19]. According to this analysis, the core radius $R_{core} \propto N_B^{3/5}$ while the overall micelle radius $\propto N_B^{4/25} N_A^{3/5}$.

Experimental Procedure

Materials

Two diblock copolymers of poly(2-ethyl-2-oxazoline-dimethylsiloxane) with approximate PEOX-PDMS block molecular weights M_n = (20 kg/mole)-(5 kg/mole) and (8 kg/mole)-(2 kg/mole), respectively, were used in this study. These copolymers are referred to hereafter as 20K-5K and 8K-2K, respectively. These polymers were synthesized by living polymerization techniques that have been described elsewhere [21]. For both copolymers, the block length ratio N_{PDMS}/N_{PEOX} = 0.33. In addition, the following homopolymers were studied: homopolymers PEOX, M = 5 kg/mole and M = 20 kg/mole, designated as 5K and 20K, respectively, and PDMS with M = 14 kg/mole, designated as 14K. While the absolute molecular weights of the diblocks and the homopolymers were not measured, previous work has shown that the target molecular

weights, cited here as the approximate molecular weights, are quite accurate. The PEOX homopolymers typically have M_w/M_n = 1.1-1.5 [21]. The PEOX 20K was synthesized first and was then used in the synthesis of the 20K/5K diblock copolymer. Approximate degrees of polymerization, DP, for these polymers are listed below in Table 5.1. HPLC-grade isopropanol, designated as IpOH, was obtained from Fisher Scientific. Deionized water with a resistivity of 17 mega-ohm-cm was obtained from a Barnstead NANOPURE II™ water purification system.

PEOX has a χ parameter of 0.489 at 25°C in water [22] and is fully soluble in IpOH at 25°C as well, although its χ parameter in IpOH is not known. PDMS is insoluble in water but is marginally soluble in anhydrous IpOH.

Sample Preparation

Stock polymer solutions (10 g/100 ml) were prepared in water and isopropanol and were stored at 4°C until used for dilutions. Polymer solutions were mixed in various water/isopropanol compositions so that the polymer concentration varied from 0.05 g/l to 10 g/l and the solvent composition, expressed as mole fraction IpOH, X_{IpOH}, varied from 0 to 1. Prior to the light scattering experiments, all polymer solutions were filtered through two 0.2 micron PTFE Gelman Acrodisc® filters in series.

Table 5.1. Polymer Characterization Data

Polymer	Approximate Molecular Weight M_n, kg/mole	Degree of polymerization DP
PEOX 5	5	50
PEOX 20K	20	201
PDMS 14K	14	189
PEOX/PDMS, 20K-5K	20/5	202/68
PEOX/PDMS, 8K-2K	8/2	81/27

Dynamic Light Scattering

Dynamic light scattering measurements were made with a Brookhaven BI-2030AT digital correlator equipped with 136 channels. All measurements were made at 25$\pm$0.1°C. A Lexell argon ion Model 95-2 laser was used at a wavelength of 514.5 nm and at a light intensity of typically 20-25 mW. The scattering intensity was measured over the angular range 30-135°. Borosilicate glass sample cells were used in the goniometer with a decalin bath. A comprehensive treatment of the theory of dynamic light scattering (DLS) can be found elsewhere [23] and so it is only briefly reviewed below.

The scattering intensity was measured to generate the autocorrelation function which, for polydisperse systems, can be written in terms of the cumulant expansion [24,25]

$$\ln[b^{1/2}g(m\Delta t)] = \ln b^{1/2} - \Gamma_{avg}(m\Delta t) + \mu_2(m\Delta t)^2/2 + \quad ..(1)$$

where μ_2 is the second cumulant, m is the channel number, Δt is the sample time, b is an optical constant, and Γ_{avg} is the average linewidth which is related to the diffusion coefficient D by

$$\Gamma_{avg} = Dq^2 \qquad (2)$$

The scattering vector q is defined by

$$q = 4\pi n \sin(\theta/2)/\lambda \quad (3)$$

where n is the solvent refractive index, θ is the scattering angle, and λ is the wavelength. All of the light scattering data reported in this work were obtained from the second cumulant expansion. The polydispersity of the solutions can be characterized by the polydispersity factor, PD, defined as

$$PD = \mu_2/\Gamma_{avg}^2. \quad (4)$$

Solutions and suspensions typically have values of PD = 0.02-0.08 for narrow distributions [25].

For scattering particles that are large compared to the wavelength λ, it is necessary to perform scattering experiments at sufficiently low angles to probe the z-average translational diffusion regime [23], i.e.,

$$D_z = \lim_{q \to 0} \Gamma_{avg}/q^2. \quad (5)$$

For spheres, the diffusion coefficient D_z is related to the hydrodynamic diameter D_h by the Einstein equation

$$D_z = kT/3\pi\eta D_h \quad (6)$$

where k is Boltzmann's constant, T is temperature, and η is the liquid phase viscosity. Values of the solvent refractive index n and viscosity for mixtures of water and isopropanol at 25°C were obtained from the literature [26]. The minimum size measurement limit for the Brookhaven light scattering instrument is approximately 3 nm.

For prolate ellipsoids, the translational diffusion coefficient D_z is related to the aspect ratio p = a/L, where a is the semi-minor axis length and (L/2) is the semi-major axis length [27]:

$$D_z = kT/f \tag{7}$$

where f is the friction factor. For any value of $p < 1$,

$$f = 6\pi\eta r/p^{2/3}S \tag{8a}$$

where:

$$S = (1-p^2)^{-1/2} \ln[\{1+(1-p^2)^{1/2}\}/p] \tag{8b}$$

$$r = (La^2/2)^{1/3} \tag{8c}$$

and r is defined as the radius of the sphere with the same volume as the ellipsoid. In the limit $p << 1$, equation (8a) for f reduces to the friction factor for a cylinder,

$$f = 6\pi\eta a/\ln(2/p). \quad (9)$$

Results and Discussion

Translational Diffusion Coefficients

Values of D_z were obtained from the slope of a plot of Γ_{avg} versus q^2 corresponding to angles ranging from 30 - 135° for PEOX-PDMS 20K-5K and 8K-2K copolymer in a variety of solvent compositions. The polymer concentrations and solvent compositions were chosen to span the range of observed micellar structures. A typical plot of Γ_{avg} versus q^2 in Figure 5.2 for PEOX-PDMS 20K-5K copolymer at polymer concentration C_p= 10 g/l and mole fraction IpOH X_{IpOH} = 0.231 shows the lack of curvature even at high angles. The extrapolated values of D_z are shown in Table 5.2 along with diffusion coefficients measured at the scattering angle $\theta = 90^0$, D_{90}. Diffusion coefficients containing mixed contributions from translational and internal flexing modes are larger than the z-average translational diffusion coefficient D_z since the internal flexing modes occur on a much shorter time scale than translation of the center of mass [23]. In all cases for the 20K-5K copolymer, the diffusion coefficients measured at $\theta = 90^0$ contained no significant contributions from internal flexing modes. The 8K-2K copolymer appears to exhibit some internal flexing modes $X_{IpOH} \leq 0.032$ but none for

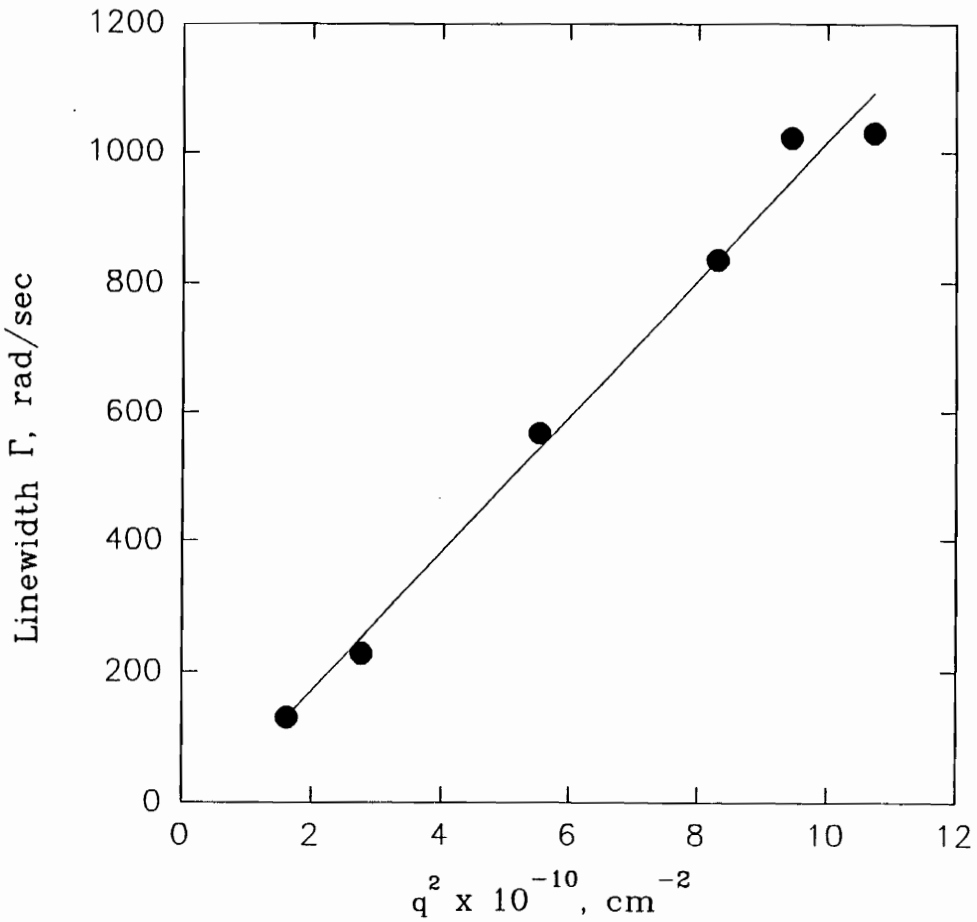

Figure 5.2. Extrapolation of linewidth Γ versus square of scattering vector q^2 to determine effects of internal flexing modes for micelles of PEOX-PDMS 20K-5K copolymer at mole fraction isopropanol X_{IpOH} = 0.23 and polymer concentration C_p = 10 g/l, ●.

Table 5.2. Angular Extrapolation of Diffusion Coefficients of PEOX-PDMS Copolymer at 25°C

Polymer	Polymer Concentration C_p, g/l	Isopropanol Mole Fraction X_{IpOH}	Diffusion Coefficient, $cm^2/sec \times 10^8$ at 90^0 D_{90}	zero-angle limit D_z
20K-5K	0.05	0.0	15.2	15.0
	1.0	0.03	10.0	10.8
	1.0	0.20	3.74	3.81
	5.0	0.0	13.4	13.7
	5.0	0.23	1.70	1.75
	10.0	0.0	20.4	20.6
	10.0	0.23	1.02	1.16
8K-2K	0.1	0.0	3.20	2.39
	0.1	0.03	2.28	2.14
	0.1	0.09	2.00	2.07
	0.1	0.23	1.89	2.09

higher IpOH concentrations. The mode of association of the 8K-2K copolymer is believed to differ from that of the 20K-5K copolymer. This will be discussed below in the section on the 8K-2K copolymer. All of the values for the hydrodynamic diameter D_h and micelle length L reported in this work were calculated with values of D_{90} using equations (6) and (7-8), respectively. The reproducibility of the resulting values of D_{90} or D_h were typically 10% or less and no effect of time was observed for periods over two weeks.

PDMS and PEOX Homopolymer Solutions

The hydrodynamic diameter of PDMS 14K at a concentration of 10 g/l was measured in anhydrous isopropanol and chlorobenzene to separate the effects of solvent composition on the PDMS block from the PEOX block. Chlorobenzene was chosen to provide a comparison with IpOH since chlorobenzene is a good solvent for PDMS [29] while there are no published data on the solubility of PDMS in IpOH. The measured hydrodynamic diameters were compared with theoretical values of the hydrodynamic diameter $D_{h\Theta}$ calculated from [28]:

$$D_{h\Theta} = 1.33R_{g\Theta} \tag{10a}$$

where

$$R_{g\Theta} = (L_c L_k/6)^{0.5}. \tag{10b}$$

L_c is the contour length and L_k is the Kuhn length which characterizes the effective stiffness of the polymer backbone. Equations (10a-b) are valid for non-draining Gaussian coils at the Θ-state. While this is not necessarily the case for the PEOX and PDMS chains at low molecular weights, these equations provide useful, approximate values of D_h. Values of L_k can be determined from equation (10b) using values of $R_{g\theta}$ determined by light scattering or from:

$$L_k = (M_{Mon}/L_{Mon})*(6R_g^2/M_w) \quad (11)$$

where M_{mon} and L_{mon} are the monomer molecular weight and length, respectively, and the ratio R_g^2/M_w is available for many polymers [29].

For PDMS 14K in pure IpOH, very weak scattering was obtained, giving $D_h \leq$ 4 nm while D_h = 4 nm in chlorobenzene. Given the literature value of $R_g/M_w^{0.5}$ = 0.025 nm for PDMS [29], L_k = 1.1 nm from equation (11) which corresponds to four monomer units in the PDMS backbone acting as a rigid segment. From equation (10a), $D_{h\Theta}$ = 4.5 nm. The results suggest that PDMS is near its theta state in pure IpOH at 25°C.

The hydrodynamic diameters D_h of PEOX 5K and 20K at a polymer concentration of 10 g/l were also measured at various solvent compositions to understand better the effects of solvent composition on the PEOX blocks in the corresponding copolymers. The values of D_h for PEOX 20K, listed in Table 5.3, range from 6-8 nm with D_h being

Table 5.3. Effect of Solvent Composition on the Hydrodynamic Diameter of PEOX Homopolymer at Polymer Concentration C_p = 10 g/l

Isopropanol Mole Fraction X_{IpOH}	Hydrodynamic Diameter, D_h^*, nm	
	PEOX 5K	PEOX 20K
0.00	16	8
0.23	3	6
1.00	3	6

* from equation [6] at scattering angle θ = 90°.

slightly higher in pure water. This suggests water is a better solvent for PEOX than isopropanol. This is reasonable given that water can form stronger hydrogen bonds with the carbonyl group in the PEOX repeat unit than can IpOH. A review of the literature reveals no light scattering studies or values of R_g^2/M_w for PEOX. However L_k values in the range 1.1-1.4 nm appear to constitute reasonable lower bounds given that L_k = 1.1 nm for PDMS which is known to be quite flexible. With L_k = 1.1-1.4 nm, the estimated Θ-state value of D_h for PEOX 20K varies between 4.1-4.6 nm. The difference between this range and the measured values of 6-8 nm is probably due to the approximations involved in equations (10a-b), excluded volume effects, and instrument uncertainty. Finally, the value of D_h= 16 nm for PEOX 5K in water was much larger than the expected value of ≈1 nm from equation [10a] and much larger than D_h = 8 nm measured for PEOX 20K in water. The reason for these differences will be discussed in the section below on the copolymer PEOX-PDMS 8K-2K.

PEOX-PDMS 20K-5K Copolymer Solutions

Table 5.4 and Figure 5.3 summarize the diffusion coefficients measured at θ = 90^0, D_{90}, for the PEOX-PDMS 20K-5K copolymer as a function of polymer concentration, C_p, and isopropanol mole fraction, X_{IpOH}. The diffusion coefficients initially decreased with increasing X_{IpOH} at all polymer concentrations due to an increase in the solvent viscosity. For C_p = 0.05 g/L and X_{IpOH} > 0.03, D_{90} could not be measured because of very weak scattering presumably due to the formation of isolated

Table 5.4. Summary Of Translational Diffusion Coefficients for PEOX-PDMS 20K-5K Copolymer

Polymer Concentration	Isopropanol Mole Fraction	Diffusion Coefficient	Hydrodynamic Diameter	Micelle Length	Aspect Ratio
C_p, g/l	X_{IpOH}	D_{90}, cm^2/sec x10^8	D_h^*, nm	L^{**}, nm	P, 2a/L
0.05	0.0	15.2	32	--	--
	0.03	12 .1	28	--	--
1.0	0.0	17.1	29	--	--
	0.03	10.0	34	--	--
	0.11	9.92	20	--	--
	0.17	9.65	17	--	--
	0.20	3.74	39	40	0.8
	0.23	37.5	4	--	--
5.0	0.0	13.4	36	--	--
	0.11	4.95	33	--	--
	0.17	6.32	25	--	--
	0.23	1.70	85	208	0.15
	0.27	6.17	22	--	--
	0.31	26.7	5	--	--
10.0	0.0	20.4	24	--	--
	0.03	10.9	31	--	--
	0.11	7.95	25	--	--
	0.14	6.48	27	--	--
	0.17	3.62	43	50	0.64
	0.23	1.02	136	454	0.06
	0.27	33.9	4	--	--
	0.31	31.5	4	--	--
	1.00	39.3	5	--	--

* from equation [6] for spherical geometry

** from equations [7] and [8] with prolate ellipsoid minor axis 2a = 32 nm

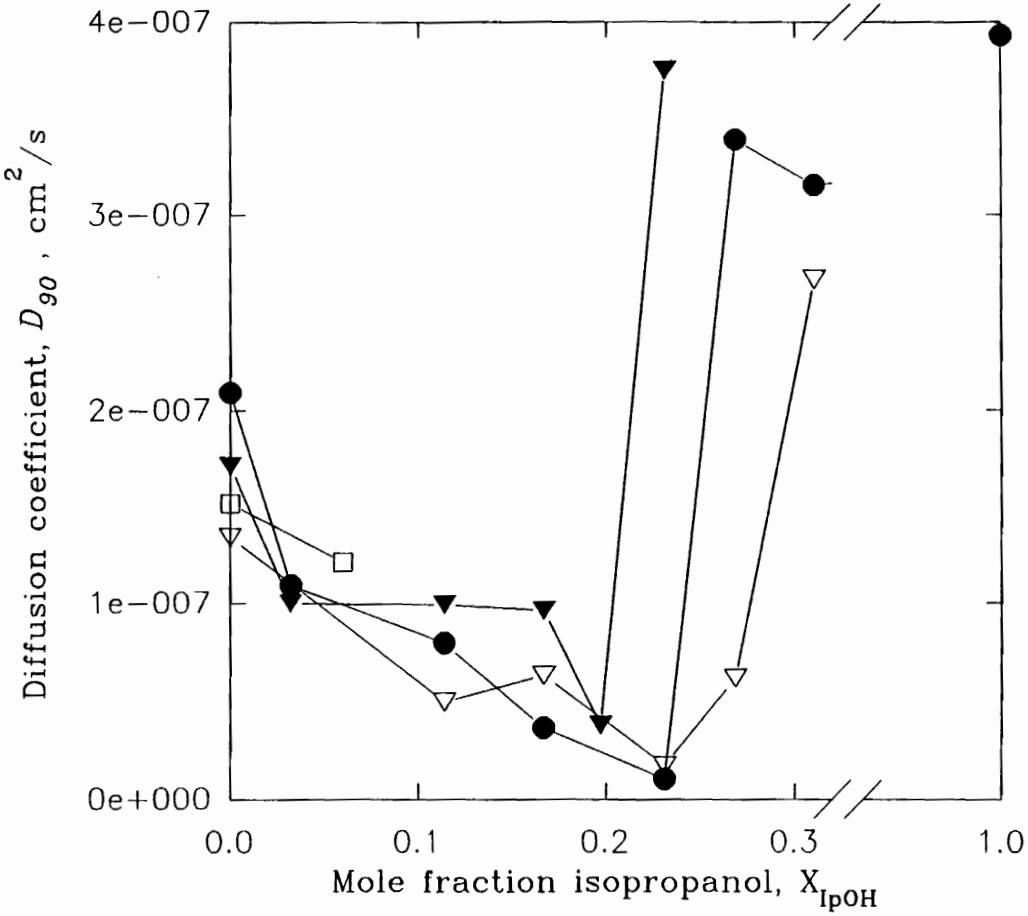

Figure 5.3. Effect of solvent composition on the diffusion coefficient of PEOX-PDMS 20K-5K copolymer at different polymer concentrations: □ C_p = 0.05 g/l; ▼ C_p = 1 g/l; ▽ C_p = 5 g/l; ● C_p = 10 g/l.

chains. At polymer concentrations of 1, 5, and 10 g/l, the diffusion coefficients reached minimum values in the range X_{IpOH} = 0.20-0.23 and then increased to the point where single chains formed. Three regimes were observed as the solvent composition and polymer concentration changed: (i) Regime I- spherical micelles in pure water and in mixtures of water/isopropanol for isopropanol mole fraction $X_{IpOH} \leq 0.17$ depending on the polymer concentration, (ii) Regime II- nonspherical micelles at intermediate solvent compositions X_{IpOH} = 0.08-0.26, and (iii) Regime III- isolated, single chains in isopropanol-rich solvents for $X_{IpOH} > 0.23$-0.26, again, depending upon the polymer concentration.

Regime I - Spherical Micelles in a Selective Solvent

In pure water, the copolymer formed micelles with D_h = 29-36 nm. The insensitivity of D_{90} to changes in polymer concentration C_p in the range 0.05-5 g/l, as shown in Table 5.5, leads us to conclude these micelles are approximately spherical in shape. The higher value of D_{90} at C_p = 10 g/l may represent a trend of D_{90} increasing with C_p. If so, this would be consistent with the behavior of spherical micelles with repulsive pair interactions in the dilute regime where [23]:

$$D_z = D_z(0)[1 + K(C_P - cmc) + \ldots] \qquad [12]$$

where $D_z(0)$ is the diffusion coefficient at the critical micelle concentration, cmc, and K

is a constant. The spherical micelle sizes are consistent with the experimental values of D_h = 6-8 nm for the PEOX 20K homopolymer and $D_h \sim$ 2 nm for PDMS 5K calculated from equations (10a-b) if the PEOX chains in the micelle corona are slightly extended and for reasonable values for the aggregation number.

An upper limit for the cmc in water is 0.05 g/l or polymer volume fraction = 5 x 10^{-5} assuming the polymer density to be 1 g/ml. At C_p = 0.05 g/l, only spherical micelles were observed up to X_{IpOH} = 0.03 beyond which very weak scattering was measured, indicating a transition from spherical micelles to single chains. This is due to a decrease in solvent incompatibility with PDMS and hence an increase in cmc with X_{IpOH}. This implies that the cmc lies relatively close to 0.05 g/l in water.

The micelles had relatively low values of the polydispersity factor PD as evident from Table 5.5. In Figure 5.4, the plot of D_h versus scattering angle θ for PEOX-PDMS 20K-5K at C_p = 10 g/l shows that D_h decreases somewhat with decreasing θ which is opposite the expected trend if the micelles were highly polydisperse [23].

Table 5.5. Spherical Micelle Regime Results For PEOX-PDMS 20K-5K Copolymer at Mole Fraction Isopropanol $X_{IpOH} = 0$

Polymer Concentration C_p, g/L	Diffusion Coefficient D_{90}, $cm^2/sec \times 10^8$	Hydrodynamic Diameter, D_h^*, nm	Polydispersity Index, PD**
0.05	15.2	32	0.12
1	17.1	29	0.13
5	13.4	36	0.15
10	20.4	24	0.12

* from equation [6]

** from equation [4]

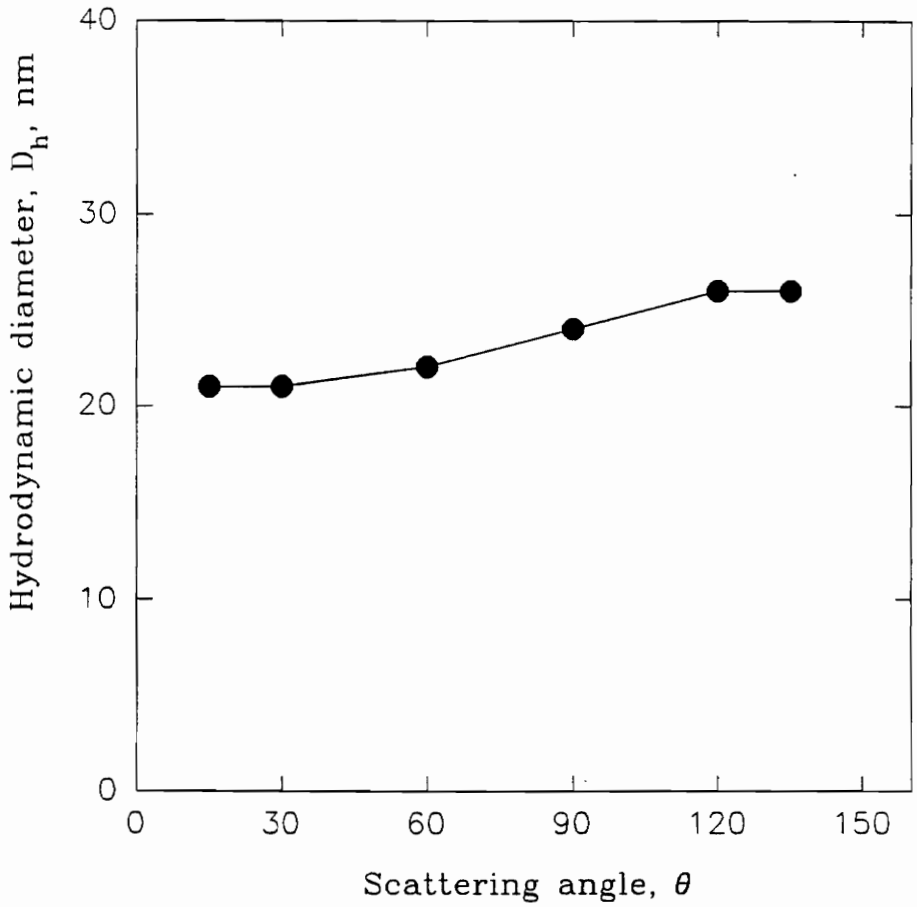

Figure 5.4. Hydrodynamic diameter, D_h, of PEOX-PDMS 20K-5K copolymer versus scattering angle θ at polymer concentration C_p = 10 g/l in water, ●.

Spherical micelles are predicted by the theory of Munch and Gast [9] for a high degree of incompatibility $\chi_{BS}N_B$, when the insoluble block B (PDMS) is smaller than the soluble A block (PEOX) and when the solvent size N_s is small with respect to the total degree of polymerization N, characterized by the ratio N/N_s. The theory assumes that there is no partitioning of solvent into the micellar core and that the block comprising the corona is in an athermal solvent. However, $\chi_{PEOX} > 0$ for water and probably for IpOH as well. For these reasons, no quantitative analysis of our results were made based on this theory.

Regime II - Mixed Solvent Effects

For C_p 1-5 g/l, the hydrodynamic diameter D_h generally decreased slightly upon initially increasing X_{IpOH} as shown in Figure 5.5 and Table 5.4. This is due to the decreasing incompatibility of the solvent, resulting in an increase in cmc and a shift in equilibrium from micelles to single chains. Upon further increasing X_{IpOH}, sharp increases in D_h occurred, reaching a maximum in the range $0.20 \leq X_{IpOH} \leq 0.23$ followed by a sharp decrease. The increase in D_h with X_{IpOH} cannot be due to expansion of PDMS cores in spherical micelles because PDMS in pure IpOH is close to its theta state as shown by the scattering experiments for the PDMS 14K homopolymer. The increase in D_h is probably not due to expansion of the PEOX chains in the corona because of the extremely large degree of expansion needed to account for the hydrodynamic sizes shown in Figure 5.4.

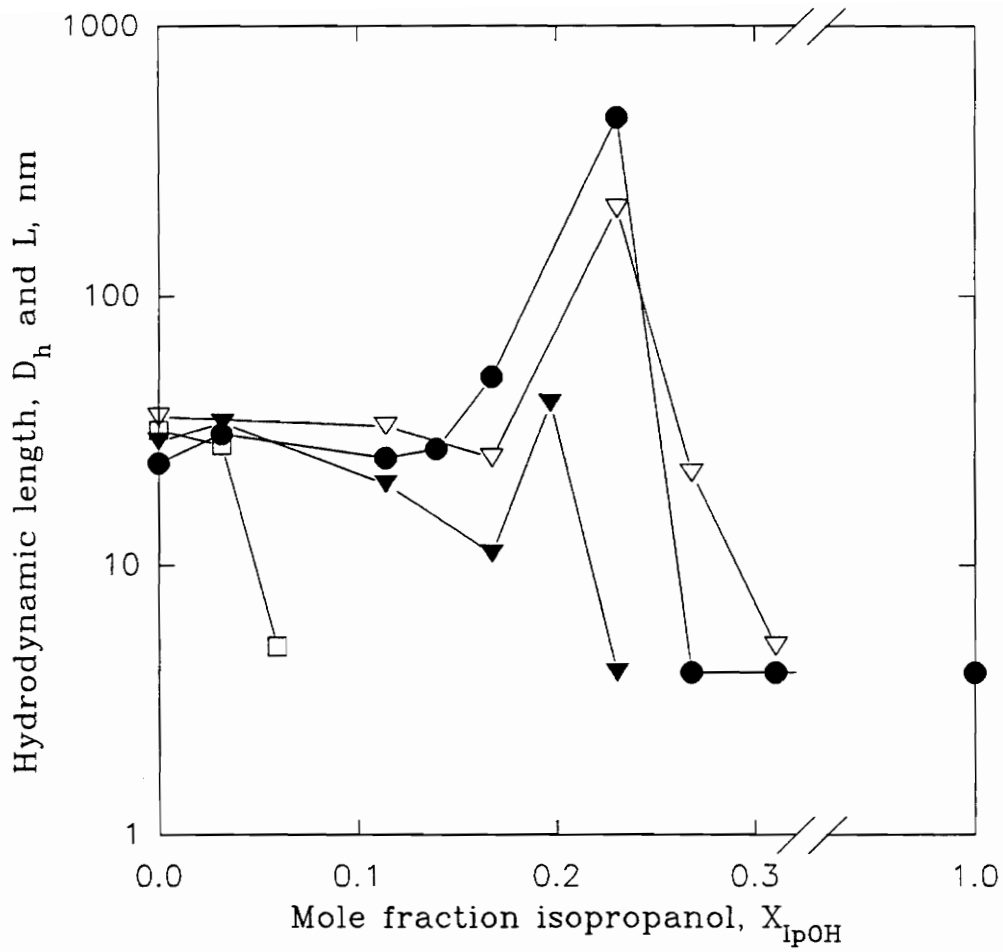

Figure 5.5. Hydrodynamic diameter D_h and length L of PEOX-PDMS 20K-5K copolymer versus mole fraction isopropanol X_{IpOH} at different polymer concentrations: □ C_p = 0.05 g/l; ▼ C_p = 1 g/l; ▽ C_p = 5 g/l; ● C_p = 10 g/l.

For example, for C_p = 10 g/l and X_{IpOH} = 0.23, the PEOX chains would have to be essentially fully extended to account for the observed D_h = 136 nm calculated from equation (6) for spherical geometry.

We believe the significant increase in the hydrodynamic size is due to a transition from spherical to ellipsoidal micelles since the lower surface/volume ratio of an ellipsoid would minimize the contact of the hydrophobic PDMS core with the aqueous phase. The hydrodynamic lengths L of micelles were calculated from equations (7)-(8) for those conditions of C_p and X_{IpOH} giving D_h > 36 nm as calculated for spheres from equation (6). A prolate ellipsoid minor axis of 2a = 32 nm was used in all of the calculations. It was assumed that the ellipsoidal micelles had a minor axis length equal to the average hydrodynamic diameter of the spherical micelles. The results for ellipsoidal micelle length L are tabulated in Table 5.4 and are plotted in Figure 5.5 along with values of hydrodynamic diameter D_h calculated from equation (6) assuming spherical geometry before the transition in micelle shape occurs.

It is highly probable that ellipsoidal micelles with L > 100-200 nm could form flexible, threadlike or wormlike structures similar to those reported for low molecular weight surfactants in aqueous solutions rather than rigid structures [30-32]. However, the ellipsoidal micelles at C_p = 1-5 g/l with L = 40-208 nm may be relatively rigid given the absence of internal flexing modes as shown in Table 5.2 and Figure 5.2. The highest value of L, 454 nm at C_p = 10 g/l, is extremely large for a rigid, ellipsoidal micelle and therefore may reflect effects of hindered diffusion of ellipsoids at relatively high polymer

concentration as illustrated by equation (12). Since the aggregation number is not known for these micelles, the hydrodynamic volume fraction of micelles cannot be calculated and hence a definitive interpretation of micellar structure at C_p = 10 g/l cannot be given. Further elucidation of the structure will require static light scattering measurements of R_g or depolarized dynamic light scattering measurements of the rotary diffusion coefficient.

In terms of the theory by Munch and Gast, the incompatibility parameter $\chi_{BS}N_B$ decreases as X_{IpOH} increases. If spherical micelles predominated in this regime, the cmc and the aggregation number should increase and the micelle radius should decrease due to corona contraction. However, we observe that the micelle size increases sharply with polymer concentration at fixed values of X_{IpOH} in the range 0.20-0.23, as seen in Figure 5.4, and hence spherical geometry is ruled out in this transition region. The increase in length L from 40-454 nm as C_p increased from 1-10 g/l is consistent with previously observed trends in low molecular weight surfactant systems where ellipsoidal micellar length increased with surfactant concentration [30].

Regime III - Isolated Chains in a Nonselective Solvent

In anhydrous isopropanol, X_{IpOH} = 1, and for sufficiently high values of X_{IpOH}, the copolymer existed as isolated chains with D_h = 5 nm. This is reasonable since both PEOX and PDMS blocks are solvated as shown above in the section on homopolymer solution behavior. The hydrodynamic diameter of the 20K-5K diblock was slightly lower

than that of the PEOX 20K homopolymer, 6 nm. However, this difference is experimentally insignificant.

The formation of single chains under solvent conditions that are relatively nonselective is consistent with the study by Duval and Picot [17] cited earlier where the PS-PMMA block copolymer formed single chains in solutions of dioxane, a good solvent for both blocks, for dioxane weight fraction $\Phi > 0.4$. Their results for $\Phi < 0.4$ are also relevant to our results in Regimes I and II in that they observed spherical micelles for $\Phi < 0.1$ and micelles with anomalously large hydrodynamic diameters for $0.1 < \Phi < 0.4$. Qualitatively similar results were also obtained by Mandema et al. [7].

PEOX 8K-PDMS 2K Copolymer Solutions

Anomalously large values of D_h were observed in solutions of the 8K-2K copolymer as shown in Table 5.6. Hydrodynamic diameters as large as 173 nm were calculated assuming spherical geometry from equation [6]. These sizes are clearly larger than expected if the copolymer formed spherical micelles. In water/IpOH mixtures, the micelle size generally decreased with increasing X_{IpOH} at a fixed polymer concentration $C_p = 0.1$ g/l. For $X_{IpOH} > 0.23$, very weak scattering was obtained indicating the transition from a micellar to a single chain regime. For $X_{IpOH} = 0$, D_h was roughly insensitive to changes in polymer concentration.

Table 5.6. Summary of Translational Diffusion Coefficients for PEOX-PDMS 8K-2K Copolymer

Polymer Concentration C_p, g/l	Isopropanol Mole Fraction X_{IpOH}	Diffusion Coefficient D_{90}, $cm^2/sec \times 10^8$	Hydrodynamic Diameter D_h^*, nm
0.1	0.0	3.20	153
	0.02	3.08	129
	0.07	2.28	150
	0.09	2.00	104
	0.23	1.89	75
0.025	0.0	2.87	171
0.050	0.0	3.07	160
0.100	0.0	3.20	153
0.500	0.0	3.32	148
5.00	0.0	2.83	173

* from equation [6] assuming spherical geometry

While it is conceivable that this copolymer may be forming threadlike or wormlike micelles whose contour length greatly exceeds the minor axis dimensions [30-32], we believe the anomalously large micelle sizes are due to aggregation of relatively small micelles, possibly spherical in shape, caused by interchain hydrogen bonding between carbonyl groups on PEOX chains in different micelles. Evidence for this comes from the light scattering data for the PEOX 5K homopolymer, shown in Table 5.3, which demonstrate that homopolymer association occurred at $X_{IpOH} = 0$ but not at higher IpOH concentrations. For PEOX 5K homopolymer in pure water, $D_h = 16$ nm which is much greater than the theta-state value of $D_{h\Theta} \simeq 1$ nm estimated from equation (10). For $X_{IpOH} \geq 0.23$, $D_h \simeq 3$ nm which is at the limit of dynamic light scattering resolution. Thus, PEOX 5K either does not associate at all for $X_{IpOH} > 0.23$ or it associates only very slightly. This decrease in association is plausible because increasing IpOH concentration reduces the probability that a water molecule can form a hydrogen bond between any two PEOX chains. This is also consistent with the observed trend of D_h decreasing with increasing X_{IpOH} for the 8K-2K copolymer at $C_p = 0.1$ g/l as shown in Table 5.6. For $X_{IpOH} > 0.23$, very weak scattering was observed, indicating the disappearance of the micelle structure and the formation of single copolymer chains.

Relatively few interchain hydrogen bonds per chain would be needed to give rise to the observed association for PEOX 5K homopolymer. By contrast, chain association was not observed for the PEOX 20K homopolymer as shown in Table 5.3. This effect of molecular weight on homopolymer chain association can be explained if the PEOX

chains undergo a conformational change leading to chain extension due to multiple inter-hydrogen bonding. Such a conformational change is possible in principle if multiple hydrogen bonds form between any two chains. The loss in entropy due to chain extension of PEOX 5K may be more than compensated by the decrease in free energy due to hydrogen bonding. Given the degree of polymerization of PEOX 5K, DP = 50, and a conservative estimate of the lower limit on the Kuhn length of the chain, L_K = 1.1 nm, the 5K chain would contain no more than approximately 13 effective Kuhn segments. Thus, even in the absence of interchain hydrogen bonding, the segmental distribution function is expected to be somewhat non-Gaussian [33] and anisotropic and thus the entropy loss due to chain extension caused by interchain hydrogen bonding may be relatively low. However, in the case of PEOX 20K, the loss in entropy due to chain extension would be greater given the greater number of effective Kuhn segments, approximately 52, and hence the decrease in free energy upon association due to hydrogen bonding would not be enough to offset the entropic penalty for association.

A similar aggregation effect was reported by Winnik for aqueous solutions of poly(ethylenoxide), PEO, where hydrogen bonds form between ether oxygens in the chain and water [11]. The hydrogen bonds between PEOX and water should be stronger than those formed between PEO and water due to the higher polarity of the carbonyl oxygen on the PEOX and hence the association of PEOX should be even more pronounced than the association of PEO.

Conclusions and Future Work

Solutions of poly(2-ethyl-2-oxazoline-dimethylsiloxane), PEOX-PDMS, block copolymers in water-isopropanol mixtures have been studied by dynamic light scattering. A diblock consisting of PEOX with M = 20 Kg/mole and PDMS with M = 5 Kg/mole, 20K-5K, exhibited three regimes of association. In pure water and at low mole fractions of isopropanol, the 20K-5K copolymer formed spherical micelles having hydrodynamic diameters of about 32 nm, where the hydrophobic PDMS blocks formed the core and hydrophilic PEOX blocks formed the corona. At a critical isopropanol mole fraction and for $C_p \geq 1$ g/l, anomalously large micelles were observed which are believed to be ellipsoidal in shape. The length of the ellipsoids increased with polymer concentration. For mole fractions isopropanol $X_{IpOH} > 0.23$, unassociated polymer chains existed at all copolymer concentrations. A second diblock consisting of a PEOX block with M = 8 kg/mole and PDMS with M = 2 kg/mole formed micelles having unusually large hydrodynamic diameters which are believed due to the aggregation of micelles caused by hydrogen bonding between PEOX chains comprising micellar coronas. This was suggested by the observed association of PEOX homopolymer with M = 5 kg/mole in water. The micelle size of the 8K-2K copolymer decreased with increasing IpOH concentration due to a reduction in the hydrogen bonding capability of the solvent. For $X_{IpOH} \geq 0.23$, only single chains existed in solution, a regime consistent with the 20K-5K copolymer results.

Future studies of these copolymers by dynamic light scattering will include the use of the program CONTIN to determine micelle size distribution. Static light scattering will be used to characterize the variation in molecular weight M_w, second virial coefficient A_2, and radius of gyration R_g of the copolymer as a function of IpOH concentration. Small angle x-ray scattering will be used to measure the R_g of the micellar core in solutions where the electron density of the solvent matches that of the corona, thus making the core visible [10]. This may be done in solutions of PEOX-PDMS in N-ethylacetamide which is virtually identical to the repeat unit of PEOX.

References

(1) Tadros, Th.F. *Surfactant*; Academic Press Inc: Orlando, Florida, **1984**.

(2) Napper, D.H. *Polymeric Stabilization of Colloidal Dispersion*; Academic Press: London, **1983**.

(3) Gast, A.P.; Munch, M.R. *Polymer Communications* **1989**, 30, 324.

(4) Gast, A.P.; Munch, M.R. *Colloids and Surfaces* **1988**, 31, 47.

(5) Patel, S.; Tirrell, M. *Colloids Surf.* **1988**, 31, 157.

(6) Mandema, W.; Emeis, C.A.; Zeldenrust, H. *Makromol. Chem.* **1979**, 180, 1521.

(7) Mandema, W.; Emeis, C.A.; Zeldenrust, H. *Makromol. Chem.* 1979, 180, 2163.

(8) Sikora, A.; Tuzar, Z. *Makromol. Chem.* **1983**, 184, 2049.

(9) Munch, M.R.; Gast, A.P. *Macromolecules* **1988**, 21, 1360.

(10) Hilfiker, R.; Chu, B.; Xu, Z. *J. Colloid and Interface Science* **1989**, 133(1), 176.

(11) Xu, R.; Winnik, M.A. *Macromolecules* **1991**, 24, 87.

(12) Zero, K.; Pecora, R. *Dynamic Light Scattering*, ed. R. Pecora, Plenum Press, N.Y., **1985**; chapter 3.

(13) Schouten, M.; Dorrepaal, J; Stassen, W.J.M.; Vlak, W.A.H.M.; Mortensen, K. *Polymer* **1989**, 30, 2038.

(14) Richards, R.W., et al. *Polymer* **1986**, 27, 643.

(15) Watanabe, H.; Kotaka, T. J. *Rheology* **1982,** 26(2), 153.

(16) Halperin, A. *Macromolecules* **1987**, 20, 2943.

(17) Duval, M.; Picot, C. *Polymer* **1987**, 28, 798.

(18) Cogan, K.A.; Gast, A.P. *Macromolecules* **1990**, 23, 745.

(19) Vagberg, L.J.M.; Cogan, K.A.; Gast, A.P. *Macromolecules* **1991,** 24, 1670.

(20) Daoud, M.; Cotton, J.P. *J.Phys.(Les Ulis,Fr.)* **1982**, 43, 531.

(21) Liu, Q.; Wilson, G.R.; Davis, R.M.; Riffle, J.S. *Polymer London*, in Press, 1992; Riffle, J.S.; Sinai-Zingde, G.; DeSimone, J.M.; Hellstern, A.M.; Chen, D.H.; Yilgor, I. *Polymer Preprints* **1988**, 29(2), 93.

(22) Wilson, J.; Davis, R.M., in preparation.

(23) Pusey, P.N.; Tough, R.J.A. *Dynamic Light Scattering*; Plenum Press, N.Y., **1985**; chapter 4.

(24) Pusey, P.N. *Journal of Chemical Physics* **1975**, 62, 1136.

(25) *Instruction Manual for Model BI-2030 AT Digital Correlator*; Brookhaven Instruments Corporation, N.Y., **1986.**

(26) Chu, K.; Thompson, R. *Journal of Chemical and Engineering Data* **1962**, February, 358.

(27) Richards, E.G. *An Introduction to Physical Properties of Large Molecules in Solution*; Cambridge University Press, **1980.**

(28) Tanford, C. *Physical Chemistry of Macromolecules*; John Wiley & Sons, Inc., N.Y., **1961**; chapter 6.

(29) Brandrup, J.; Immergut, E.H. *Polymer Handbook*; John Wiley & Sons, Inc., N.Y., **1975**.

30) Candau, S.J.; Hirsch, E.; Zana, R. *Journal de Physique* **1984**, 45, 1263.

(31) Imae, Toyoko *J. Phys. Chem.* **1990**, 94, 5953.

(32) Brown, W., et al., *J. Phys. Chem.* **1989**, 93, 5888.

(33) Yamakawa, H.; Stockmayer, W. *J. Chem. Phys.* **1972**, 57, 2843.

Chapter 6

Novel Thin Films of Titanium Dioxide Particles Synthesized by a Sol-Gel Process

Introduction

There is considerable interest in thin films for applications such as ultraviolet filters for optics and packaging material, narrow band pass interference filters with controlled refractive index gradients, antireflection coatings for photovoltaic cells and passive solar collectors [1], and thin ceramic films or membranes with controlled porosity [2a]. This work concerns the fabrication and properties of novel composite thin films of ultra-fine TiO_2 particles dispersed in a matrix of the thermoplastic polymer hydroxypropylcellulose, HPC. Sub-100 nm size TiO_2 particles are synthesized in a sol-gel process using HPC initially as a steric stabilizer to limit particle size. In a second step, suspensions of TiO_2 in HPC solutions are used in a spin-coating process to form thin, transparent composite films which absorb strongly in the ultraviolet part of the spectrum. It is possible to burn out the HPC polymer at 450°C, resulting in a porous and transparent TiO_2 film where the porosity can be controlled by the original TiO_2/HPC ratio and the sintering temperature.

Thin, transparent ceramic films have been made previously by various vapor-phase methods including chemical vapor deposition, reactive evaporation, electron beam evaporation, and sputtering [1]. These methods require relatively high temperatures and sophisticated equipment [2b]. High temperatures limit the choice of substrates on which the films can be formed. The film properties depend on deposition conditions such as oxygen pressure, rate of deposition, and substrate temperature. Films made by these processes tend to be crystalline and nonporous. While these methods are useful for making films with single layers, they are more cumbersome when multilayer films are required.

Relatively thick polymer films containing TiO_2 were made by Meldrum et al. by dispersing sub-100 nm TiO_2 particles in molten polypropylene [3]. These films had ultra-violet barrier properties with potential applications in the packaging industry. However, the difficulty of dispersion and mixing of the TiO_2 particles in a highly viscous polypropylene melt complicates processing.

By comparison, films derived from alkoxides using sol-gel processes require considerably less equipment, resulting in generally lower processing costs. A major advantage of sol-gel processes over the vapor-phase methods is the ability to control the microstructure of the deposited film, i.e., the pore size, pore volume, and surface area [2b]. Films made from sol-gel processes are mainly deposited by dip coating, spin coating, or spray coating. TiO_2 films made by the sol-gel process have been made by partially hydrolyzing titanium tetraethoxide (TEOT) where [molarity H_2O]/[molarity

TEOT] < 2 in the presence of acid as a catalyst [4-7] according to the reactions:

$$Ti(OC_2H_5)_4 + 4H_2O \rightarrow Ti(OH)_4 + 4C_2H_5OH \text{ ..... Hydrolysis (1)}$$

$$Ti(OH)_4 \rightarrow TiO_2 \cdot xH_2O + (2 - x)H_2O \text{ ..... Condensation (2)}$$

TEOT hydrolyzes in a step-wise manner in the first reaction and, in the subsequent step-wise condensation reaction, forms TiO_2. The low concentrations of water used in the reaction necessitates strict control of the moisture level in the reagents and during the film formation step. In a study by Brinker and Hurd, TiO_2 films were made by partially hydrolyzing TEOT in ethanol using $[H_2O]/[TEOT] = 1$ in the presence of HCl [8]. The partially hydrolyzed species condensed to form oligomers composed of Ti-O-Ti about 1 nm in diameter. Films made by these species continued to hydrolyze and condense due to atmospheric moisture. The as-deposited film had a refractive index of 1.7 at a film thickness of about 200 nm. Upon heating for 5 minutes at 450°C the refractive index increased to 2.2 and the film thickness decreased by 30-40 %.

The films made by the procedure described in the present paper have the following advantages: (i) a wider choice of substrates is available since the films are made in the absence of any acid or base catalysts which may be corrosive; the absence of catalysts results in films relatively free of impurities that might limit

optical or electronic applications, (ii) the film properties do not change with time as the TEOT is fully hydrolyzed and condensed into TiO_2 particles prior to film formation, (iii) crack-free films with thicknesses greater than 1 μm are produced relatively easily whereas conventional sol-gel films with thicknesses greater than 1 μm suffer from a serious problem of cracking [2a], (iv) film properties such as mean refractive index can be controlled easily by varying the TiO_2/polymer weight ratio as well as the type of polymer used as the matrix, and (v) multilayer films with controlled refractive index gradients can be made by controlling each layer's composition.

This chapter is organized as follows. TiO_2 particle formation is briefly described followed by a description of the process for making the TiO_2-HPC composite films by spin-coating. Next, we describe a sintering process for burning out the HPC to obtain an anatase TiO_2 film. The properties of the TiO_2-HPC composite films and the sintered TiO_2 films are then discussed.

Experimental Procedure

Materials

Tetraethyl ortho-titanate, TEOT, (≈ 95 % TEOT, 5% ethanol) was obtained from Alfa Chemicals and was used as received. Anhydrous ethanol, 200 proof, was obtained from the Aaper Alcohol and Chemical Company. A.C.S. Certified dimethyl sulphoxide, DMSO, was obtained from Fisher Scientific. Samples of hydroxypropyl cellulose, HPC, were kindly donated by the Aqualon Company, a subsidiary of Hercules, Inc. HPC is a cellulose derivative with a glass transition temperature T_g in the range 100-150°C [9]. The structure of the repeat unit of HPC is shown in Figure 6.1. In all of the experiments, the grade HPC E was used with a weight-average molecular weight of 68.5 kg $mole^{-1}$. Deionized water with a resistivity of 16-18 x 10^{-6} mhos was used in all of the experiments. Polished and ground quartz wafers were obtained from Quartz Scientific Inc. Silicon wafers were obtained from the Polish Company of America.

Synthesis of TiO_2 Particles

To make transparent films consisting of TiO_2 particles, it is imperative to minimize scattering by controlling the particle size and refractive index. We synthesized sub-100 nm TiO_2 particles by the hydrolysis and condensation of tetraethyl-orthotitanate (TEOT) in the presence of HPC dissolved in ethanol.

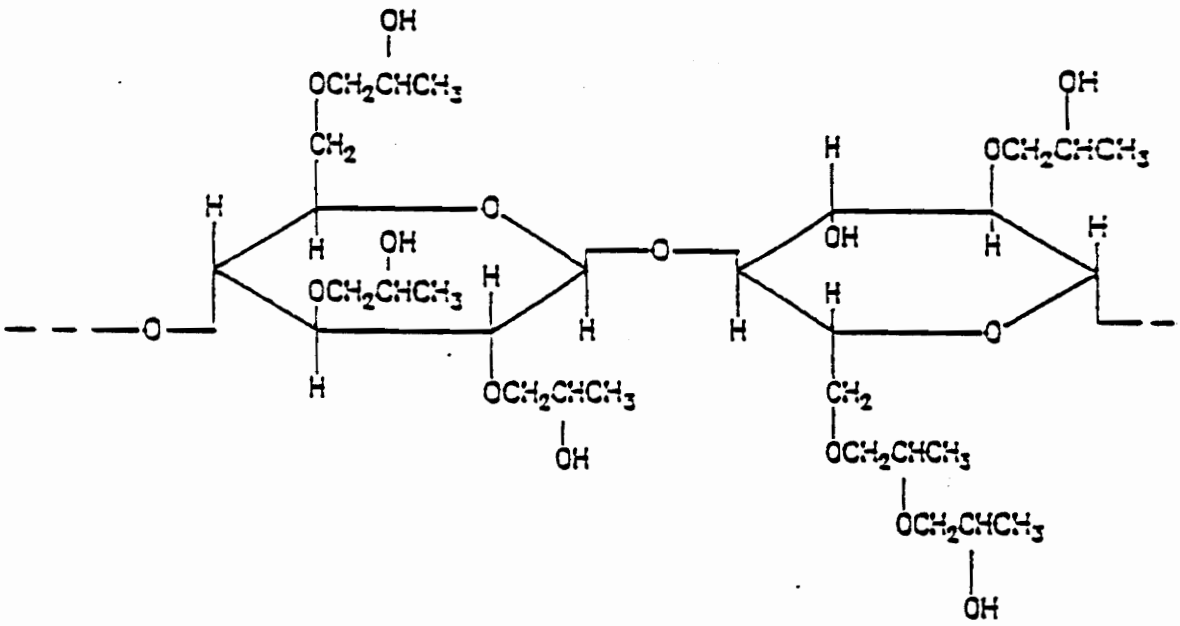

Figure 6.1. Structure of Hydroxypropylcellulose, HPC

The polymer HPC adsorbed onto the precipitating TiO_2 particles, providing steric stabilization and thus limiting the size. Complete details of this process have been given in chapter 2 [10] and so the procedure is only briefly reviewed here.

The hydrolysis and condensation reactions, (1) and (2) respectively, were conducted without any added acid or base. In all experiments, the TEOT concentration was in the range of 0.02-0.0375 M, the water concentration was in the range of 2.3-4.5 M. The HPC E concentration was in the range of 1.7-3.4 g l^{-1}. These conditions lead to full conversion of the TEOT with the final reaction mixture having the TiO_2/HPC ratio of 48/52 wt%/wt%. All growth experiments were done at room temperature. The reaction mixture was kept quiescent for twenty four hours although the reaction probably went to completion within one hour. After the reaction was complete, the resulting TiO_2 suspension was concentrated in a Buchi 461 Rotavaporator at 70°C to a solids concentration of $\approx$ 4 % by weight. HPC does not phase separate at 70°C in ethanol and hence steric stability of particles is not affected by suspension concentration.

Particle Size Analysis

The mean size of the TiO_2 particles was determined by electron microscopy and by dynamic light scattering. Size analyses were done before and after the suspensions were concentrated to determine if the concentration step affected particle size. The electron microscopy was done with a Philips 420T STEM Transmission Electron

Microscope. A range of particle size was determined by visual inspection of the TEM micrographs since the particles' edges were so ill-defined that image analysis could not be done.

Dynamic light scattering, DLS, provided measurements of the hydrodynamic diameter D_h by fitting the autocorrelation function with a single exponential fit as well as a second cumulant fit [11]. The DLS experiments were done with a Brookhaven BI-2030AT digital correlator equipped with 136 channels and a Lexel 95-2 argon ion laser operated at a wavelength of 514.5 nm. Scattering measurements were made at a scattering angle of 90° and a temperature of 25.0 $\pm$ .1°C. DLS measures the diffusion coefficient D which is related to the hydrodynamic diameter D_h by

$$D = kT/(3\pi\eta D_h) \qquad (3)$$

where η is the liquid phase viscosity.

In a suspension of TiO_2 particles made with HPC in ethanol, scattering will come from both TiO_2 particles and HPC molecules in solution. This can complicate the analysis of dynamic light scattering size measurements. A solution to this problem comes from considering the Rayleigh theory for the time-averaged light scattering intensity I from a suspension of spheres of radius R which, at a fixed angle, varies as [12]:

$$I \propto N_p R^6 n_0^4 \lambda^{-4} [(m^2 - 1)^2/(m^2 + 2)] \quad (4)$$

where N_p is the number of particles/volume, λ is the wavelength, and $m = n_p/n_0$ where n_p is the refractive index of the scattering species and n_o is the refractive index of the solvent. Scattering is minimized especially when the particle size R is less than $\lambda/20$. Also, equation (4) is valid only if $m < 2$.

In a mixture consisting of two components in a solvent, equation (4) shows that scattering from one of the components can be minimized by matching the refractive index of the solvent with that of the component. HPC has a refractive index of 1.483 as measured by the prism coupling technique to be discussed later while ethanol has a refractive index of 1.361. To minimize the scattering due to HPC, TiO_2 particles made with HPC were resuspended in dimethyl sulfoxide, DMSO, a good solvent for HPC [9] which has a refractive index of 1.477. For this purpose, a drop of suspension was diluted in 10 ml of DMSO. TiO_2 particles were also diluted in ethanol using this same procedure for comparison. All suspensions were filtered through 0.2 μm Acrodisc™ filters before the scattering experiments. The DLS size analysis was done before and after sonicating the diluted suspensions for ten minutes.

TiO_2-HPC Film Formation

The film casting procedure is depicted in Figure 6.2. Spin coating was done onto 2.54 cm diameter quartz disks and 1 x 1 cm silicon wafers at a coater speed of

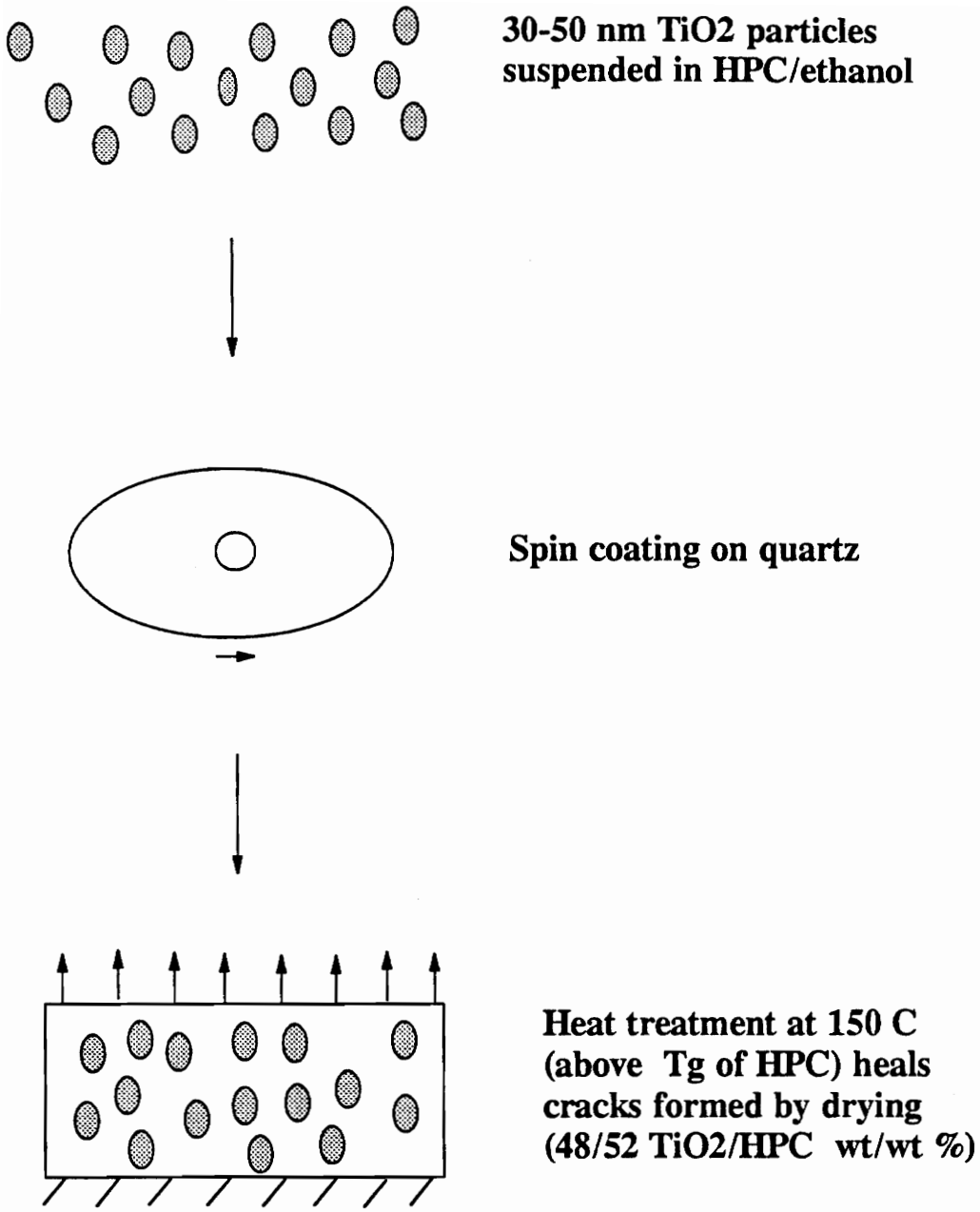

Figure 6.2. TiO_2/HPC film formation process.

2000 RPM. After each coating, the films were dried at 160°C for 1 hour in a convection oven. As many as four coats were deposited on a film to determine the effect of thickness on film properties. Some films were also cast directly onto copper grids for electron microscopy tests. To test the effect of the ratio of TiO_2/HPC on film properties, some of the stock suspension was diluted with solutions of HPC in ethanol to obtain suspensions with the TiO_2/HPC weight ratios ranging from 20 to 48% TiO_2. These suspensions were then used to cast films.

Film Characterization

Unless otherwise stated, the films were made with suspensions consisting having the TiO_2/HPC wt/wt ratio of 48/52. The film morphology was determined by scanning electron microscopy with an Electroscan E3 Environmental Scanning Electron Microscope (E-SEM). The film composition was characterized by: (i) Auger Electron Spectroscopy with a Perkin Elmer Scanning AUGER Microprobe Model 610, (ii) ESCA with Kratos Model XSAM 800 with Magnesium Anode operated at 260 watt, and (iii) microprobe analysis with a Cameca SX50 electron microprobe. The film crystallinity was determined by X-ray diffraction with a Siemens Crystallex 4 instrument. Stresses within the films were measured with a Flexus F2400 Stress analyzer. The optical properties of the films were characterized by a variety of techniques including: (i) optical microscopy from Hacker Instruments, (ii) UV-Visible transmission spectrophotometry with an Hitachi U-2000 instrument, and (iii)

refractive index and film thickness for films cast on both quartz and silicon wafers using a Metricon Model 2010 Prism Coupler instrument at a wavelength of 633 nm. This last technique involves measuring angles at which a prism will couple light from a laser beam into the sample films. The thickness and refractive index are calculated from the measured angles [13-17]. Adams et al. evaluated the prism coupling technique along with three other techniques to measure the film refractive index and thickness on silicon substrate [17]. The other techniques were reflectance spectroscopy, ellipsometry, and the mechanical measurement of a step height. The four techniques showed good agreement but it was concluded that the prism coupling technique was much more precise. The refractive index and film thickness were also calculated by the fringe envelope method described by Manifacier et al. [18]. This method is reliable only if the difference in the film and substrate refractive index is large, which is not the case in our work when the films are cast on quartz. Hence, the refractive index of the films was not reliably obtained by this method.

Results and Discussion

Particle Size

There was a striking change in the appearance of the TiO_2 particles observed by TEM as a result of the suspension concentration step in the Buchi Rotavaporator. Before the concentration step, there were a number of relatively large particles, 80-

100 nm in size, with discrete boundaries as seen in Figure 6.3(a). There were also a number of smaller particles approximately 10-20 nm in size in the background. After the concentration step, the largest particle size was only about 30-50 nm as seen in Figure 6.3(b). The reduction in particle size was due most likely to heating at 70°C during the concentration step which broke up the TiO_2 aggregates. The aggregates observed in Figure 6.3(a) very likely consist of smaller TiO_2 particles bound together loosely by adsorbed HPC. The particle size results from both TEM and DLS are summarized in Table 6.1.

The hydrodynamic diameters of the TiO_2 particles measured in ethanol and DMSO agreed very well, giving an average $D_h \approx 135$ nm as seen in Table 6.1. The total hydrodynamic diameter represents the sum of the TiO_2 particles' hydrodynamic diameter and twice the adsorbed HPC layer's hydrodynamic thickness. These measurements represent the size of TiO_2 particles with adsorbed HPC and not those of free HPC chains in solution since HPC does not scatter significantly in DMSO. The particle size distributions in both solvents were relatively narrow given the good agreement between the hydrodynamic diameter D_{h1} determined by the single exponential fit to the autocorrelation function and D_{h2} determined by the second cumulant fit. Sonication had no significant effect on D_h both before and after the concentration step. The mean value of D_h before concentration was about 30-40% higher than the size determined by TEM.

(a)

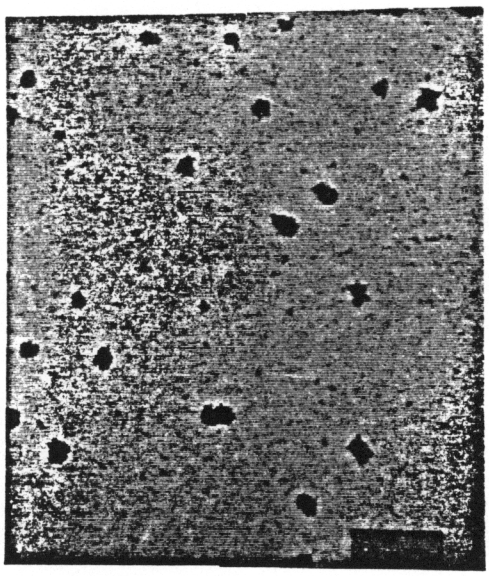

500nm

(b)

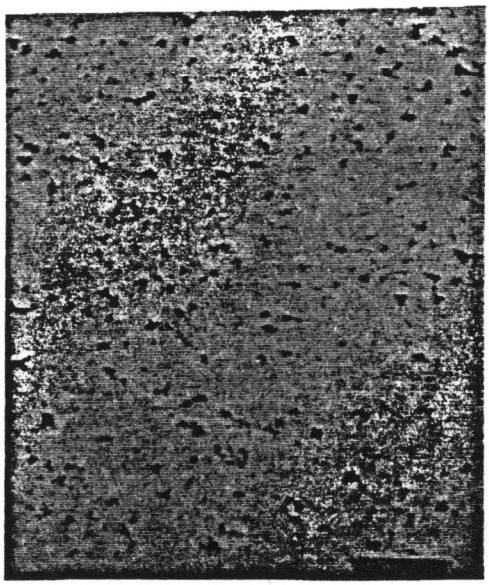

500nm

Figure 6.3. TEM micrographs of TiO_2 particles in TiO_2/HPC suspension (a) before and (b) after concentration.

Table 6.1. Particle Size analysis by Dynamic Light Scattering and Transmission Electron Microscopy

	Solvent	Hydrodynamic diameter, D_h, nm				TEM nm
		No sonication		Sonication		
		D_{h1}*	D_{h1}**	D_{h1}	D_{h2}	
Before Concentration						
	Ethanol	136	128	140	131	80-100
	DMSO	136	125	139	129	
After Concentration						
	Ethanol	138	133	136	135	30-50
	DMSO	131	130	133	132	

* from dynamic light scattering, single exponential fit
** from dynamic light scattering, second cumulant fit[11]

The difference is due partly to the shrinkage of the adsorbed HPC layer around the particle when it is dried for the TEM experiment. The adsorbed HPC layer shrinks by at least a factor of 10 upon drying. In a related study, Ring et al.[19] measured sizes of TiO_2 particles grown in HPC at a water concentration $R = 6.3$. They observed a reduction in particle size of about 33% when measuring TiO_2 particles size by TEM compared to DLS. This reduction was attributed in part to the highly porous nature of TiO_2 particles which shrank due to the collapse of pores upon the removal of solvent.

The hydrodynamic diameter did not change as a result of the concentration step, unlike the change observed by TEM. It may be that the disaggregated particles in Figure 6.3(b), when still in solution, are tethered together by linking HPC chains which would lead to a relatively high value of D_h but would appear as disaggregated particles in TEM since the dried HPC tether chains would not be visible in the TEM. This is plausible given that the average or end-to-end distance of the fully stretched chain of the HPC used in this work is approximately 100 nm [9].

TiO_2/HPC Composite Film Properties

Optical Microscopy

The films on both quartz and silicon substrates developed large cracks when the films were allowed to dry in air after spin-coating. However, crack-free films were obtained upon annealing at 160°C for one hour after every coating step. Annealing

above the glass transition temperature of HPC allows the polymer chains to diffuse across the cracks, thus erasing them. This procedure was adopted in making all films discussed in this paper.

SEM Analysis

Figure 6.4(a) is a high resolution scanning electron micrograph of a TiO_2/HPC film cast with four coats at 2000 RPM and annealed at 160°C after every coat. The bright regions consist of closely packed TiO_2 particles mostly in the size range 30-40 nm which corresponds roughly to the size measurement from TEM after the suspension concentration step. The dark spots approximately 20-30 nm in size are voids between the particles.

Auger Depth Profile

Auger Electron Spectroscopy, AES, determined the film composition along its thickness. The films were cast with 3 coatings at 2000 RPM. The electron beam voltage was 3.0 KEV at 0.05 μA and the argon ion beam voltage was 4.0 KEV at 5 μA. The film was sputtered at a rate of 30 nm/min. The elemental composition along the depth is shown in Figure 6.5. The titanium, carbon, and oxygen elemental composition remained constant along the film thickness indicating that there was no segregation of the TiO_2 particles in the thickness direction.

(a)

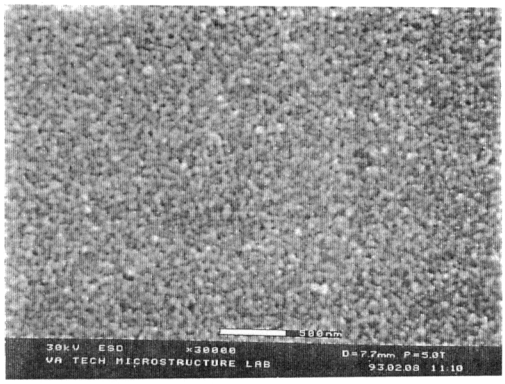

150°C
Transparent

(b)

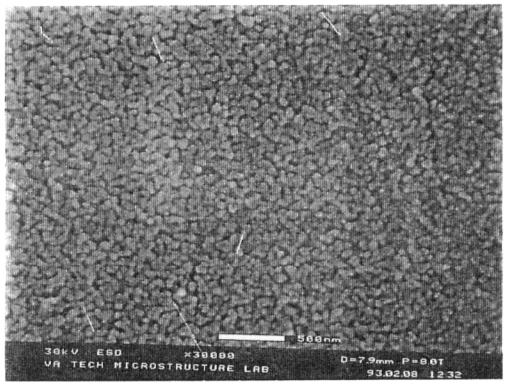

700°C
Transparent

(c)

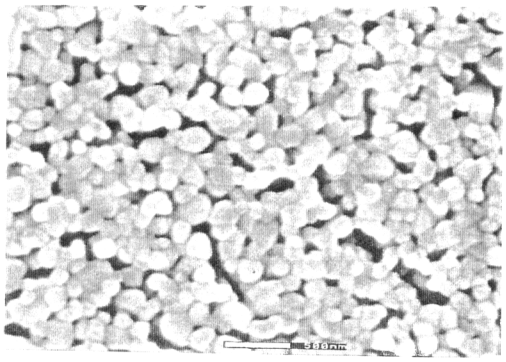

950°C
Opaque

Figure 6.4. Scanning electron micrographs of: (a) non-sintered TiO_2/HPC film, annealed at 160°C, (b) TiO_2 film sintered at 700°C, and (c) TiO_2 film sintered at 900°C.

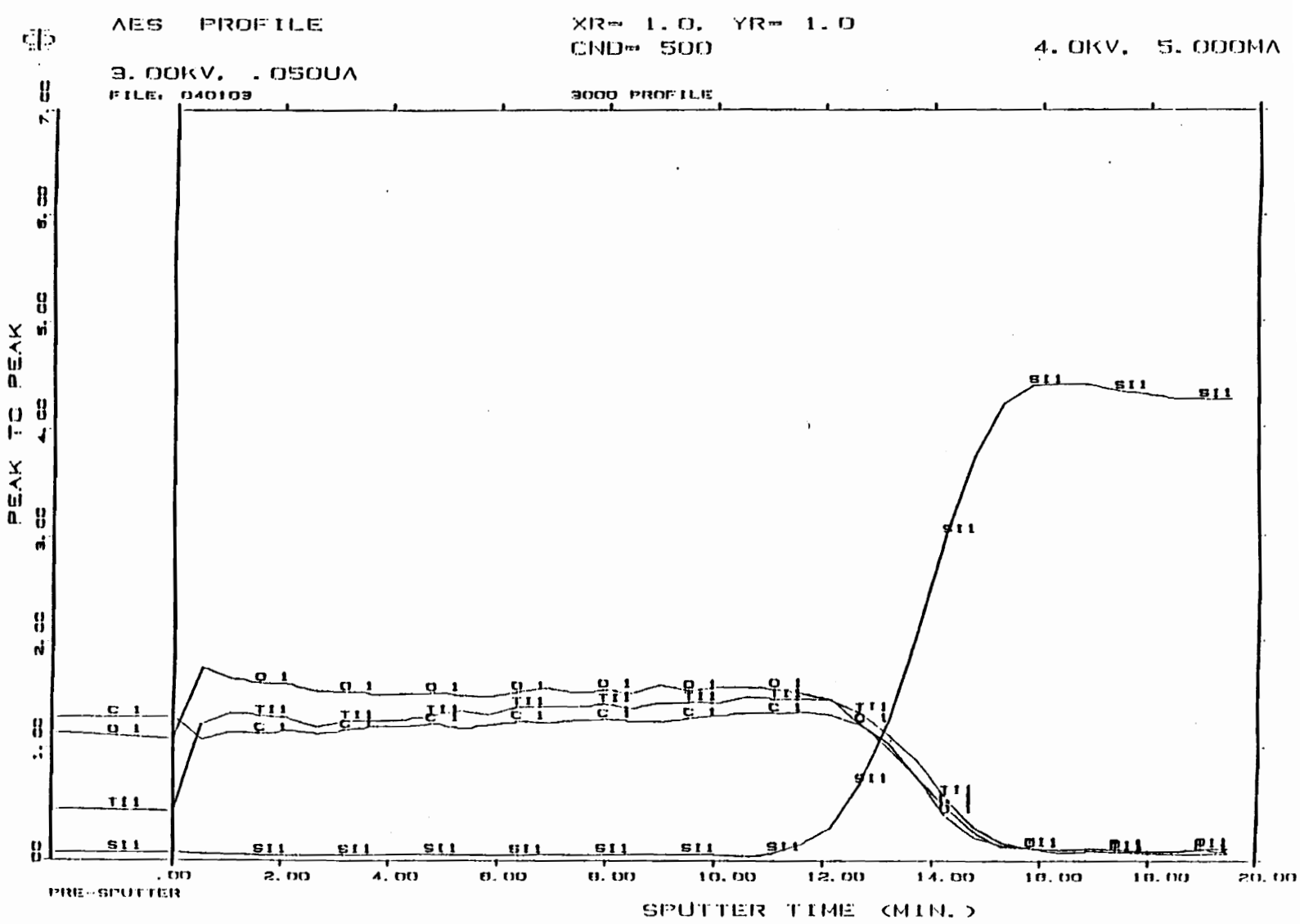

Figure 6.5. Auger electron spectroscopy of a TiO_2/HPC film, approximately 400 nm thick.

Microprobe Analysis

Microprobe analysis provided another measure of the elemental composition of the films. A film was cast with four coats onto a 1 x 1 cm^2 silicon wafer at 2000 RPM. The analysis was done at 6 KEV. Twenty spots were probed, each with an area of 100 μm^2. They were randomly chosen to provide a representative sampling of the entire film surface. The analysis results are shown in Table 6.2 in percent composition by weight of titanium, carbon, and oxygen. The small standard deviations conclusively establish the film's surface homogeneity. Table 6.2 also shows that the elemental composition determined by micrprobe analysis agrees quite closely to the expected theoretical elemental composition for TiO_2/HPC weight ratio of 48/52 on dry basis.

X-ray Diffraction

The X-ray diffraction in Figure 6.6(a) revealed that the films annealed at $T \leq$ 500°C were amorphous since no crystal peaks were observed. The X-ray source was Cu (K_α) at a wavelength of 0.154 nm.

Table 6.2. Elemental Composition of Composite TiO_2/HPC Film by Microprobe Analysis

Elements	% elemental composition	Standard deviation	% elemental composition (theoretical)
Ti	16.5	1.72	12
C	39.5	0.78	42
O	43.0	0.38	46

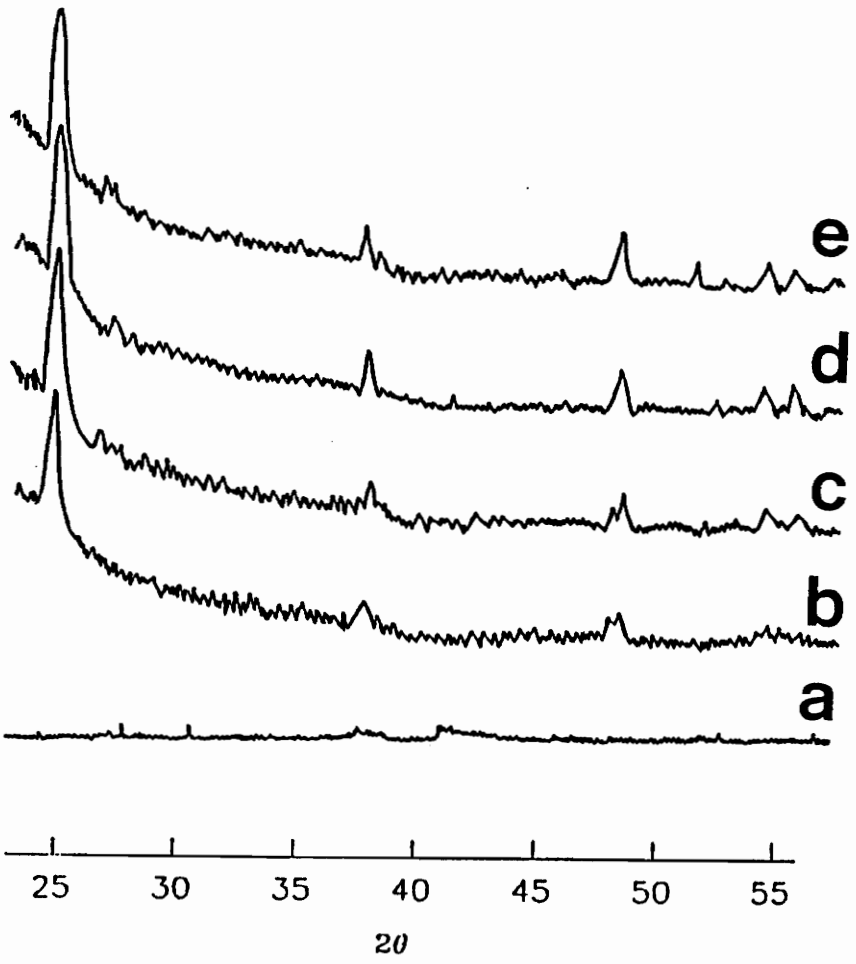

Figure 6.6. X-ray diffraction patterns versus temperature of TiO_2 film obtained by sintering TiO_2/HPC film at: (a) 500°, (b) 600°, (c) 700°, (d) 800°, and (e) 900°C.

Film Stress Measurements

Figure 6.7 shows the stress measurement on a film with a thickness of approximately 1600 nm cast on a silicon wafer. The film was allowed to dry for about one hour in air at room temperature and was then placed in the Flexus film stress analyzer where it was heated at a rate of 3°C/minute. There was an initial increase in tensile stress due to solvent evaporation up to about 78°C followed by a stress relaxation up to 160°C. This stress relaxation is probably due to the glass transition of HPC. Recall that the T_g of pure HPC is in the range 100-150°C. The TiO_2 particles may serve to decrease T_g somewhat by increasing the effective free volume of the HPC chain, an effect sometimes observed in filled polymer systems [20]. The TiO_2 phase does constitute a significant amount of the volume of the film with the volume fraction ranging from 22-30% when the TiO_2 density is taken as 3.84 g cm^{-3} for anatase TiO_2 [21] and as 2.7 g cm^{-3} for amorphous TiO_2 [22], respectively. However, these results do not definitively show a substantial depression of T_g. Upon cooling from 160°C, there is no tensile stress build-up as would be expected for a pure HPC film on a silicon substrate given that the thermal expansion coefficient of HPC is at least 10 times that of silicon [21,23]. The plateau in the stress upon cooling suggests that the mean thermal expansion coefficient of the composite film is lower than that of pure HPC.

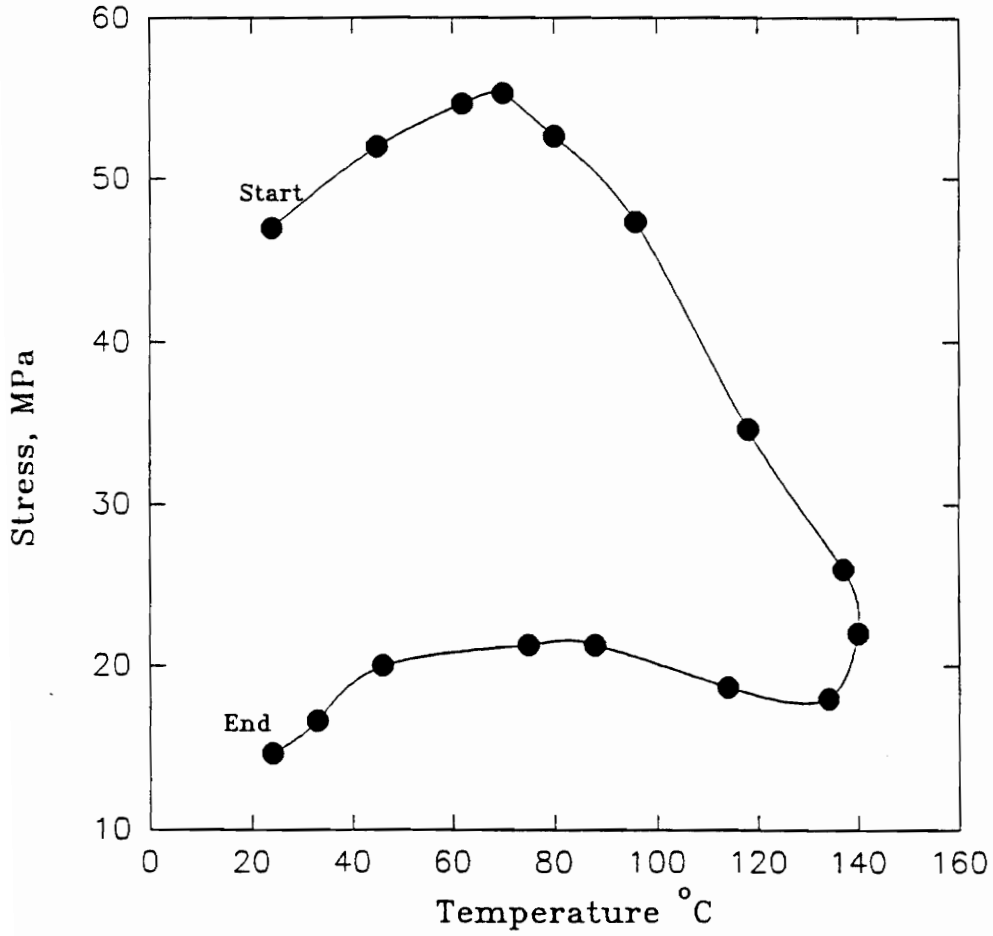

Figure 6.7. Stress analysis versus annealing temperature of a TiO_2/HPC film.

Optical Transmission Properties

Films on quartz wafers were characterized by UV-Visible spectrophotometry between the wavelengths 190-1100 nm. Measurements of the percent transmission, %T, versus wavelength, λ, provided a direct test of the film's UV filter properties as observed in Figures 6.8(a-c). These show the progressive decrease in transmission with the increasing number of coats. In Figure 6.8(d), a relatively thick film of pure HPC made with four coats was transparent even in the ultra-violet region whereas a TiO_2-HPC composite film with a similar thickness (also made with four coats) completely blocked transmission below a wavelength of 300 nm. The film thickness required for complete cut-off for $\lambda < 300$ nm increased with decreasing TiO_2 concentration in the suspension. For example, a film made with two coats containing 48 wt % TiO_2 had a transmission of 0.8 % at $\lambda = 300$ nm whereas a film made with two coats containing 20 wt % TiO_2 had a transmission of 17%. The TiO_2 concentration in the films could be easily controlled by spin coating with TiO_2-HPC suspensions made by mixing the appropriate amounts of original suspension containing 48 % TiO_2 with HPC solutions in ethanol.

The transmission scans of the composite film in Figures 6.8(b-d) exhibited local maxima and minima due to constructive and destructive interference caused by the difference in refractive index between the substrate and the film.

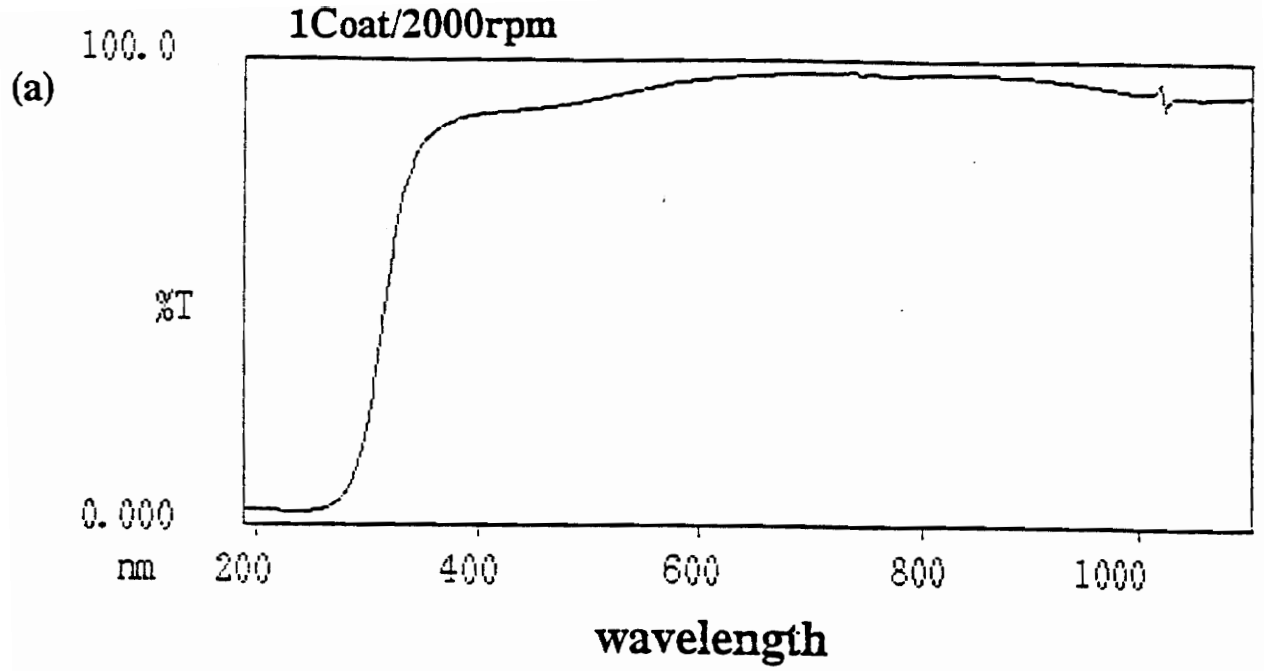

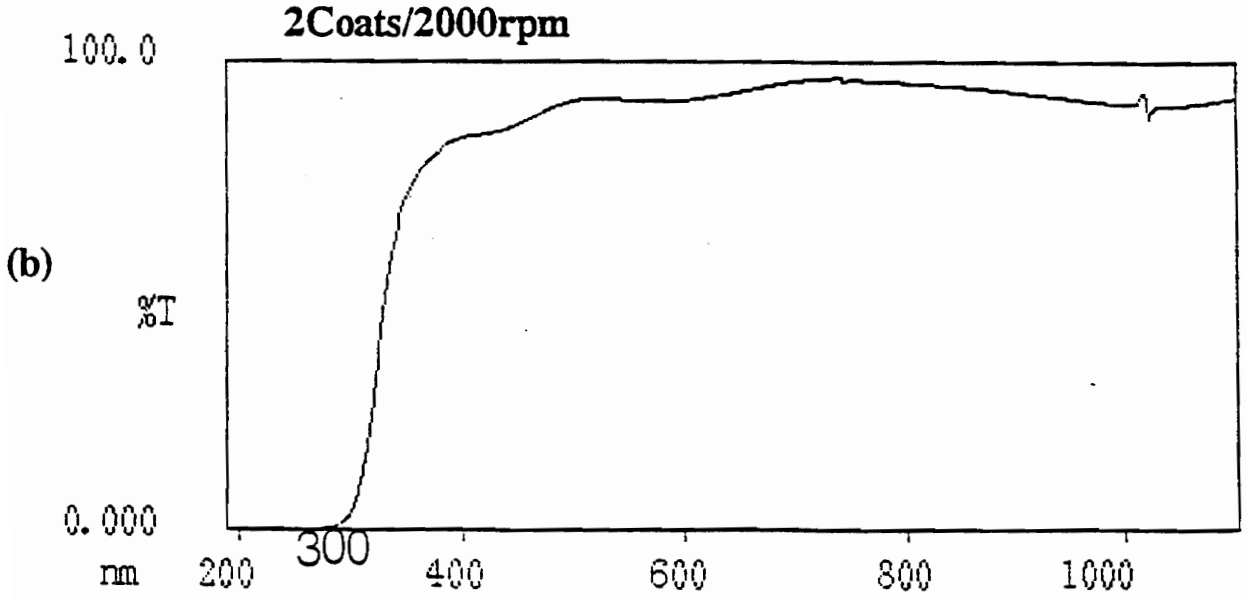

Figure 6.8. UV/VIS transmission versus wavelength of TiO_2/HPC films on quartz. The films were deposited at a spin-coater speed of 2000 RPM and annealed at 160°C after every coat. (a) One coat, (b) two coats of a TiO_2/HPC suspension.

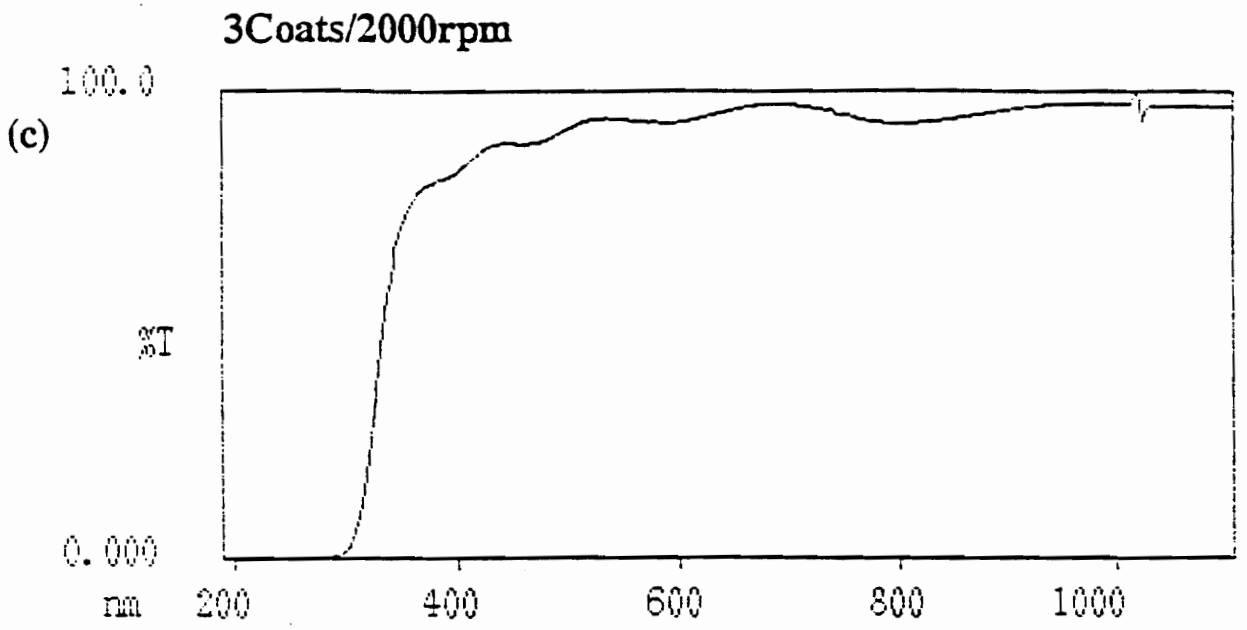

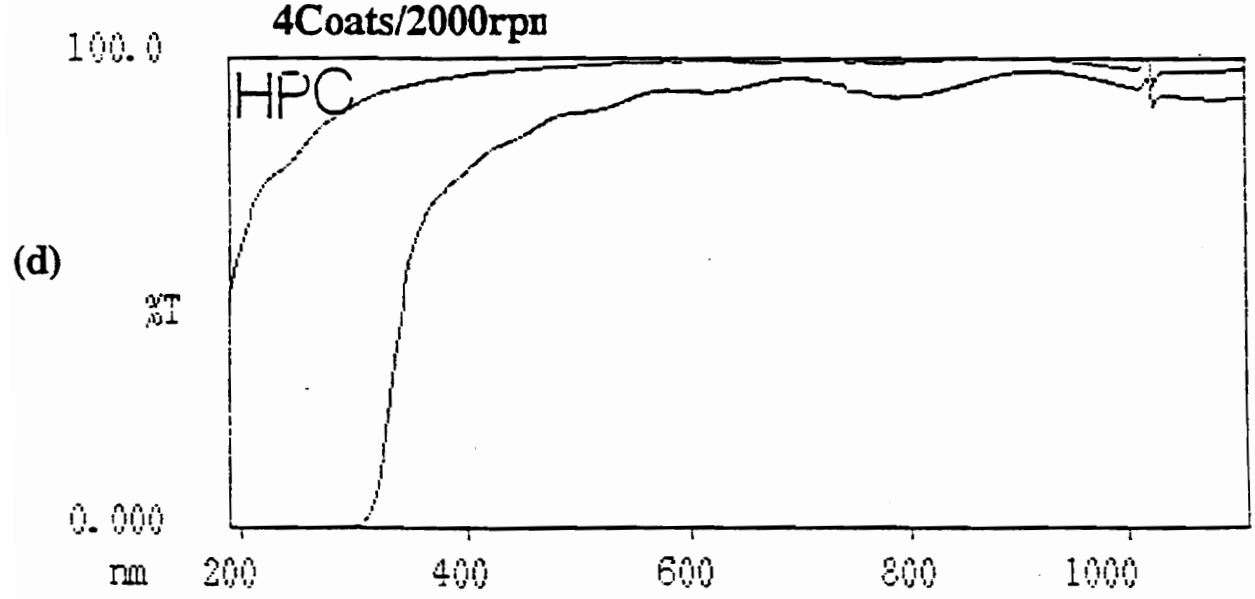

Figure 6.8. UV/VIS transmission versus wavelength of TiO_2/HPC films on quartz. The films were deposited at a spin-coater speed of 2000 RPM and annealed at 160°C after every coat. (c) Three coats, (d) four coats of a TiO_2/HPC suspension and four coats of pure HPC solution in (d).

These interference patterns are commonly seen in uniform films made by vapor-phase techniques and indicate that the films are highly uniform in thickness and composition. The number of peaks and crests in Figures 6.8(b-d) also increased with the number of coatings due to the increasing film thickness.

Refractive Index and Film thickness

The values of refractive index for the composite films were in the range 1.657-1.665 as seen in Table 6.3. This is much lower than expected if the TiO_2 phase were dense and nonporous as can be seen from the effective medium approximation for a composite film. The Lorentz-Lorenz equation gives the mean film refractive index as [2b]:

$$[n_f^2 - 1]/[n_f^2 + 2] = \phi_{TiO2} [n_{TiO2}^2 - 1]/[n_{TiO2}^2 + 2] + \phi_{HPC} [n_{HPC}^2 - 1]/[n_{HPC}^2 + 2] \quad (5)$$

where n_f is the measured film refractive index, n_{TiO2} is the refractive index of the TiO_2 phase, and ϕ_{TiO2} is the volume fraction of the TiO_2. The volume fraction of TiO_2, ϕ_{TiO2} , is 0.29 assuming that the density [22] of the TiO_2 phase is 2.7 g cm^{-3}. For the film made with four coats on quartz from Table 6.3, n_f = 1.657 which leads to n_{TiO2} = 1.62 from equation (5). This value is significantly lower than the refractive index of pure anatase TiO_2, i.e. 2.554 [21] and is likely due to the combination of the amorphous nature of the TiO_2 particles and the porosity of the particles.

Table 6.3. Refractive Index and Film Thickness of TiO_2/HPC Films Measured by the Prism Coupling Technique

# Coatings	Film thickness t, nm		Refractive index n	
	Quartz	Silicon	Quartz	Silicon
3	--	497	--	1.657
4	770	741	1.657	1.657
5	975	978	1.664	1.665

The size and refractive index effects cannot be separated at present because there is no reliable value for the refractive index of amorphous TiO_2. Thus, the transparency of the composite film is due to both the small particle size and a low mean refractive index of the TiO_2 phase.

The thicknesses and the refractive indices of the films coated on quartz and silicon wafers agree closely when given the same number of coats at 2000 RPM. The film refractive index increased from 1.657 to 1.665 upon an increase in film thickness from 497 to 978 nm on a silicon substrate. This may be a significant increase since the standard deviations in the measurement of refractive index and thickness are 0.0002 and 0.003 respectively. More experiments are underway to elucidate the effect of film thickness on the refractive index. As a calibration check, the refractive index of a pure HPC film on silicon obtained by this technique was 1.483 which was close to the value of 1.486 reported by Samuels [24].

Sintered TiO_2 Films

The polymer HPC decomposes at 450°C in air and, upon burnout, leaves behind a very low ash content and no organic residues [9]. HPC is often used as a temporary binder in the production of ceramics, glazes, refractories, and powdered metal products. Pure TiO_2 films were obtained by first casting TiO_2-HPC films onto quartz and silicon using a suspension with the composition TiO_2/HPC = 48/52 wt/wt. After every coat was deposited at a spin-coating speed of 2000 RMP, the composite films

were sintered at 500°C for one hour in air in a tube furnace open at both ends. A film consisting of eight coats was made this way for the X-ray diffraction experiment to characterize film crystallinity. After the initial diffraction measurement, the same film was sintered further for one hour each at 600°, 700°, 800°, and 900°C. An X-ray diffraction measurement was made after each sintering step. The X-ray diffraction patterns in Figure 6.6(a) showed that the film was amorphous up to 500°C. Anatase TiO_2 appeared at 600°C as seen in Figure 6.6(b). The anatase peaks became more pronounced and sharper at 700°C and 800°C. The film turned opaque at 800°C due to the densification of TiO_2 particles since the transition to anatase was already essentially complete at this temperature. At 900°C, the film was predominantly anatase, although some broad rutile peaks were observed indicating the formation of very fine grains of rutile.

In a second set of experiments, films were cast from the same suspension on quartz and silicon wafers and were sintered at 700°C after every coat. The films were analyzed by optical microscopy, UV-VIS transmission, the prism coupling technique, and by X-ray diffraction.

Optical Microscopy

Optical microscopy revealed that it was essential to sinter the film after every coat to obtain a uniform and crack-free TiO_2 film. For example, films cracked if they were sintered after four coats of TiO_2/HPC suspension were deposited.

ESCA analysis on non-sintered and sintered films

ESCA analysis was done on films cast on silicon wafers with the TiO_2/HPC weight ratio of 48/52. The non-sintered film was annealed at 160°C after every coating and the sintered film was sintered at 700°C after every coat. Figures 6.9(a) and (d) are the carbon (1s) and oxygen (1s) ESCA curves of a pure HPC film on silicon. The binding energy B.E. = 284.6 eV due to carbon-hydrogen bonds in Figure 6.9(a) served as a reference. For the pure HPC film, there was also a peak in Figure 6.9(a) at B.E. = 286.2 eV due to carbon-oxygen bonds in the polymer. The carbon (1s) curve in Figure 6.9(b) obtained from the non-sintered film was very similar to the curve in Figure 6.9(a). The carbon-oxygen peak at B.E. = 286.2 eV vanished in Figure 6.9(c) for the sintered film, leaving only a single carbon peak corresponding to carbon-carbon bonds due most likely to carbon contamination from the atmosphere.

Confirmation of complete burnout of the HPC came from examining the oxygen 1s curves in Figures 6.9(d),(e), and (f). For the unsintered film in Figure 6.9(e), the oxygen peak occurring at B.E. = 532.4 eV was due to the oxygen bonded to carbon in the HPC. This was corroborated by the presence of the oxygen peak at 532.4 eV in Figure 6.9(d) for the pure HPC film. The shoulder in Figure 6.9(e) at B.E. = 529.9 was due to oxygen in TiO_2 [25]. After sintering, there was only a single oxygen peak in Figure 6.9(f) occurring at a B.E. = 529.7 due to TiO_2.

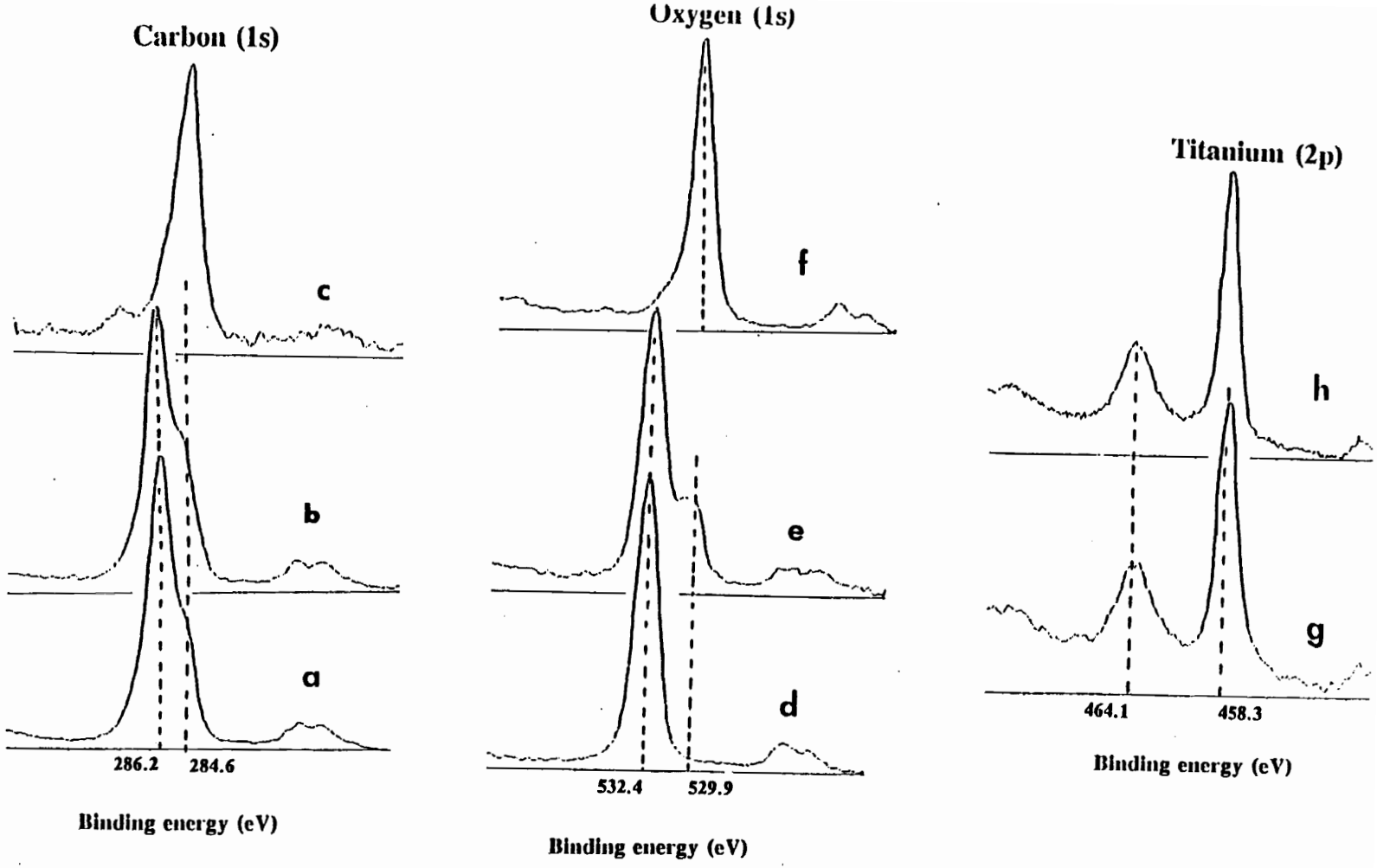

Figure 6.9. Carbon, oxygen, and titanium elemental analysis by ESCA on HPC, non-sintered TiO_2/HPC and anatase TiO_2 film obtained by sintering TiO_2/HPC film at 700°C; (a) carbon in pure HPC, (b) carbon in non-sintered film, (c) carbon in sintered film, (d) oxygen in pure HPC, (e) oxygen in non-sintered film, (f) oxygen in sintered film, (g) titanium in non-sintered film, and (h) titanium in sintered film .

The TiO_2 curves of TiO_2 in non-sintered and sintered films occurred at the same binding energy. Figures 6.9(e) and (f) show a $Ti2p^{1/2}$ peak at a B.E. of 464.1 eV and a $Ti2p^{3/2}$ peak at a B.E. of 458.3 eV.

Scanning Electron Microscopy

Figures 6.4(b) and (c) show the morphology of the anatase TiO_2 films sintered at 700°C and 900°C respectively. It is interesting to compare the morphological features of the non-sintered and the sintered films. Recall that the bright regions in Figure 6.4(a) consisted of densely packed TiO_2 particles, mostly in the size range 30-50 nm, indicating little porosity. However, the particle size in Figure 6.4(b) for the sintered film ranges between 60-120 nm. The increase in particle size is due to the inter-particle densification. The dark areas in the micrograph are the inter-particle voids due to the burning of the polymer. These voids are about 60-100 nm long and about 20 nm wide. The particle and the void size are both at least 4 times smaller than the wavelength of visible light and hence the film transparency is retained. Sintering at higher temperature led to a larger grain size and higher porosity, as seen in Figure 6.4(c). The average grain size in this figure is about 200 nm and the grains are fused with each other to form a network. The increase in grain size made the films opaque due to an incresed scattering of light. Thus, it is possible to control the particle size and the film porosity by controlling the polymer concentration, sintering time and temperature. This should be useful in designing TiO_2 films for membrane

applications.

Film Refractive Index and Thickness

The thicknesses of films cast onto quartz and silicon and sintered at 700°C, shown in Table 6.4 agreed well with each other. The higher refractive indices of the sintered films compared to those of the composite films shown in Table 6.3 were due to the burnout of the HPC which had a diluent effect on the film refractive index as seen by equation (5). The intra-particle and inter-particle densification also accounted for some of the increase of the refractive index of the TiO_2 phase and hence that of the sintered film. However, the refractive index of the sintered film was much lower than that of pure anatase, 2.554 due to inter-particle and intra-particle porosity.

The sintered film porosity was estimated using the effective medium approximation which is given by a modified form of equation (5):

$$[n_f^2 - 1]/[n_f^2 + 2] = \phi_{TiO2}\,[n_{TiO2}^2 - 1]/[n_{TiO2}^2 + 2] \quad (6)$$

where n_f is the film refractive index, n_{TiO2} is the refractive index of anatase, 2.554 [25], and ϕ_{TiO2} is the volume fraction of anatase TiO_2. For the film cast on silicon, the data from Table 6.4 and equation (6) give $\phi_{TiO2} = 0.622$. Thus, approximately 38 % by volume of the film consists of pores occupied by air. Finally, the refractive index

Table 6.4. Refractive Index and Film Thickness of TiO_2 Films Sintered at 700°C Measured by the Prism Coupling Technique

Substrate	Film thickness t, nm	Refractive index n
Silicon	488	1.742
Quartz	493	1.726

of the sintered film on silicon was somewhat higher than that obtained on quartz. More work is in progress to establish the effect of substrate type on the refractive index of the sintered film.

Transmission Properties

UV-Vis spectrophotometry revealed that the film on quartz sintered at 700°C was essentially transparent down to a wavelength of 330 nm below which the transmission dropped to zero as shown in Figure 6.10. By comparison, the TiO_2-HPC composite films in Figure 8 exhibited a cut-off at a wavelength of 300 nm. The 30 nm shift towards the higher wavelength is probably due to the increased volume fraction of TiO_2 in the sintered film as seen from the Beer-Lambert law for transmission T [26]:

$$T = 10^{-ecl} \qquad (7)$$

where e is the absorption coefficient, c is the concentration of the absorbing species, and l is the path length. The volume fraction of TiO_2 in the composite films lay in the range 0.2-0.3 depending on the assumed value of the density of amorphous TiO_2. In the sintered film made with eight coats, $\phi_{TiO2} = 0.622$.

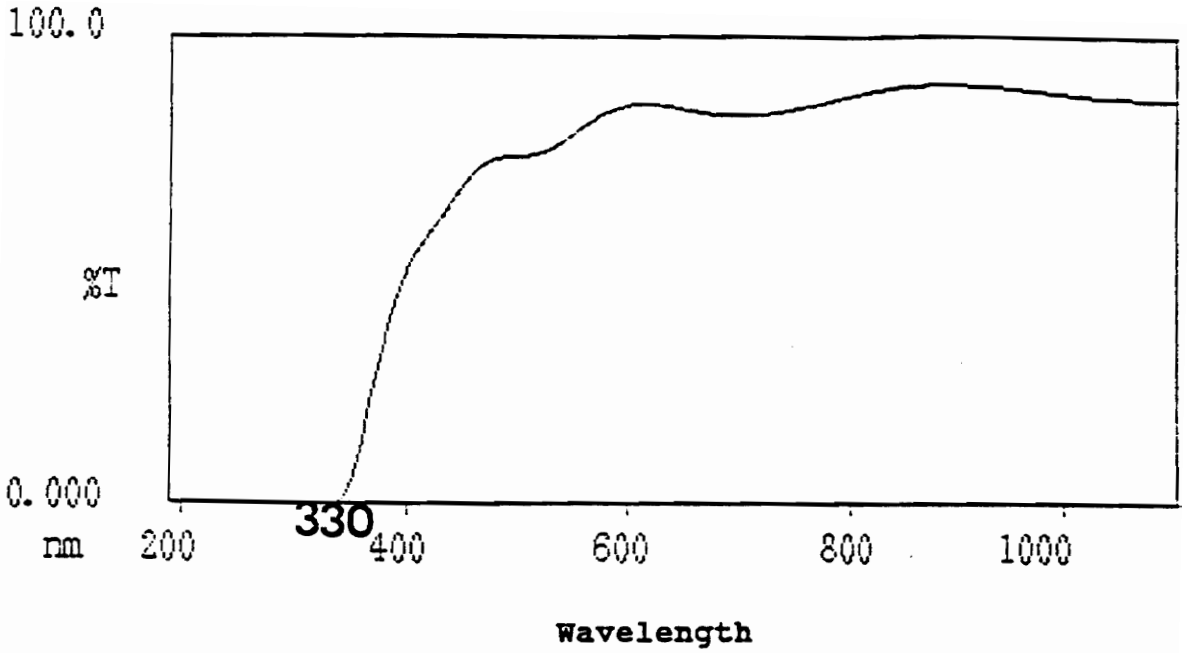

Figure 6.10. UV/VIS transmission versus wavelength of an anatase TiO_2 film obtained by sintering a TiO_2/HPC film at 700°C.

Thus, the effective path length, cl, is higher for the sintered TiO_2 film than for a composite film with a comparable thickness such as the case in Figure 6.3(c) for the film with thickness = 497 nm. The transmission scan of the sintered film also showed interference patterns, indicating its excellent uniformity.

Conclusions and Future Work

Thin composite films of TiO_2 and the polymer hydroxpropylcellulose, HPC, were made by spin-coating suspensions of sub-100 nm TiO_2 particles in a solution of HPC onto quartz and silicon substrates. The TiO_2 particles were formed from the hydrolysis and condensation of tetraethylorthotitanate in a solution of HPC which functioned as an in-situ steric stabilizer. After solvent evaporation and annealing at 160°C, the films were crack-free, uniform in thickness, and had excellent transparency down into the ultraviolet range where the transmission dropped abruptly to almost zero. Films were transparent due to the small size and porosity of the particles. Sintering the film at 700°C in air resulted in the complete burnout of the HPC and the formation of an anatase film. The sintered film had UV cut-off and interference fringe properties similar to those of the annealed composite films. However, the refractive index of the films increased significantly upon sintering. This work demonstrates a simple, general technique for making UV filters from relatively inexpensive materials [28].

Multilayer films can be made easily. In future work, films with controlled refractive index gradients will be made by controlling the composition of each layer. These films may find application as narrow band pass filters. The spin-coating model of Rehg and Higgins [29] will be tested to rigorously link processing parameters such as suspension viscosity, spinning speed, and drying conditions to film thickness. The polymer in which the TiO_2 particles are dispersed can be selected to control film properties. For example, a polyimide which is chemically stable at high temperatures, i.e. in excess of 250°C, can be used instead of HPC to obtain films that could function at high temperatures. The porosity of the film may be exploited for use as porous membranes and catalyst supports. It should be possible to vary the film porosity by controlling the TiO_2/HPC ratio in the initial suspension and the sintering temperature. It should be possible to dope the porous TiO_2 particles, either before or after sintering, with various compounds to obtain specific optical, electronic, and catalytic properties. Such porous films could find use in microsensors for specific chemical species and in the development of catalysts where the location of active catalytic groups is controlled.

References

1. *Thin-Film Optical Filters*, edited by H.A. Macleod (2nd edition, Macmillan Publishing Company, New York, 1986.
2. C.J. Brinker and G.W. Scherer, *Sol-Gel Science: The Physics and Chemistry of Sol-Gel Processing*, (Academic Press Inc., 1990), (a) Chapter 14; (b) Chapter 13.
3. B.J. Meldrum, *Proceedings of The Society of Plastic Engineers ANTEC 1991 Conference*, **37**, 5 (1991).
4. H. Schroeder, in *Physics of Thin Films*, edited by G. Hass and R.E. Thun, (Academic, New York, 1969), Vol.5, p. 87.
5. B.E. Yoldas, J. Mater. Sci. **14**, 1843 (1979).
6. B.E. Yoldas, J. Non Cryst. Solids **38 & 39**, 81 (1980).
7. B.E. Yoldas, Applied Optics **21(16)**, 2960 (1982).
8. A. Hurd and C.J. Brinker, J.Phys. France **49**, 1017 (1988).
9. *KLUCEL, Hydroxypropyl Cellulose, Physical and Chemical Properties*, Aqualon Company, subsidiary of Hercules, Inc. (1981).
10. V.J. Nagpal, R.M. Davis, and J.S. Riffle, "In-Situ Steric Stabilization of Titanium Dioxide Particles Synthesized by Sol-Gel Process", submitted to *Colloids and Surfaces*.

11. N.C. Ford, Chapter 2 in *Dynamic Light Scattering*, edited by R. Pecora (Plenum Press, N.Y., 1985).

12. M. Kerker, *The Scattering of Light and Other Electromagnetic Radiation* (Academic, New York, 1969).

13. P.K. Tien, R. Ulrich, and R.J. Martin, Appl. Phys. Lett. **14**, 291 (1969).

14. P.K. Tien and R. Ulrich, J. Opt. Soc. Am. **60**, 1325 (1970).

15. D.J. Walter, Thin Solid Films **23**, 153 (1974).

16. D.J. Walter and D. Krause, Thin Solid Films **46**, 7 (1977).

17. A.C. Adams, D.P. Schinke, and C.D. Capio, J. Electrochemical Society **126(9)**, 1539 (1979).

18. J.C. Manifacier, J. Gasiot and J.P. Fillard, Journal of Physics E: Scientific Instruments **9**, 1002 (1976).

19. J.H. Jean and T.A. Ring, Colloids and Surfaces **29**, 273 (1988).

20. P.C. Hiemenz, *Polymer Chemistry: The Basic Concepts*, (Marcel Dekker, Inc., 1984), Chapter 4.

21. *Handbook of Chemistry and Physics*, (CRC Press, 68th edition, 1987-88).

22. J-L Look and C.F.Zukoski, J. Am. Ceram. Soc. **75(6)**, 1587 (1992).

23. *Polymer Handbook*, edited by J. Brandrup and E.H. Immergut (Wiley-Interscience Publication, New York 1975).

24. R.J. Samuels, J. Poly. Sci., Part A-2 **7**, 1197 (1969).

25. *Handbook of X-Ray Photoelectron Spectroscopy*, edited by J. Chastain (Perkin

Elmer Corporation, 1992).

26. G.W. Castellan, *Physical Chemistry*, (2nd edition, Addison-Wesley Publishing Co.,Reading, MA, 1971), Chapter 33.

27. V.J. Nagpal, R.M. Davis, and S. B. Desu, "Novel Thin Films of Ceramic Particles Derived by Sol-Gel Process", U.S. Patent pending.

28. T.J. Rehg, B.G. Higgins, AIChE Journal **38(4)**, 489 (1992).

Chapter 7

Future Work

Particle Synthesis

1. Particle growth via the hydrolysis and condensation of titanium tetraethoxide at the typical reaction conditions occurs within minutes. The fact that in-situ steric stabilization could be successfully achieved in such a reactive system lends strong possibility to the fact that in-situ steric stabilization can also be achieved towards the synthesis of other transition metal oxide systems as well, e.g., zirconium oxide or tantalum oxide via the hydrolysis and condensation of their respective ethoxides.

2. Co-hydrolysis of mixed alkoxides should be studied to produce composite ceramic materials where the heterogeniety occurs on the length scale of 1-10 nm. For this purpose, hydrolysis and condensation of individual alkoxides might be studied first. Sequential addition of alkoxides might be necessary to account for the rates of hydrolysis and condensation of the alkoxide species.

3. Particle synthesis in the presence of well defined block copolymers should be pursued. It is anticipated that block copolymers would perform better as stabilizers than homopolymers in terms of minimum polymer concentration and molecular weight

needed to achieve steric stabilization. A di-block copolymer can be used such that the short anchor block adsorbs at the surface whereas the long tail block, which does not adsorb at the surface, forms a steric layer. For surfaces like titania which have hydroxyl surface groups, this would mean that the anchor block should have a tendency to form strong hydrogen bonds. Hence, polymers carrying carbonyl or hydroxyl groups can be a good candidate anchor blocks. The criteria for the candidate tail block would be that it should be reasonably soluble in the given solvent system. Also, the copolymer should not form micelles which can happen if the anchor block is in a bad solvent. Micelle formation can be easily detected by dynamic light scattering.

One such di-block copolymer can be poly(2-ethyl-2-oxazoline)(PEOX)-b-poly(methylvinylether)(PMVE) where the short PEOX block adsorbs strongly at the hydrophilic surface and the long PMVE block constitutes steric layer thickness. The block lengths should be such that n_{tail}/n_{anchor} should be at least 4 where n is the degree of polymerization. A tail block with molecular weight of about 10,000 would be a good starting point.

4. In Chapter 4 it was mentioned that monofunctional Jeffamine M2000 did not work as a steric stabilizer whereas a difunctional D2000 did. This was surprising because a difunctional polymer carrying adsorbing groups at either ends can cause bridging flocculation whereas a monofunctional polymer cannot do so and hence M2000 was

expected to also give steric stabilization. The fact that it did not suggests that M2000 does not adsorb at the surface within the time scales of particle growth. This can be tested by carrying out equilibrium adsorption studies with both the end-functionalized D2000 and M2000 polymers on previously synthesized titania powder. The carbonyl group in the end-functionalized polymers adsorbs in the UV region and hence a change in polymer concentration can be easily detected and hence adsorption isotherms can be constructed. Also, the colloidal stability of titania particles after equilibrium adsorption can be tested by simulating flocculation by electrolyte addition in the suspension. The suspension with less steric stability will flocculate first and sediment. These experiments would shed some light on the adsorption behavior of the two polymers.

5. The end-attachment of the functionalized PPO chains should be enhanced by the condensation of the -Si-OH end groups onto a TiO_2 surface. This may be realized by end-functionalizing the PPO as before and adding it to TEOT solutions that are slightly acidic. This should enhance the adsorption of the deprotonated silanol to the TiO_2 surface since the TiO_2 would be even more positively charged than it was under our normal neutral reaction conditions. If hydrolyzed -Si-OH endgroups can be made to condense sufficiently rapidly, then covalent end-grafting and improved steric stabilization may be realized.

6. The particle growth experiments in this thesis were done under neutral pH conditions to minimize the effects of electrostatic stabilization and thus to highlight the effects of steric stabilization. Previous work [1] had shown that electrostatic stabilization accomplished by controlling the pH could result in TiO_2 particle sizes as small as 0.3 microns. Growth experiments could be done with in-situ steric stabilization at pH conditions where electrostatic stabilization would also be important. The combined effects of these two modes of stabilization may lead to even smaller particle sizes.

7. The dynamic light scattering data in chapter 2 suggests that HPC reacts with TEOT when mixed together before hydrolysis. This can possibily be verified by FT-IR analysis before and after the premixing.

Thin Films

1. The composition of thin TiO_2/HPC films discussed in Chapter 6 can be easily changed by changing HPC concentration. This will change the film refractive index. Multiple films with controlled refractive index gradients can then be constructed. By appropriately controlling the film thickness and refractive index, these films can be used to construct optical band pass filters. The filter performance would depend upon the film thickness and refractive index of each layer. The design parameters of these filters are commercially available as a software package.

2. Pure titania films were obtained when the polymer was burnt at 700°C. The burning of the polymer led to inter-particle porosity of 38% and the pore size was about 40 nm. These films might be suitable for filtration applications for removing particles from liquids or gases in highly aggressive environments. The film porosity and the pore size can be controlled by simply varying the polymer concentration in the starting mixture. For example, higher polymer concentrations in the suspension used for spin coating would result in more inter-particle voids and hence greater porosity. Sintering time and temperature would determine the pore size. Higher sintering time and temperatures lead to greater local densification and increase the grain size. This in turn increases the pore size. In Chapter 6 it was mentioned that the films turned opaque when sintered at 900°C due to large grain size and pores.

3. The sintered porous titania films will have high surface area and hence can be studied for their properties as catalyst supports.

Reference

1. J-L Look, and C.F. Zukoski, Faraday Discuss. Chem. Soc., 90 (1990) 345.

Vita

Vidhu J. Nagpal was born on July 4, 1963, in Kanpur, India, as the eldest of the two children. He mostly grew up in Bombay and obtained a bachelor's degree in Chemistry from the Bombay University in 1984. He then joined the University Department of Chemical Technology (U.D.C.T.), Bombay, for a three year bachelor's degree program in Chemical Technology. He then came to Virginia Tech in Fall 1987, where he first joined the Chemistry Department and then moved to the Department of Chemical Engineering in Fall 1988 where he started working with Professor Rick Davis as a Ph.D. candidate in the Materials Engineering and Science Program. He finished his Ph.D. in August 1993 and he is currently a Post-Doctoral Research Associate with Professor Seshu Desu in the Department of Materials Science and Engineering.